Towards a verified mechanistic model of plankton population dynamics

Mark E. Baird

Submitted for the degree of:
Doctor of Philosophy

Department of Biological Sciences
University of Warwick
Coventry CV4 7AL
UNITED KINGDOM

July 1999

Preamble

For the first time in my life, I saw the horizon as a curved line. It was accentuated by a thin seam of dark blue light - our atmosphere ... I was terrified by its fragile appearance.

Ulf Merbold, Space Shuttle Astronaut (1988)

We are presently changing many of the physical, chemical and biological properties of our planet. In order to understand these changes, and minimise their negative impacts, we must be able to forecast global physical, chemical and biological cycles. To predict the future behaviour of a such a complex dynamical system, a forecaster must concentrate on those aspects of the system that cannot change in time. If he/she can constrain the system using only time-invariant laws and parameters, and define all initial conditions, then the future behaviour of the system can be predicted.

Such a task, on a planetary scale, is certainly daunting. Nonetheless, climate modellers, concentrating on thermodynamic relationships which constrain atmospheric and oceanographic dynamics, are achieving forecasting results on time-scales of days-to-decades thought unachievable when the nature of complex systems was first recognised in the early 1970s. But the atmosphere system is coupled to the global land, ocean and biosphere. The strength of this coupling has been highlighted by increasing concern over anthropogenic release of buried carbon, and deforestation, on atmospheric carbon dioxide. The planet is warming at an unprecedented rate. The chief cause, according to our most advanced models, is increased atmospheric insulation by carbon dioxide. To predict future carbon dioxide levels, and therefore global climate, we must predict the

behaviour of the global biosphere (ourselves included).

We therefore need a model of the biosphere based on time invariant laws, and parameters, with globally measurably initial conditions. This thesis, by working towards a verified, mechanistic model of plankton population dynamics, hopes to contribute in part, to achieving this goal.

Mark Baird

Coventry, UK 1999.

Contents

List of Symbols

Let no one who is not a mathematician read my works.

Leonardo da Vinci

The units used in this document comply with the Système International d'Unités (International System of Units or SI). Fundamental constants refer to physical constants which do not change over time; base variables refer to quantities which vary in time, and derived variables refer to quantities, made up of base variables, which are convenient to define. The use of one symbol to represent more than one parameter is unfortunate, but is a result of conforming to the nomenclature of the variety of different fields that have been used in this project. Symbols are listed complete with all sub- and superscripts used to define them. In some case they appear without their qualifiers in the text, but retain their definition.

Base variables

a	maximum nutrient uptake rate to a cell	mol cell s^{-1}
$a_{j,\lambda}$	fraction of light absorbed by a cell of species j, at wavelength λ	-
A	experimentally-determined constant for Arrhenius equation	s^{-1}
A_j	projected area of a cell of species j on a plane perpendicular to the incident light	m^2
A_s	surface area	m^2
b	extracellular nutrient concentration at half the maximum	

	uptake rate	mol m^{-3}
$b_{j,\lambda}$	chlorophyll a specific scattering coefficient of cell j	
	at wavelength λ	m^2 mg(Chl a)$^{-1}$
$b_{w,\lambda}$	scattering coefficient of sea water and its non-phytoplankton	
	constituents at wavelength λ	m^{-1}
C	fraction of cloud cover ($\times 8$)	oktas
C_b	nutrient concentration in the bulk fluid	mol m^{-3}
$C_{\mathrm{Chl}\,a,j}$	concentration of chlorophyll a in phytoplankton species j	mol m^{-3}
c_p	specific heat	J kg^{-1} K^{-1}
$C_{D,j}$	drag coefficient of cell j	m
C_w	nutrient concentration at the cell wall	mol m^{-3}
$C_{\xi,j}$	concentration of pigment ξ, in species j	mg(pig) m^{-3}
D_i	molecular diffusivity of chemical species i	m^2 s^{-1}
E_a	activation energy	J mol^{-1}
e	eccentricity of a spheroid	-
F^{rad}	radiative flux density	W m^{-2}
g	gravitational acceleration	m s^{-2}
g_1	dimensionless scattering coefficient	-
g_2	dimensionless scattering coefficient	-
G	dimensionless scattering coefficient	-
h	number of herbivore species	-
H_k	concentration of herbivore species k	mol m^{-3}
$I_{z,\lambda}$	radiation at depth z, wavelength λ	W m^{-2}
$J_{i,j}$	uptake rate of nutrient i to phytoplankton species j	mol $cell^{-1}$ s^{-1}
k	thermal conductivity	W m^{-1} K^{-1}
$k_{g,\lambda}$	partial attenuation coefficient of gilvin at wavelength λ	m^{-1}
k_j	reaction rate constant for species j	s^{-1} $mol^{-(n+1)}$
k_p	reaction rate constant for phytoplankton (Ch. 3)	s^{-1} $mol^{-(n+1)}$
$k_{w,\lambda}$	partial attenuation coefficient of water at wavelength λ	m^{-1}

K	wall concentration at half the maximum uptake rate of intracellular processes	mol m^{-3}
K_D	Kolmogorov length scale	m
K_o	value of K at $Q = 0$	mol m^{-3}
K_z	vertical eddy diffusivity at depth z	m^2 s^{-1}
m	mass	kg
$m_{i,j}$	stoichiometric coefficient for nutrient i, phytoplankton j	mol mol^{-1}
$m_{I,j}$	stoichiometric coefficient for energy (in photons) phytoplankton species j	mol mol^{-1}
M	thickness of layer of fluid	m
$M_{path,\lambda}$	average pathlength of a photon through a layer at wavelength λ	m
n	number of nutrient species	-
N_{in}	concentration of N in the dilutant	mol m^{-3}
N_i	concentration of nutrient species i in the extracellular fluid	mol m^{-3}
p	number of phytoplankton species	-
p	pressure	N m^{-2}
P_j	concentration of phytoplankton species j	mol m^{-3}
Pe	Peclet number	-
Q_H	heating function	W m^{-2}
Q^*	fraction of nutrient reservoir filled $Q^* = Q/Q^{max}$	-
$Q_{i,j}$	concentration of nutrient species i stored in phytoplankton species j	mol cell^{-1}
$Q_{i,j}^{max}$	maximum concentration of nutrient species i, stored in phytoplankton species j	mol cell^{-1}
q^*	fraction of energy reservoir filled $q^* = q/q^{max}$	-
q_j	energy in photons stored in phytoplankton species j	mol cell^{-1}
q_j^{max}	maximum energy in photons stored in phytoplankton species j	mol cell^{-1}
r	spherical radius	m
r_a	aspect ratio = axial radius/normal radius	-

r_1, r_2, r_3	orthogonal radii	m
R	abundance ratio of isotopes	-
Pe	Peclet number	-
S	salinity	ppt
S_z	concentration of a scalar at depth z	mol m^{-3}
$Sh_{i,j}$	Sherwood number of nutrient i advected towards phytoplankton species j	-
T	temperature	K
t	time	s
$T_{ref,j}$	temperature of phytoplankton species j growth rate maximum	K
$T_{ref,k}$	temperature of herbivore species k growth rate maximum	K
u	fluid velocity	m s^{-1}
$U_{j,k}$	velocity of cell j relative to k	m s^{-1}
V	maximum rate of intracellular uptake processes	mol m^{-3}
V_j	volume of cell j	m^3
W_ξ	halfwidth of the ξth Gaussian band	nm
$Y_{j,k}$	yield of predator per prey	mol mol^{-1}
α_j	growth efficiency of phytoplankton species j	-
γ_ξ	peak specific absorption coefficient of pigment ξ	m^2 mg(pig) $^{-1}$
δ	isotopic composition relative to standard	‰
ϵ	mean dissipation rate of turbulent kinetic energy	m^2 s^{-3}
ϵ_b	isotopic fraction rate by internal biochemical reactions	‰
ϵ_d	isotopic fraction rate by diffusion	‰
ϵ_p	isotopic fraction rate of phytoplankton growth	‰
ϵ_{Ru}	isotopic fraction rate by Rubisco	‰
η	dynamic viscosity	kg m^{-1} s^{-1}
θ	azimuth angle	rad
Θ	potential temperature	K
λ	wavelength	nm

λ_ξ	wavelength of maximum absorption for pigment ξ	nm
μ_j	growth rate of phytoplankton species j	s^{-1}
μ_j^{max}	max. growth rate of phytoplankton species j	s^{-1}
$\mu_j^{max\,ob}$	max. observed growth rate of phytoplankton species j	s^{-1}
μ_k	growth rate of herbivore species k	s^{-1}
ρ	fluid density	kg m^{-3}
ρ_j	density of species j	kg m^{-3}
ρ_w	density of water	kg m^{-3}
τ_λ	transmission coefficient of a cloudless atmosphere and zenith sun at wavelength λ	$airmass^{-1}$
Υ	number of pigment types	-
υ	molecular diffusivity of momentum	m^2 s^{-1}
$\phi_{j,k}$	encounter rate coefficient of species j with species k	m^3 s^{-1}
ψ_j	diffusion shape factor for phytoplankton species j	m
$\mathcal{D}$	dilution rate	s^{-1}
$\mathcal{P}$	cell wall permeability	m s^{-1}
$\mho$	effective conductance of uptake	m^3 s^{-1}

Subscripts and Superscripts

i	Nutrient species	
j	Phytoplankton species	
k	Herbivore species	
z	depth	m
λ	wavelength	nm
ξ	pigment species	
max	maximum	

Derived variables

$\overline{aA}_{\lambda,j}$	absorption cross-section of cell j at wavelength λ	m^2
$\overline{\gamma C}_{\lambda,j}$	absorption coefficient of cell j at wavelength λ	m^{-1}

Fundamental constants

A_v	Avogadro constant	6.02214×10^{23} mol^{-1}
h_P	Planck constant	6.62608×10^{-34} J s^{-1}
k_B	Boltzmann constant	1.38066×10^{-23} J K^{-1}
R	universal gas constant	8.31451 J K^{-1} mol^{-1}
G_c	gravitational constant	6.67259×10^{-11} N m^2 kg^{-2}

Non-fundamental constants

Ω	rotation rate of earth	7.292×10^{-5} s^{-1}

Mathematical symbols

if $\mathbf{u} = u_x x + u_y y + u_z z$ and $\mathbf{v} = v_x x + v_y y + v_z z$,

$$\nabla \equiv \left(\frac{\partial}{\partial x} + \frac{\partial}{\partial y} + \frac{\partial}{\partial z} \right)$$

$$\mathbf{u} \times \mathbf{v} \equiv (u_y v_z - u_z v_y)\, x + (u_z v_x - u_x v_z)\, y + (u_x v_y - u_y v_x)\, z$$

$$\mathbf{u} \cdot \mathbf{v} \equiv u_x v_x + u_y v_y + u_z v_z$$

$$\frac{Ds}{Dt} \equiv \frac{\partial s}{\partial t} + u_x \frac{\partial s}{\partial x} + u_y \frac{\partial s}{\partial y} + u_z \frac{\partial s}{\partial z} \equiv \frac{\partial s}{\partial t} + \mathbf{u} \cdot s$$

$$\nabla^2 \mathbf{u} = \nabla \cdot \nabla \mathbf{u} = \frac{\partial^2 \mathbf{u}}{\partial x^2} + \frac{\partial^2 \mathbf{u}}{\partial y^2} + \frac{\partial^2 \mathbf{u}}{\partial z^2}$$

Abbreviations

APEX	Artificial Plankton Experiment
BATS	Bermuda Atlantic Time-series
Chl	Chlorophyll
CR	Chemical Reaction growth equation
DIC	Dissolved Inorganic Carbon
DOC	Dissolved Organic Carbon
FTSC	Forward-Time Space-Centred integration scheme
GFDL	Geophysical Fluid Dynamics Laboratory, Princeton
HOTS	Hawaiian Ocean Time-series
HW	Hill-Whittingham uptake equation
JGOFS	Joint Global Ocean Flux Study
KE	Kinetic Energy
LM	Law of the Minimum growth equation
MT	Mass Transfer limited uptake equation
MOM	Princeton's Modular Ocean Model circulation model
MP	Multiplicative growth equation
NERC	Natural Environment Research Council
NPZ	Nutrient / Phytoplankton / Zooplankton
IPCC	Intergovernmental Panel on Climate Change
OCC	Orthogonal curvilinear coordinates
ODE	Ordinary Differential Equation
OWS	Ocean Weather Station
PDB	Standard Pee Dee Belemnite
PDE	Partial Differential Equation
pig	pigment
PAR	Photosynthetically Available Radiation
POM	Princeton Ocean Model (circulation model
RUBISCO	Ribulose-1,5-bisphosphate carboxylase
SeaWiFS	Sea-viewing Wide Field-of-View Sensor
SC	Spherical coordinates

List of Figures

List of Tables

Acknowledgements

As to the fable that there are Antipodes, that is to say, men on the opposite side of the earth, where the sun rises when it sets to us, men who walk with their feet opposite ours, that is on no ground credible.

St. Augustine, 5th Century

My biggest thanks go to fellow Ph.D. student Steve Emsley. Steve has been an integral part of the development and publishing of the work presented in Chapter 2 in an article in the *Journal of Plankton Research*, and has produced the most realistic oceanic simulations of the plankton population model by coupling it to the Princeton Ocean Model. He has become a close friend, and I have thoroughly enjoyed working together. Thank you also to Lyndi, who graciously put up with our nightmare model development / programming sessions in Devon.

I thank the Natural Environmental Research Council, UK, for providing the studentships that supported myself and Steve. Prof. J. McGlade, A. Taylor and J. Aiken were the principal investigators on the grant, and helped us out whenever we were in Plymouth. NERC also provided the funding for my attendance at the Mathematical Modelling of Plankton Population Dynamics' workshop, Isaac Newton Institute for Mathematical Sciences, Cambridge (Northern summer, 1996), and the Geophysical and Environmental Fluid Dynamics summer school, Cambridge (September, 1998).

I thank my supervisors at the University of Warwick, Prof. J. M. McGlade, Dr. E. J. Milner-Gulland and Dr. G. F. Medley for the freedom to pursue my own ideas, and encouragement to keep going.

I have also benefited from the feedback of researchers around the world, who have given their time either in person, or through correspondence. In particular to Dr. Andrew Yool and Dr. Markus Kirkilionis (both formerly of the University of Warwick) who reviewed Chapter 2 thoroughly before its publication in the *Journal of Plankton Research*. I also thank Prof. Marlin Atkinson (Univ. of Hawaii), Dr. Hugo van den Berg (Univ. of Warwick) Prof. Bob Bilger (Univ. of Sydney), Dr. Matthew England (Univ. of New South Wales), Dr. Richard Geider (Marine Biological Association of UK), Prof. George Rowlands (Univ. of Warwick), Dr. Dennis McGillicuddy (Wood's Hole Oceanographic Institute), Dr Wade McGillis (Wood's Hole Oceanographic Institute), Dr. David Morse (Univ. of Warwick), Prof. Tim Pedley (Univ. of Cambridge), Prof. Brian Popp (Univ. of Hawaii), Dr. Andrew Price (Univ. of Warwick), Dr. Iain Suthers (Univ. of NSW), and Dr. Deiter Wolf-Gladrow (Alfred-Wegener-Institute for Polar and Marine Research)

I also thank my fellow Ph.D. students at Warwick, and at the University of New South Wales, Australia, who have stimulated angles and ideas which have improved this thesis greatly.

Thank you especially to Ginny, my lovely wife, who has kept me sane these past three years. She is also the best proof reader ever. Without her efforts at improving the grammar, the equations would have been easier to understand than the text (really).

Declaration

Do not tempt me to beat my chest and say this is what I have done.

Nelson Mandela

This thesis is the result of original research conducted by myself unless stated in the text or acknowledgements. This research was conducted at the University of Warwick under the supervision of Prof. J. M. McGlade, Dr. E. J. Milner-Gulland and Dr. G. F. Medley. All sources of information have been acknowledged or referenced.

No part of this thesis has been submitted for a degree at any other university.

Summary

Plankton are a significant component of the biogeochemical cycles that impact on the global climate. Plankton ecosystems constitute around 40 % of the annual global primary productivity, and the sinking of plankton to the deep ocean (the so-called biological pump) is the largest permanent loss of carbon from the coupled atmosphere-surface ocean-land system. The biological pump need only increase by 25 % to cancel the anthropogenically-released flux of CO_2 into the atmosphere.

Mechanistic models of atmosphere-ocean dynamics have proved to have superior predictive capabilities on climate phenomena, such as the El Niño, than empirical models. Mechanistic models are based on fundamental laws describing the underlying processes controlling a particular system. Existing plankton population models are primarily empirical, raising doubts to their ability to forecast the behaviour of the plankton system, especially in an altered global climate.

This thesis works towards a mechanistic model of plankton population dynamics based primarily on physical laws, and using laboratory-determined parameters. The processes modelled include: diffusion and convection to the cell surface, light capture by photosynthetic pigments, sinking and encounter rates of predators and prey. The growth of phytoplankton cells is modelled by analogy to chemical kinetics. The equations describing each process are verified by comparison to existing laboratory experiments. Process-based model verification is proposed as a superior diagnostic tool for model validation than verification based on the changing state of the system over time. To increase our ability to undertake process-based verification, a model of stable isotope fractionation during phytoplankton growth is developed and tested.

The developed model has been written to complement other process-based models of biogeochemical cycles. A suite of process-based, biogeochemical models, coupled to an atmosphere-ocean circulation model, will have superior predictive capabilities compared with present global climate models.

Chapter 1

Introduction

---

mechanism /'mɛk(e)nɪz(e)m/' *n.* **6** *Philos.* the doctrine that all natural phenomena, including life, allow mechanical explanation by physics and chemistry.

The Concise Oxford Dictionary

1.1 Outline

This thesis is divided into 4 chapters and 2 appendices. Chapter 1 briefly introduces the topic of plankton ecology, and then surveys a variety of global biogeochemical models. Chapter 1 concludes by recognising the need for a predictive plankton population model, and proposes that this is most likely to be produced by a mechanistic model. Chapter 2 works towards a mechanistic model of plankton population dynamics. This involves using theoretical descriptions of particle interactions in the physical sciences to describe plankton interactions. Laboratory experiments on single species populations are used to validate the choice of equations. Chapter 3 furthers this verification process, by analysing population dynamics and stable isotope fractionation predicted using the model of phytoplankton growth based on an analogy to chemical kinetics developed in Chapter 2. In particular, this chapter proposes that a governing set of equations describing phytoplankton growth may be derived, and that process-based model verification has advantages over model verification based on the changing state of the system over time alone. Chapter 4 discusses the progress made in Chapters 2 and 3 in developing and

verifying the mechanistic model, and the significance of the such a model in predicting global biogeochemical cycles. Appendix A gives biogeochemical values useful for application of the model. Appendix B provides geometric information on the shapes which phytoplankton cells are assumed to take in this thesis, and provides a methodology for expanding this to include more complicated shapes.

1.2 An overview of the plankton

Plankton are small aquatic organisms whose position (horizontal and vertical) in a body of water is determined primarily by fluid motion. They range in size from less than 1μm diameter bacterial cells to larval fish centimetres long. They can span virtually the whole food chain, from primary producers gaining energy from chemosynthesis and photosynthesis, through to herbivores, carnivores and even cannibals. There is also a vast number of a varieties, many adapted to particular environments, but others whose presence in the water bodies of the world seems ubiquitous.

Although small in size, plankton numbers are large. Given favourable conditions, some species can double in number in less than a day. Their numbers are so large, and their distribution so widespread, that the solar radiation reflected from the ocean surface has reduced strength at the peak absorbances of the photosynthetic pigments that the plankton contain. We use this to measure the biomass of photosynthetic plankton in the ocean from satellites (Fig. 1.1). With such a large and dynamic biomass, the plankton are a major component of global biogeochemical cycles (such as carbon, nitrogen etc).

Plankton also affect local aquatic environments. The photosynthetic plankton provide the energy and organic matter that feeds, along with benthic algae, all aquatic animals. Some of the most important living resources of the ocean, such as fish, begin their lives as plankton, and many continue to feed off plankton even in their adult stages. But the plankton can also have negative impacts. A number of species are toxic to other marine organisms, and even humans (e.g. the red-tide forming dinoflagellates). Textbooks which introduce the fundamentals of plankton ecology include Valiela (1992), Mann and Lazier

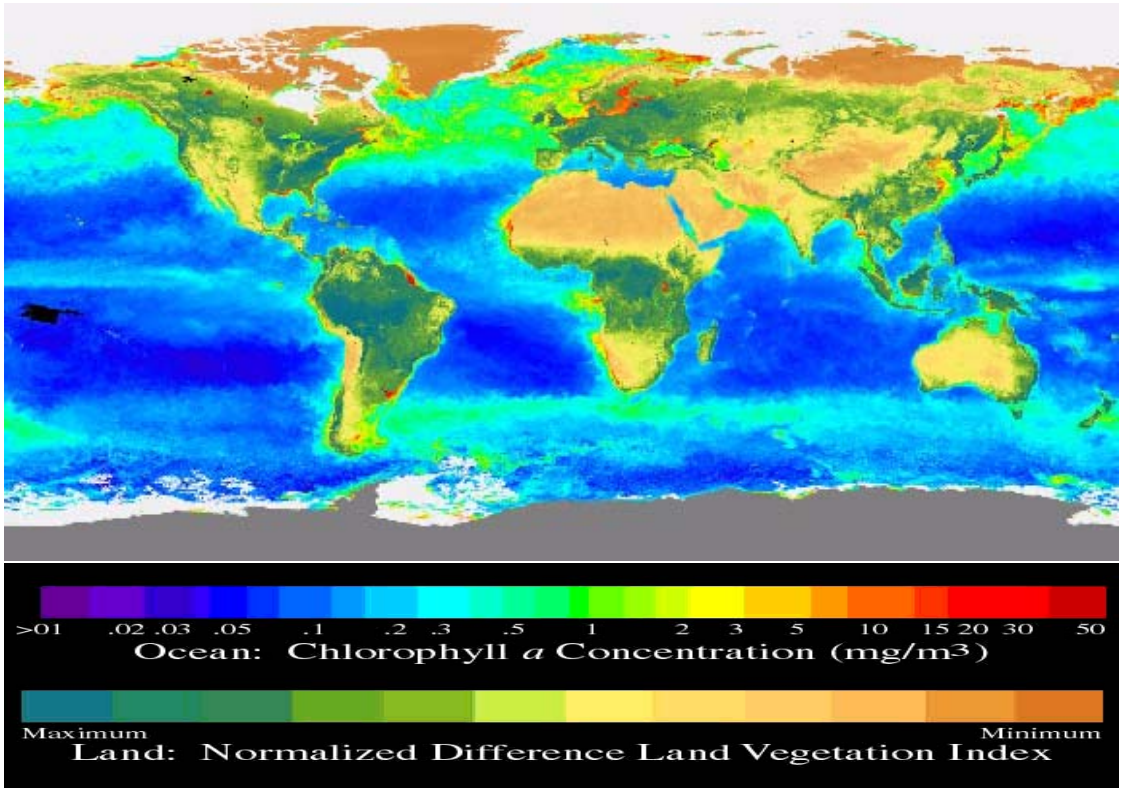

Figure 1.1: Global chlorophyll *a* concentrations from March - May 1998. Chlorophyll *a* inferred from satellite measurement of irradiance at 8 wavelengths by the sun-synchronously orbiting SeaWiFS satellite (`http://seawifs.gsfc.nasa.gov/SEAWIFS.html`).

(1991), Newell and Newell (1973) and Bold and Wynne (1985).

A large number of models have been written to quantitatively simulate plankton ecology (Riley (1947); Wroblewski (1977); Steele and Henderson (1981); Fasham *et al.* (1990); Hurtt and Armstrong (1999); Bissett *et al.* (1999b) and Oschlies and Garçon (1999)). This thesis provides another such model, derived in Chapter 2. All plankton population models, by necessity, provide only an abbreviated description of a plankton ecosystem, based on very simple ecological processes (such as photosynthesis, grazing etc.). The model presented in this thesis is based on the same general concepts as other plankton population models. The unique element of the model presented in this thesis is the extent to which fundamental physical laws have been preferred to field-determined empirical relationships. Using fundamental physical laws, instead of field-based observa-

tions, has improved predictive capabilities of atmospheric and ocean circulation models (Kerr, 1998). Could such an approach improve our ability to forecast plankton population dynamics ?

1.3 Derivation of numerical models

Numerical models are used to explain a large variety of time-evolving natural phenomena. The method of equation derivation, and the techniques of numerical integration, can have significant impacts on the model output. This thesis considers only the impact of equation derivation on model output. Section 1.3 introduces concepts in equation derivation which will be important for understanding novel aspects of the model presented in Chapter 2.

1.3.1 The language of modellers

The theoretical modelling approach adopted in this thesis shares a number of characteristics with those of the physical sciences, but is, nonetheless, an ecological model. There is a conflict in terminology between these two fields. Table 1.1 defines terminology used in this thesis to avoid ambiguity. In particular, it should be noted that the term mechanistic is often used in the biological modelling (Hurtt and Armstrong, 1999) where, according to the definitions of Table 1.1, process-based would be more appropriate.

1.3.2 Empirical versus mechanistic equation derivation

Most plankton populations models are derived empirically from field data sets (e.g. Hurtt and Armstrong (1999) and Steele and Henderson (1981)). Such models are diagnostic. That is, they provide a summary of data obtained from the field, but cannot predict phenomena beyond the bounds of this data. The model developed in this thesis is process-based, and, as far as possible, mechanistic. Mechanistic models, it has been shown in the physical sciences, can be prognostic. That is, using an understanding of underlying processes alone, mechanistic models can predict the behaviour of a complex system.

Adjective	Description
Equation derivation	
mechanistic	an equation based on theoretical consideration of underlying physical processes only.
semi-empirical	an equation based on theoretical considerations, with experimentally determined constants.
empirical	an equation based on experimental data only.
heuristic	intuitively determined equation based on endpoints and chosen from simple functional forms.
Model structure	
process-based	a model whose structure allows description of physical interaction between model components.
prognostic	a model with predictive capabilities, especially with respect to changing environmental forcings.
diagnostic	a model that can be used to explain observations, but which cannot be formulated independently of observation.
dynamic	a model inwhich state-variables change with time.

Table 1.1: Definition of adjectives as used in this thesis to describe the method of deriving equations and model structure. The descriptions of equations is mutually exclusive, but the model structure descriptions are not.

Given the lack of understanding of fundamental plankton interactions, the model presented in Chapter 2 contains some empirically derived relationships. To get a feel for the difference between a mechanistically-derived and an empirically-derived equations, it is instructive to look at what could be considered the first mechanistic model, and its empirical predecessor.

Kepler's empirical model of planetary motion

A set of empirical laws describing the motion of the planets (assuming the sun to be at a fixed point) were developed by Johannes Kepler:

Empirical Law 1 *The path of each planet about the sun is an ellipse with the sun at one of the foci of the ellipse.*

Empirical Law 2 *Each planet moves so that an imaginary line from the sun to the planet sweeps out equal areas in equal periods of time.*

Empirical Law 3 *If T_1 and T_2 are the periods of the two planets (i.e. the time they take for a complete orbit about the sun) and r_1 and r_2 are their mean distances from the sun, then the following equations holds:*

$$\left(\frac{T_1}{T_2}\right)^2 = \left(\frac{r_1}{r_2}\right)^3 \tag{1.1}$$

It takes six parameters to define an ellipse in 3 dimensional space: the major axis of the ellipse, the eccentricity, the direction of the major axis in the plane of the orbit, the time of perihelion (when the two bodies are closest together), and two numbers giving the orientation of the orbital plane in space. With these six parameters, and a state variable[1] defining the location of the planet on the ellipse, Kepler was able to geometrically describe the observed planetary motion. Had Kepler written a numerical model based on the above three equations to predict the position of all planets through time, he would have needed six parameters and one initial condition (to give the initial value of the state variable) for each planet.

Newton's mechanistic model of planetary motion

Issac Newton, on the other hand, described planetary motion in terms of a set of physical laws: three describing the nature of motion and one describing the interaction of bodies at a distance (law of gravity):

Mechanistic Law 1 *A body at rest remains at rest, and a body in motion continues to move at constant velocity unless acted upon by an external force.*

Mechanistic Law 2 *The rate of change of momentum of a moving object is proportional to the resultant force and is in the direction of that force.*

Mechanistic Law 3 *Whenever a body exerts a force on another body, the latter exerts a force of equal magnitude and opposite direction on the former.*

[1] A parameter is a variable whose value is assumed to be constant in a particular system. A state variable is a variable whose value changes with time. The state of a system is assumed to be completely described by the knowledge of the value of each state variable.

Mechanistic Law 4 *The attractive force between two masses, m_1 and m_2 [kg] at a distance d [m] is given by:*

$$g = \frac{Gm_1m_2}{d^2} \tag{1.2}$$

where the gravitational constant, $G_c = 6.67259 \times 10^{-11}$ N m^2 kg^{-2}. These equations demonstrated Newton's belief in causality. The observed paths were not a property of the system itself, but rather emerged from the fundamental laws that governed it. To model planetary motion, Newton required three equations (Law 1 is a special case of Law 2), a fundamental constant (G_c) of the whole system, and, for each body (the planets and the sun), one parameter (m) and six state variables defining the each body's position (in x, y and z) and velocity (in x, y, and z).

For a n planet system with a sun, Kepler needed $6n$ parameters and n initial conditions while Newton required $n+2$ parameter values, and $6\,(n+1)$ initial conditions to describe the system's behaviour. In total, Kepler required $7n$ quantities, while Newton needed $7n+8$. So why were Kepler's empirical laws almost immediately consigned to history ? Firstly, Newton was able to show that Kepler's empirical laws could be derived from his mechanistic laws (although not vice versa). In doing so, Newton showed that Kepler's empirical laws were for the case when the planets did not interact with each other, were rigid spheres, and were in a frictionless medium, orbiting around a motionless sun. Secondly, Newton's laws were able to explain more than just planetary motion: they described motion at all of the then observable scales.

In terms of modern day predictive models, we can see two additional advantages of Newton's model. Firstly, the derivation of the mechanistic laws could be done independent of planetary motion. Planetary motion is an application of the equations, rather than their origin. Secondly, the parameters required by Newton's laws are better suited for predictive models. The gravitational constant, G, can be measured anywhere with great accuracy. Newton's equations were adopted, however, not because they did a better job of explaining data (although they do), but rather because they provided a better understanding of the system. Today's scientific community prefers to adopt models as

theories only with improved prediction of observable phenomena. Such an approach is referred to as the scientific method. In Newton's day, before science and philosophy became distinct methods of investigation, his model was quickly adopted. When Newton's theories were superseded at the beginning of this century by those of Albert Einstein, using essentially the same theoretical methods Newton himself developed, the scientific method slowed the acceptance of relativity as a theory, waiting instead for observable phenomena. Einstein's model required an extra fundamental constant (the speed of light), but was able to remove the assumptions of absolute space and time, and improve the accuracy of predicting planetary motion.

So as physicists derived more accurate models of planetary motion, we see the number of parameters and state variables increase. But the greater certainty with which the parameters can be determined, and their independence from the system's properties and state, results in a model with superior predictive capabilities.

1.4 Modelling global physical and biogeochemical cycles

The land, atmosphere and oceans are coupled through the transport of energy (heat, light and momentum) and mass (sediment, aerosols, nutrients, organic matter) (Fig. 1.2). A significant component of the land and oceans is the biological material they contain. In the oceans, the majority of the biological material is contain in the plankton. In this thesis, we will consider the dynamics of the plankton as a function of ocean circulation and solar irradiance only (label 6. in Fig. 1.2). To obtain a complete description of the behaviour of one component of the global biogeochemical system, however, it is necessary to quantify the fluxes of energy and mass to and from the other components. We shall briefly survey the models used to predict the dynamics in physical and biogeochemical models in the other components of the global system. The survey is by no means complete (there is an enormous number of such models), but is designed to give as both an overview, and also to gain insights which may be useful for constructing a model of plankton population dynamics. The survey therefore provides an example, and a challenge, upon which the development of the plankton population model in Chapters

2 and 3 will be based.

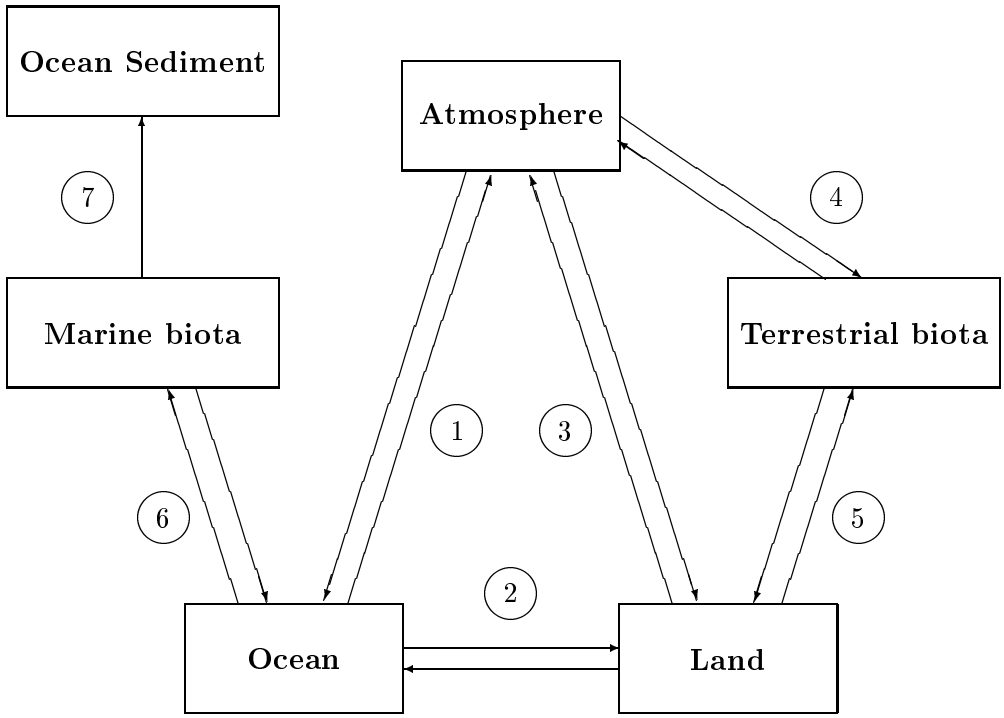

Figure 1.2: A simple model of the global physical and biogeochemical interactions 1. Atmosphere-ocean interactions such as momentum, heat and mass fluxes; 2. Ocean-Land interactions such as nutrient input; 3. Atmosphere-Land interactions such as rainfall, evaporation; 4. Terrestrial biota-Atmosphere interactions such as oxygen, nitrogen and carbon dioxide fluxes; etc. 5. Terrestrial biota-Land fluxes such as ground water use and nutrient supply; 6. Marine biota-Ocean fluxes such as carbon and nutrient uptake; 7. Marine biota-Ocean sediment fluxes, such as exchanges of benthic communities and planktonic organisms sedimenting.

1.4.1 Atmospheric and oceanic circulation

Modelling of the earth's atmosphere, both on short (weather) and long (climate) time scales is a highly advanced science. The resources devoted to obtaining forecasts of weather phenomena dwarf that spent on the modelling the other components of the global biogeochemical system. It is therefore natural that we look first at the progress

made in atmospheric circulation modelling. For most of the history of weather and climate prediction, empirical models have been used. With the development of highly advanced mechanistic models (Mellor and Yamada, 1974), and high speed computers, however, mechanistic models are becoming more popular. The prediction of the 1998 El Niño six months before the event by the most advanced mechanistic models, and the relative failure of empirical models (Kerr, 1998), is probably a turning point. It is unlikely that empirical models (based on large satellite-measured data sets of only a few decades, and getting larger at only 1 year per year), will be able to compete with the mechanistic models, whose performance now appears primarily limited by computing power.

In looking at atmospheric circulation, it is impossible to ignore ocean circulation. Not only are the atmosphere and oceans strongly coupled, but the mechanistic models used to describe their behaviour are very similar. The atmosphere and oceans are both fluids on a rotating sphere. It is therefore possible to write three fundamental laws describing their dynamics (Gill, 1982).

Conservation of mass:

$$\frac{\partial \rho}{\partial t} + \nabla \cdot \mathbf{u} = 0 \tag{1.3}$$

Conservation of momentum:

$$\frac{Du}{Dt} + 2\Omega \times u = \frac{\nabla p}{\rho} - g + \nu \nabla^2 u \tag{1.4}$$

Conservation of energy:

$$\frac{\rho T c_p}{\Theta} + \frac{D\Theta}{Dt} = \nabla \cdot (k \nabla T - I) + Q_H \tag{1.5}$$

where the rotation rate of earth, $\Omega = 7.292 \times 10^{-5}$ s^{-1}; u is the fluid velocity [m s^{-1}]; g is the gravitational acceleration [m s^{-2}]; ρ is the fluid density [kg m^{-3}]; p is the pressure [N m^{-2}]; k is the thermal conductivity [W m^{-1} K^{-1}]; υ is the molecular diffusivity of

momentum [m^2 s^{-1}]; Θ is the potential temperature [K]; c_p is the specific heat [J kg^{-1} K^{-1}]; T is the temperature [K]; F^{rad} is the radiative flux density [W m^{-2}] and Q_H is the heating function [W m^{-2}] which takes into account heating due to changes of phase, chemical reactions and viscous dissipation. The techniques for applying these equations differ. Different co-ordinate systems (e.g. Lagrangian versus Eulerian) can be chosen, different boundary conditions, and different numerical approximations. There is little disagreement, however, over their mathematical form (Denman and Gargett, 1995).

Atmospheric modellers have also developed a variety of tools for interpreting simulation outputs for the purpose of providing practical forecasts. These include evaluation of model performance based on its theoretical correctness, knowledge of initial conditions, and the spatial and temporal resolution of the model. Forecasts are often based on the results on a large number (or ensemble) of simulations (Buizza and Palmer, 1998). Improved forecasts have also been achieved by the assimilation of real-time data into model runs (Todling *et al.*, 1998). Global weather forecasts now show significant skill (model results are better than using mean weather statistics) for 5-7 days, and long term forecasts can predict annual variability over 6 months ahead. Ocean circulation forecasts are at the moment restricted to regional scales. However, an international collaboration (Global Ocean Data Assimilation Experiment) aims to provide global forecasts of ocean circulation by 2003. Such advanced techniques require resources well beyond the 20th century plankton population modeller. Nonetheless, they provide a good indication of the direction plankton population modelling may take, and what levels of predictive performance can be achieved in models of global scale phenomena.

1.4.2 Land geochemical cycles

A number of process-based models of land biogeochemical cycles have been developed such as models of volcanic eruptions and erosion (see the intrusion of fluid mechanics into geology (Huppert, 1986)). Constructing a global model of the effects of land biogeochemical cycles, however, is problematic. The processes that dominate in a particular geographic location change in time due to unpredictable (on long time scales) events such

as volcanic eruptions and landslides. These unpredictable events can have global impacts (e.g. the cooling of the planet in 1992 due to aerosols released by the volcanic eruption of Mount Pinatubo, The Philippines). A model of global land processes, therefore, must in some way average the sometimes very significant effects of individual events.

Some land geochemical processes can be successfully globally averaged. One example is the flux of the potent greenhouse gas methane between the soil and atmosphere. Ridgwell *et al.* (1999) have constructed a model of methane fluxes based on the specific processes which exchange the methane between the atmosphere and the soil. They contrast this approach to models which estimate the size of the flux based on "extrapolations from field and laboratory studies". Ridgwell *et al.* (1999) believe that such empirical estimates "are valuable as initial estimates [of global methane fluxes] and for defining maximum and minimum limits, but they cannot necessarily provide information about fluxes under novel conditions, particularly those arising as a result of climate change". Where feasible, Ridgwell *et al.* (1999) describe processes mechanistically, such as using Fick's law of diffusion, to determine fluxes of methane within the soil. This process-based approach is similar to the models of ocean circulation. Although the use of mechanistically-derived equations was limited, it was preferred where possible.

1.4.3 Land biological processes

The modelling of biological, both terrestrial and marine, systems has also proved to be more difficult than atmospheric and oceanographic circulation modelling. Cao and Woodward (1998b), amongst others, have developed a process-based, ecosystem-level model of terrestrial productivity. Carbon is contained within the soil, vegetation or atmosphere. Processes considered are photosynthesis, respiration, litter production, and decomposition. These processes are parameterised according to the soil (sand, sandy loam, loam, clay loam and clay), and vegetation type (18 in all). This model is complex, and includes a considerable number of mechanistic descriptions of biologically important processes such as evapotranspiration, soil moisture and stomatal conductance. A limitation of the development of mechanistic descriptions for this model is the use of

the ecosystem as the model scale. This does not allow changing characteristics within this ecosystem (for example the invasion of a exotic species etc.) and parameterisations must be based on ecosystem-scale field data. Cao and Woodward (1998a) conclude that "the dynamic simulation of ecosystem carbon fluxes in this study ... will lead to a full coupling between ecosystem carbon processes and climate systems that is essential for the more realistic predictions of both ecosystem response and climate change".

1.4.4 Marine biological processes

The biological component of the oceans can be divided into benthic and pelagic environments. There are some process-based models of benthic ecosystems. A good example is the modelling of primary productivity of reef flats on Eniwetak Atoll (Atkinson, 1992), based on an understanding of the fundamental processes of nutrient uptake to benthic surfaces (Bilger and Atkinson, 1992; Atkinson and Bilger, 1992; Baird and Atkinson, 1997). However, modelling benthic ecosystems has the same scale problems as the terrestrial ecosystem models mentioned above. A benthic species-level model has been constructed (Chen and Coughenour, 1996), although it is limited to the photosynthesis of a single aquatic macrophyte.

This thesis concentrates on modelling the pelagic biological component, and in particular, the plankton. A quick survey of some existing plankton population models follows that will be useful as a comparison to the theoretically derived and verified model presented in Chapters 2 and 3.

The Steele and Henderson (1981) model

The Steele and Henderson (1981) model is a very widely cited simple plankton population model. The Steele and Henderson (1981) model contained 3 state variables, 10 processes describing the interaction of the state variables, and 15 parameters describing properties of the system (Table. 1.2). Parameters were obtain from either field measurements, or 'tuning' to fit the whole model to a particular data set. In hindsight, John Steele (Steele and Clark, 1998) described the approach used in the construction of this

$$\frac{dN}{dt} = \underbrace{-\frac{N}{k_1+N}\frac{k_2}{k_3+k_4P}P}_{nutrient\ uptake} + \underbrace{\frac{k_5P}{1+k_6P} + k_7k_8H}_{excretion} + \underbrace{k_{13}(k_{14}-N)}_{mixing}$$

$$\frac{dP}{dt} = \underbrace{\frac{N}{k_1+N}\frac{k_2}{k_3+k_4P}P}_{growth} - \underbrace{\frac{k_9}{1+k_6}P}_{grazing\,loss} - \underbrace{k_{10}P}_{mortality} - \underbrace{k_{15}P}_{sinking}$$

$$\frac{dH}{dt} = \underbrace{\frac{k_{11}P}{1+k_6P}H}_{grazing\ gain} - \underbrace{k_{12}H}_{mortality}$$

Table 1.2: An empirical model of plankton population dynamics (Steele and Henderson, 1981) N - nutrient; P - phytoplankton biomass; H - herbivore biomass; k_{1-15} - coefficients.

model as:

"Traditional nutrient, phytoplankton, zooplankton (N/P/Z) simulations treat P and Z as single entities. Usually there is no formal optimising procedure, but a process of first defining the physical context, then selecting functional relationships and finally choosing parameter values. The results are judged by comparison with observations of, say, chlorophyll or zooplankton biomass. 'Tuning' is done by varying the least known (or knowable) parameters, such as predation rate (e.g. Fasham et al., 1990)".

The Steele and Henderson (1981) paper became the starting point for a large number of empirical models. The most cited plankton population model, the Fasham *et al.* (1990) paper, is one such model.

The Fasham *et al.* (1990) and Fasham (1993) models

The Fasham models used the same approach as Steele and Henderson (1981), but extended the food web to contain 7 state variables, 33 processes and 30 parameters. This level of complexity provided a good middle ground between the mathematical modellers (who required a simple model whose dynamics could be explored) and the ecologists (who demanded a model that contained some of the complexity of real food webs).

Nonetheless, Yool (1997) showed that much of the added complexity did not improve (or even change) the model's performance.

Chapter 2 compares the presented model output with that of Fasham *et al.* (1990) and Fasham (1993). Fasham's models were chosen as a benchmark because firstly they are well known, and secondly, since they use a simplified mixing model, the biological performance of the two models could be compared directly. Fasham's models have been coupled to a coarse resolution circulation model of the North Atlantic (Sarmiento *et al.*, 1993). They are referenced in almost all papers on plankton population dynamics, illustrating their dominance in the development of plankton population models. And yet, they are a simple diagnostic model, and have not been used successfully to predict plankton population dynamics.

The Hurtt and Armstrong (1999) model

The Hurtt and Armstrong (1999) model is developed and calibrated by simultaneously fitting data the from the Bermuda Atlantic Time-series (BATS) site from 1988 to 1991 and Ocean Weather Station (OWS) India from 1971 to 1975 in the the North Atlantic. Hurtt and Armstrong (1999) use only a relatively simple model to fit the annually averaged data at both sites. The model is then used to predict the behaviour at the Hawaiian Ocean Time-series (HOTS) site. They obtain the 'best fit' to data using a simulated annealing algorithm. Not surprisingly, given their main criteria for choosing model equations and parameter values is their ability to fit the data, the complicated mathematical techniques they use achieve a better fit to the field data set than other numerical models such as Fasham *et al.* (1990). However, the world's ocean environments vary both spatially and temporally, and may be undergoing permanent shifts due to global climate change. It is therefore unlikely that a model based purely on the average conditions over a few years of two vertical profiles of sites located conveniently near oceanographic institutes in the North Atlantic will provide predictive forecasts of global marine biogeochemical cycles. In fact, because the data is based on averages over a number of years, the model is unable to even predict one year of the original data

(see Hurtt and Armstrong (1999) Figs. 9a and b). Nonetheless, they conclude with "we believe that simple mechanistic [by which they evidently mean empirical] motivated biologically and constrained with field data are a key to making fundamental progress in understanding and predicting the role of ocean ecosystems in the air-sea balance of CO_2".

The Bissett *et al.* (1999b) model

The Bissett *et al.* (1999b) model was developed to capture biological-chemical ecosystem dynamics around Bermuda in the Sargasso Sea. In contrast to the Hurtt and Armstrong (1999) model, the Bissett *et al.* (1999b) model attempts, using a process-based approach, to capture the complex web of biological interactions that occur in plankton communities. While the equations used generally represent identifiable processes, they are nonetheless empirical. The model contains four functional groups to represent photosynthetic plankton, a heterotrophic bacteria functional group, two forms of dissolved organic nitrogen, nitrification, particulate remineralisation, and nitrogen fixation. The authors state that using "realistic vertical mixing [it] replicates the seasonal cycle of productivity, chlorophyll *a*, accessory pigments, phytoplankton species succession, dissolved inorganic carbon, dissolved organic carbon, ammonia + nitrite, nitrification, settling losses, air-sea CO_2 flux, and nitrogen fixation at the BATS site". To achieve this impressive list of predicted phenomena, the model has 21 state variables, and over 100 parameter values.

Of course, with such a large number of chosen equations and parameters, it is tempting to dismiss the Bissett *et al.* (1999b) model as having the degrees of freedom required to fit any data set. This argument is invalidated, however, if the choice of equations and parameter values is not made by the modeller, but rather from controlled, repeatable experiments. In the case of plankton, laboratory cultures can provide an environment for controlled, repeatable experiments. Bissett *et al.* (1999b) use a large number of laboratory experiments to obtain parameter values and choose model equations. However, this is not so much a principle on which the model is written, as an easy source of parameter

values. Furthermore, Bissett *et al.* (1999b) makes no attempt to ensure that model equations and parameter values are comparable between laboratory and field environments. For example, turbulence is known to change the loss rate of phytoplankton cells due to grazing. However, the model equations do not include a term for turbulence. The model equations and parameters values chosen are therefore applicable only for environments with the same turbulence level of the laboratory cultures (probably stagnant). To further compound the problem of choice of parameter values and model equations, some are based on field data sets (which are essentially uncontrolled, unrepeatable experiments). The success of the Bissett *et al.* (1999b) model, although certainly more convincing than the Hurtt and Armstrong (1999) and earlier models, may also be limited to the where it has been tested (BATS 1989-1995).

The Oschlies and Garçon (1999) model

The Oschlies and Garçon (1999) model consists of a simple empirical four component biological model coupled to the Geophysical Fluid Dynamics Laboratory (GFDL) Modular Ocean Model (MOM) version 1.1. At first, it seems strange to couple a highly advanced ocean circulation model to a basic empirical plankton population model. But in their own words (Oschlies and Garçon, 1999):

"We selected this simple biological model since the goal is to understand the impact of physical [circulation] processes and their representation in a numerical model on the biology, rather than to simulate ecological complexity".

As a result, they do not resolve community structure changes that can be important to biogeochemical cycles. However, the paper does undertake a lengthy comparison of numerical experiments to determine the optimal numerical methods for plankton population models coupled to three dimensional ocean circulation models. As a result of the biogeochemical scalars often numerically approaching zero (but not being allowed to become negative), a different numerical integration scheme is suggested compared with that used in physical mixing models. This is an important realisation, and this

paper is likely to become a valuable tool for future modellers of horizontally resolved plankton populations. But while it improves our understanding of numerical tools for modelling plankton population dynamics, it does not advance our understanding of model derivation.

Summary of plankton population models

At an international workshop on models of upper ocean biogeochemistry (JGOFS, Toulouse, France, 1995) models presented ranged from three to fourteen state variables, and from less than a dozen to more than forty parameters (Hurtt and Armstrong, 1999). With the Bissett *et al.* (1999b) model we can extend this to 21 state variables and approximately 100 parameters. As pointed by Denman and Gargett (1995), there is no consensus to the form, complexity, or even approach to modelling plankton populations.

As well as not reaching a consensus on modelling approaches, the field has not reached a consensus on model verification. Hurtt and Armstrong (1999) and Fasham *et al.* (1990) use measured averages (throughout the water column, and over a period of years) of nitrate, chlorophyll and primary productivity. Bissett *et al.* (1999b), on the other hand, uses depth resolved measurements of productivity, chlorophyll *a*, accessory pigments, phytoplankton species succession, DIC, DOC, NH_4 + NO_2, nitrification, settling losses, air-sea CO_2 flux, and nitrogen fixation.

The state of disagreement over the derivation and verification of plankton population model leads Falkowski *et al.* (1998) to state:

"Given the lack of mechanistic understanding of many of the feedbacks [between phytoplankton populations and global biogeochemical cycles], and the paucity of observational data on decadal to century time scales, it is presently beyond credible capability to quantitatively represent these processes within coupled three-dimensional ocean-atmosphere models. Hence, our ability to quantitatively predict ecosystem structure and biogeochemical feedbacks on the basis of forecasted climate-change scenarios is limited".

A consensus on the form and verification techniques of plankton models is unlikely to be found by using more elaborate empirical approximations and mathematical modelling techniques. The example of models of atmospheric and ocean circulation clearly demonstrates that a consensus can be achieved by processes-based, mechanistic models.

1.4.5 Plankton populations as a feedback on the climate system

The feedback between the marine biota and climate was highlighted by Denman *et al.* (1996) in the IPCC Climate Change 1995 report (Houghton *et al.*, 1996). As plankton grow they remove CO_2 from the surrounding fluid, whose concentration is coupled to atmospheric carbon. A component of the plankton sink out of the surface waters, and is no longer coupled to the atmospheric carbon. This loss is called the biological pump. The biological pump removes 16 Gt C (Falkowski *et al.*, 1998) from the surface ocean-atmosphere every year. Considering the atmospheric CO_2 is increasing by only 3 Gt C yr^{-1} (Houghton *et al.*, 1996), any changes in the size of the biological pump could have significant feedbacks on the global climate system.

Whether the size of the biological pump will change with increased atmospheric CO_2 concentration is a matter of considerable debate. A recent paper (Joos *et al.*, 1999) has attempted to estimate the change in the size of the biological pump with the changes predicted in sea-surface temperature (SST), ocean circulation, and marine biota. During the years 1980-1989, their model simulation showed 5.6 % reduction in oceanic uptake of CO_2 due to all three components, but a 7.5 % increase due to marine biota. However, their biological model (Marchal *et al.*, 1998) parameterises biological processes in terms of the shift in the equilibrium state of the CO_2(aq) - HCO_3^- - CO_3^{2-} system, and cannot therefore be expected to resolve the biological feedbacks such as changing species assemblage that may be important (Arrigo *et al.*, 1999).

Sarmiento *et al.* (1998) also simulated the response of the ocean carbon cycle to anthropogenic climate warming. In their model simulation, an increased in atmospheric temperatures resulted in an increase in rainfall, which reduced the density of surface

waters. Fresher surface waters are more stratified, reducing vertical mixing. Vertical mixing determines the rate of exchange of temperature, and, given constant nutrient to carbon ratios in the biota, carbon from the atmosphere. In their simulation, therefore, the biological pump provides a positive feedback on atmospheric CO_2 concentration - the more CO_2 in the atmosphere, the slower it is removed by the plankton, and the quicker it builds up.

Sarmiento *et al.* (1998), however, does not consider the effects of the changing structure of the marine biota on the ocean and the atmosphere. Such a change has been hypothesised by Arrigo *et al.* (1999). They found phytoplankton community structure in the Ross Sea also varied with stratification. Notably, in strongly stratified waters, the diatom species *Nitzschia subcurvata* dominated, while in weakly stratified waters, *Phaeocystis antarctica* dominated. *P. antarctica* draws more carbon molecules per nutrient molecule out the ocean, and therefore provides a greater sink of carbon from the atmosphere than *N. subcurvata*. Given that more stratified waters will result from a warmed atmosphere (Sarmiento *et al.*, 1998), Arrigo *et al.* (1999) concludes that there will be a further 36 % reduction in CO_2 drawdown than predicted by ocean circulation changes. Arrigo *et al.* (1999) highlights the need to include a process-based description of marine biota in a global climate model.

Present models of plankton population dynamics are not sufficiently advanced to resolve the positive feedback between atmospheric CO_2 and plankton populations that Arrigo *et al.* (1999) proposes.

1.4.6 Summary of the state of global biogeochemical modelling

The conclusion of IPCC scientists in 1995 regarding global climate change were based on simulations of the physical processes (atmospheric and ocean circulation) impacting on climate only (Houghton *et al.*, 1996). Biogeochemical cycles, which have potential feedbacks with the climate, were not included. Since 1995, a large number of global biogeochemical models have been developed (some of which are discussed above). In

particular, components of the global biogeochemical cycles with the potential to directly alter global climate, such as atmospheric CO_2, methane and sulfur, have received much attention. Indirect effects like changing ocean circulation, sea-ice, cloud formation, vegetation cover and marine plankton productivity have also been modelled intensively. Many of these processes feedback on a number of different components in the global biogeochemical system. To improve forecasts of biogeochemical cycles, and therefore global climate change, process-based, predictive models of all significant feedbacks on the climate system must be constructed, and run as a globally coupled model.

1.5 Summary

Plankton are a major component of global biogeochemical cycles, and impact significantly on global climate. With the increased concern over global climate change, there is a need for a predictive model of plankton population dynamics. This is not meet by the presently available empirical models. Mechanistic models have displayed predictive capabilities beyond that achieved by empirical models in modelling of atmospheric and ocean circulation, and have recently been applied to other components of the global biogeochemical system. This thesis, through primarily theoretical considerations, will work towards a verified mechanistic model of plankton population dynamics.

Chapter 2

Towards a mechanistic model of plankton population dynamics

Throw up a handful of feathers, and all must fall to the ground according to definite laws; but how simple is this problem compared to the action and reaction of the innumerable plants and animals which have determined, in the course of centuries, the proportional numbers and kinds.

Charles Darwin, The Origin of Species

2.1 Abstract

A plankton population model is developed from literature studies with mechanistic descriptions of interactions of individual plankton cells. Interactions considered include diffusion and convection of nutrients to phytoplankton cell surfaces, light capture by phytoplankton pigment assemblages, sinking rates of phytoplankton cells, and encounter rates of predators and prey. Mechanistic formulations are based on individual species characteristics, obtained from measurements in laboratory experiments, and are functions of local fluid properties such as small-scale turbulence and viscosity. Phytoplankton growth is modelled by analogy to chemical kinetics, and is a function of intracellular nutrient and energy reserves. Results from laboratory experiments on single species populations found in the literature are used to test the applicability of the functional forms for quantifying interactions of populations of common marine plankton species. These

functional forms are then used to construct a system of equations describing plankton population dynamics. Simulations of plankton population dynamics at environmental conditions similar to the oceanic mixed layer at Bermuda (32°N, 65°W) and Ocean Weather Station (OWS) 'India' (59°N, 19°W) are performed, and compared to existing models (Fasham *et al.*, 1990; Fasham, 1993) and field data sets.

2.2 Introduction

Plankton population modelling has traditionally been based on simple empirical models (Steele and Henderson, 1981), without detailed theoretical consideration of the underlying physical processes involved. Empirical models usually capture the dynamics of a few chosen phenomena, such as the spring bloom (Taylor and Stephens, 1993), predator-prey interactions (Edwards and Brindley, 1996) or recycling of nitrate (Fasham *et al.*, 1990). However, empirical models have been unable to describe the range of phenomena necessary to become useful tools for forecasting geochemical quantities and biological populations in natural ecosystems (Botsford *et al.*, 1997). Recently, some global climate models have achieved greater accuracy in forecasting, by employing explicit physical laws, rather than empirical relationships based on historical data sets (Kerr, 1998; Stockdale *et al.*, 1998). Could such a theoretical approach improve the forecasting of biological populations?

A large number of theoretically derived, and empirically tested, mechanistic and semi-empirical functional forms (Table 1.1 defines the terms mechanistic, semi-empirical, empirical and heuristic) relevant to modelling plankton populations are described in the literature (Pasciak and Gavis, 1975; Kirk, 1975a; Gerritsen and Strickler, 1977; Brock, 1981; Mellor and Yamada, 1982; Rothschild and Osborn, 1988; Blanchard, 1989; Jackson, 1995; Blake and Otto, 1996; Karp-Boss *et al.*, 1996; Pahlow *et al.*, 1997). In the last decade, modellers have used mechanistic light (Fasham *et al.*, 1990), semi-empirical aggregation (Jackson and Lochmann, 1992) and mixing (Sharples and Tett, 1994) functions to describe environmental forcing in plankton population models. By considering an isolated mechanism in detail, these studies have given ecologists an insight into what

the affects of a particular mechanism may have on population dynamics. However, so far modellers have not attempted to incorporate mechanistic functional forms into the biological processes in a plankton population model.

The major obstacle to incorporating mechanistic functional forms into plankton population models is the quantification of phytoplankton and zooplankton in terms of total biomass of phytoplankton and zooplankton species respectively. By using a plankton population model structure based on populations of individual plankton cells, mechanistic interactions can be considered, with constants derived from controlled laboratory experiments. Laboratory-determined constants typically have greater precision than field measurements, and their use in mechanistic functional forms allows explicit quantification of the effects of environmental variables, such as small-scale turbulence and viscosity, on population dynamics. The resulting model should provide a general description of plankton population dynamics in a variety of environments.

The aim of this chapter is to develop, as far as possible, a plankton population model based on theoretically derived functional forms and laboratory-determined constants. This has necessitated functional forms describing interactions of individual plankton cells. The mechanistic functional forms are then compared to the literature describing the dynamics of populations of single plankton species in the laboratory environment. These comparisons evaluate the usefulness of functional forms, based on individual cells, in describing population dynamics. The model equations are then combined and simulations of plankton population dynamics in the oceanic mixed layer at Bermuda and OWS 'India' are performed, and compared to other models (Fasham *et al.*, 1990; Fasham, 1993) and field data sets.

2.3 The model

2.3.1 Model structure

The model structure is based on a series of ordinary differential equations (ODEs) describing the interactions of individual plankton species. With the processes described

in words, the ODEs are:

$$\frac{dN_i}{dt} = \pm \text{mixing} - \text{nutrient uptake} + \text{nutrient recycled} \quad (2.1)$$

$$\frac{dQ_{i,j}}{dt} = \pm \text{mixing} + \text{nutrient uptake} - \text{nutrient for growth} \quad (2.2)$$

$$\frac{dq_j}{dt} = \pm \text{mixing} - \text{light captured} - \text{energy for growth} \quad (2.3)$$

$$\frac{dP_j}{dt} = \pm \text{mixing} + \text{growth} - \text{sinking} - \text{grazing loss} \quad (2.4)$$

$$\frac{dH_k}{dt} = \pm \text{mixing} + \text{grazing uptake} - \text{sinking} \quad (2.5)$$

where N_i is the concentration of nutrient species i in the extracellular fluid [mol m^{-3}]; $Q_{i,j}$ is the concentration of nutrient species i stored in phytoplankton species j [mol $cell^{-1}$]; q_j is the energy in photons stored in phytoplankton species j [mol $cell^{-1}$]; P_j is the concentration of phytoplankton species j [mol m^{-3}] and H_k is the concentration of herbivore species k [mol m^{-3}].

The model structure above deals with the growth of phytoplankton populations differently to traditional treatments including internal nutrient pools (Droop, 1974). Unlike Droop (1974), the internal storage of nutrients, Q, and energy, q, are quantified as a concentration stored (i.e. taken into the cell, but as yet not combined with other elements to create organic matter). The total amount of nutrient within a cell is given by that which is stored, Q, plus that which make up the cell itself. Also unlike Droop (1974), the uptake of all nutrients into storage, and their use for growth, are coupled (i.e. a change in the energy uptake alone, will change the uptake of other nutrients). The rest of this section derives each term in Eqs. 2.1 - 2.5. For a simpler 'case study' approach to understanding the growth model presented, see Section 3.3.1.

2.3.2 Nutrient uptake by phytoplankton

The most common functional form chosen by plankton population modellers to describe nutrient uptake is a rectangular hyperbola (Dugdale, 1967):

$$J = \frac{aC_b}{b + C_b} \tag{2.6}$$

where C_b is the nutrient concentration in the bulk fluid [mol m^{-3}] [1] ; b is the extracellular nutrient concentration at half the maximum uptake rate [mol m^{-3}] and a is the maximum nutrient uptake rate to a cell [mol cell s^{-1}]. However, in addition to extracellular nutrient concentration, nutrient uptake by phytoplankton is also dependent on extracellular physical conditions, such as fluid motion, molecular diffusivity of the nutrient and phytoplankton shape (Pasciak and Gavis, 1975), and intracellular conditions, such as internal nutrient concentration and rates of biochemical reactions (Droop, 1968). To choose a more theoretical functional form for nutrient uptake by phytoplankton, the equations describing extracellular and intracellular uptake processes need to be considered separately, and then solved simultaneously.

Extracellular processes. Nutrient uptake to a single phytoplankton cell, J [mol cell^{-1} s^{-1}], can be determined mechanistically by:

$$J = \psi D \left(C_b - C_w\right) \tag{2.7}$$

where ψ is the diffusion shape factor [m] (Table 2.1); D is the molecular diffusivity of the nutrient [m^2 s^{-1}] (Table A.1); C_b is the average extracellular nutrient concentration [mol m^{-3}] and C_w is the concentration at the wall of the cell [mol m^{-3}]. For the derivation of Eq. 2.7 and ψ for a variety of shapes, see Appendix B. A semi-empirical correction to Eq. 2.7, to account for fluid motion around the cell, is provided by the Sherwood number, Sh [dimensionless]. Sh is a relative measure of the additional flux of nutrient

[1] The symbol for extracellular concentration used during the derivation of nutrient uptake terms is C_b to conform with the notation of the nutrient uptake literature referenced. Once the final form has been reached, it is replaced with the symbol N_i to conform with the state variable notation used in many plankton population models.

due to the motion of fluid surrounding the cell:

$$Sh = \frac{\text{total flux}}{\text{diffusive flux}} \tag{2.8}$$

Sh is important for a variety of engineering applications, and has been determined by a combination of theoretical and empirical methods for a variety of shapes and flow conditions (Table 2.2). So Eq. 2.7 becomes the semi-empirical formula:

$$J = \psi DSh\,(C_b - C_w) \tag{2.9}$$

Intracellular processes. The dependence of uptake on intracellular nutrient concentration has also been recognised, and the concept of an internal cell quota, introduced (Droop, 1968). One heuristic formulation used to describe the dependence of uptake on internal nutrient concentration is (Sharples and Tett, 1994):

$$J = \Theta\left(\frac{Q^{max} - Q}{Q^{max}}\right) \tag{2.10}$$

where Θ is a function of other internal and external processes affecting uptake. However, it is clear that internal nutrient concentration only directly affects the intracellular processes, which themselves must be given a functional form. A common heuristic choice for describing internal cell processes involved in uptake is the rectangular hyperbola (Eq. 2.6), primarily because of its use to mechanistically describe enzyme kinetics (Kuchel and Ralston, 1988), which is often implicated in intracellular uptake processes. This takes the form:

$$J = \frac{VC_w}{K + C_w} \tag{2.11}$$

where V is the maximum rate of intracellular uptake processes [mol m^{-3}], and K is the wall concentration at half the maximum uptake rate of intracellular processes [mol m^{-3}]. Since it is probably the rate of reaction, rather than maximum uptake potential of the internal cell processes, which is a function of internal nutrient concentration, it is

Shape	Diffusion shape factor ψ [m]
Sphere	$4\pi r_1$
Oblate spheroid	
$r_1 = r_2 \;\; r_2 > r_3$	$4\pi r_1 e \left(\frac{1}{\tan^{-1} \frac{e}{\sqrt{1-e^2}}} \right)$ where $e = \sqrt{1 - \left(\frac{r_3}{r_1}\right)^2}$
Prolate spheroid	
$r_1 > r_2 \;\; r_2 = r_3$	$8\pi r_1 e \left(\frac{1}{\ln \frac{1+e}{1-e}} \right)$ where $e = \sqrt{1 - \left(\frac{r_3}{r_1}\right)^2}$
General ellipsoid	$\frac{I_1}{I_2}$
$r_1 > r_2 > r_3$	$I_1 = 8 \int_B^C \int_0^B \frac{(\theta^2 - \lambda^2)\, d\lambda d\theta}{\sqrt{(\theta^2 - B^2)\,(C^2 - \theta^2)\,(B^2 - \lambda^2)\,(C^2 - \lambda^2)}}$
	$I_2 = \int_{r_1}^{\infty} \frac{1}{\sqrt{(x^2 - B^2)\,(x^2 - C^2)}} dx$
	$B = \sqrt{r_1^2 - r_2^2},\; C = \sqrt{r_1^2 - r_3^2}$
Cube edge $= L_1$	$0.656(4\pi L_1)$
Touching spheres	$(2\, \ln 2)(4\pi r_1)$
Cylinder	
$0 \le \frac{L}{d} \le 8$	$\left(8 + 6.95 \left(\frac{L}{d}\right)^{0.76}\right) r_1$
Thin rectangular plate $L_1 \ge L_2$	$\frac{2\pi L_1}{\ln\left(\frac{4L_1}{L_2}\right)}$
Needle-like bodies $L_1 \ge 10 L_2$	$\approx \frac{2\pi L}{\ln(\frac{4L_1}{L_2}) - 1} \pm 5\%$

Table 2.1: Diffusion shape factor ψ [m]. ψ is obtained by solving the Laplace equation, $\nabla^2 C = 0$, and the flux at the surface of the cell, $J = \psi D \triangle C$ (Eq. 2.9), where D = molecular diffusivity and $\triangle C$ = concentration difference between the average fluid and the cell wall; $r_{1,2,3}$ are orthogonal radii [m]; ψ for an arbitrary shape is $\ge \psi$ of a sphere of same volume, and $\le$ to ψ of a shape which circumscribes it (Clift *et al.*, 1978). References: sphere - Lazier and Mann (1989), spheroids - Pasciak and Gavis (1975), general ellipsoid - Wolf-Gladrow and Riebesell (1997), others - Clift *et al.* (1978).

Flow Regime	Conditions of flow	Sphere	Other shapes
Uniform flow	fluid motion due to cell swimming only $\epsilon = 0$	$Sh = 0.5\left(1 + \sqrt[3]{1+2Pe}\right)$ $Pe = \frac{U_{rel}\, r_1}{D}$	$Sh = 1 + 0.5 Sh_0 Pe + 0.5 Sh_0 \mathrm{f} Pe^2 \ln Pe$ $Sh_0 = \frac{\psi_{shape}}{\psi_{sphere,=SA}}$, $\mathrm{f} = \frac{C_D}{6\pi\mu\ r_c}$, $Pe = \frac{r_c U_{rel}}{D}$
Shear flow	Turbulent induced shear $r_1 < K_D$ $K_D = \sqrt[4]{\frac{\upsilon D^2}{\epsilon}}$	$Pe < 0.1\ \ Sh = 1 + 0.23 Pe^{0.5}$ $0.1 < Pe < 100\ \ Sh = 1.002 + 0.21 Pe^{0.5}$ $Pe > 100\ \ Sh = 0.67 Pe^{1/3}$ $Pe = \frac{E r_1^2}{D}\ \ E = 0.71\left(\frac{\epsilon}{\upsilon}\right)^{1/2}$	Prolate sp, $0.1 < Pe < 10$ $Sh = 1 + 0.363\sqrt{\frac{Pe}{r_a + 1}}$ $+0.115\frac{r_a - 1}{r_a + 1} Pe^{1/3}$ $r_a = \frac{r_1}{r_3}$, $Pe = \frac{E r_a r_3^2}{D}$
Turbulent flow	Turbulent induced shear $r_1 > K_D$ $K_D = \sqrt[4]{\frac{\upsilon D^2}{\epsilon}}$	$Sh = \alpha\left[A + B\right]^{1/6}$ $A = 2.25\left(\frac{r_1 U_{rel}}{D}\right)^2$ $B = 5.1 S^2\left(\frac{r_1^2}{D}\left(\frac{\epsilon}{\upsilon}\right)^{0.5}\right)^2$ $0.495 < S < 0.545$	no literature studies

Table 2.2: Sherwood numbers, Sh [dimensionless], for spheres and other shapes (Karp-Boss *et al.*, 1996; Pahlow *et al.*, 1997; Brenner, 1963). r_1, r_2, r_3 are orthogonal radii [m]; r_c = characteristic radii [m], used for non-spherical shapes, and taken to be the radius of a sphere with the same surface area as the non-spherical shape; ψ = diffusion shape factor [m] (Table 2.1); f = dimensionless drag; C_D = drag coefficient (Table 2.4); μ = dynamic viscosity [kg s^{-1} m^{-1}]; K_D = Kolomogorov length scale for diffusion [m]; υ = kinematic viscosity [m^2 s^{-1}]; E = shear rate [s^{-1}]; ϵ = mean rate of dissipation of turbulent kinetic energy [m^2 s^{-3}]; D = molecular diffusivity of transferred chemical species [m^{2}s^{-1}]; Pe = Peclet number = $\frac{r_1^2 \epsilon^{0.5}}{D\upsilon^{0.5}}$; Re = Reynolds number = $\frac{r_1^2 \epsilon^{0.5}}{\upsilon^{1.5}}$ U_{rel} = velocity of cell relative to fluid as a result of sinking and swimming from Eq. 2.42 [m s^{-1}]. For uniform motion in a shear flow, it has been shown for a cylinder at low Re that $Sh = Sh_{shear} + Sh_{uniform}$ (Dabros *et al.*, 1984), and this is assumed true for all shapes. For combinations of shapes and flow regimes not covered, Sh is given by the Sh of a sphere of the same equivalent surface area as the non-spherical shape by substuting r_c for r_1 in the 2nd column.

assumed that K in Eq. 2.11 is the following function of Q:

$$K = K_o \left(\frac{Q^{max}}{Q^{max} - Q} \right) \tag{2.12}$$

where K_o is the value of K at $Q = 0$. This form was chosen heuristically, based on the simplest function that met the criteria that K approaches infinity at $Q = Q^{max}$, and $K = K_o$ at $Q = 0$. The rate of uptake due to intracellular processes can now be given by:

$$J = \frac{VC_w}{K_o \frac{Q^{max}}{Q^{max} - Q} + C_w} \tag{2.13}$$

Enzyme-mediated uptake has been identified on the surface of cells (Dyhrman and Palenik, 1997). The reaction rate of such enzyme reactions will be dependent on concentration at the cell wall, C_w, and their activity, K, on the internal nutrient concentration, Q. In the formulation of nutrient uptake presented in this chapter, the effects of surface enzyme reactions are included in the internal processes. In fact, Eq. 2.13 approximates a series of biochemical reactions and transport processes, from those on the surface, through the cell membrane, to the point of storage within the cell.

Uptake rate, incorporating both extracellular and intracellular processes. Up to this point both extracellular and intracellular uptake rates have been calculated independently as a function of the concentration of the nutrient at the surface of the cell, C_w. There is no direct way of determining C_w. However, by mass balance, extracellular and intracellular uptake rates must be equal, so by solving simultaneous equations (Eqs. 2.9 and 2.13) (Hill and Whittingham, 1955; Pasciak and Gavis, 1975; Mierle, 1985b) the uptake rate as a function of extracellular nutrient concentration, fluid motion, phytoplankton shape, internal nutrient concentration, and enzyme saturation rate and maximum activity is given by solving the quadratic:

$$\frac{J^2}{\psi DSh} - \left(K_o \left(\frac{Q^{max}}{Q^{max} - Q} \right) + C_b + \frac{V}{\psi DSh} \right) J + VC_b = 0 \tag{2.14}$$

Eq. 2.14 is impractical to use for most species, since almost all literature values for K_o and V are determined using Eq. 2.6 rather than Eq. 2.11. Furthermore, there is experimental evidence (Morel, 1987) which contradicts the assumption that V is independent of Q, and K is a function of Q. However, an approximation (see below) of Eq. 2.14 is achieved by considering the physiological state of the cell directly in Eq. 2.9 using Eq. 2.10:

$$J_{i,j} = \psi_j D_i Sh_{i,j} N_i \left(\frac{Q_{i,j}^{max} - Q_{i,j}}{Q_{i,j}^{max}} \right) = \left(\frac{dQ_{i,j}}{dt} \right)_{uptake} \tag{2.15}$$

where $J_{i,j}$ is the uptake rate of nutrient i to phytoplankton species j [mol cell^{-1} s^{-1}]; ψ_j is the diffusion shape factor for phytoplankton species j [m] (Table 2.1); D_i is the molecular diffusivity of chemical species i [m^2 s^{-1}] (Table 2.13); N_i is the concentration of nutrient species i in the extracellular fluid [mol m^{-3}]; $Sh_{i,j}$ is the Sherwood number of nutrient i advected towards phytoplankton species j [-](Table 2.2); $Q_{i,j}$ is the concentration of nutrient species i stored in phytoplankton species j [mol cell^{-1}] and $Q_{i,j}^{max}$ is the maximum concentration of nutrient species i stored in phytoplankton species j [mol cell^{-1}] (Table 2.11). The expression $\left(\frac{Q_{i,j}^{max} - Q_{i,j}}{Q_{i,j}^{max}} \right)$ has been commonly used by ecological modellers (Sharples and Tett, 1994). It a very simple way to introduce a dependence of uptake on cell physiology. Since Eq. 2.15 is much simpler than Eq. 2.14, it is more suitable to an ecosystem modelling exercise such as presented and would be more readily accepted by experimentalists. Eq. 2.15 also fits in well with the ideas presented later that consider growth as an interaction of rates.

2.3.3 Light capture

Phytoplankton absorb incident light as a function of wavelength, pigment concentrations, cell geometry (Kirk, 1994) and the presence of other attenuating components of the water column. The spectrum of absorption coefficients for the pigment assemblage that is characteristic of each phytoplankton species is determined, and then the absorption characteristics of a phytoplankton cell can be calculated depending on the pathlength of light through the cell as a function of cell size, shape and orientation. For cells evenly distributed through a well-mixed layer, light capture by an individual

cell will be a function of the incident light on the top of the layer, and the absorption coefficients of all attenuating elements of the medium.

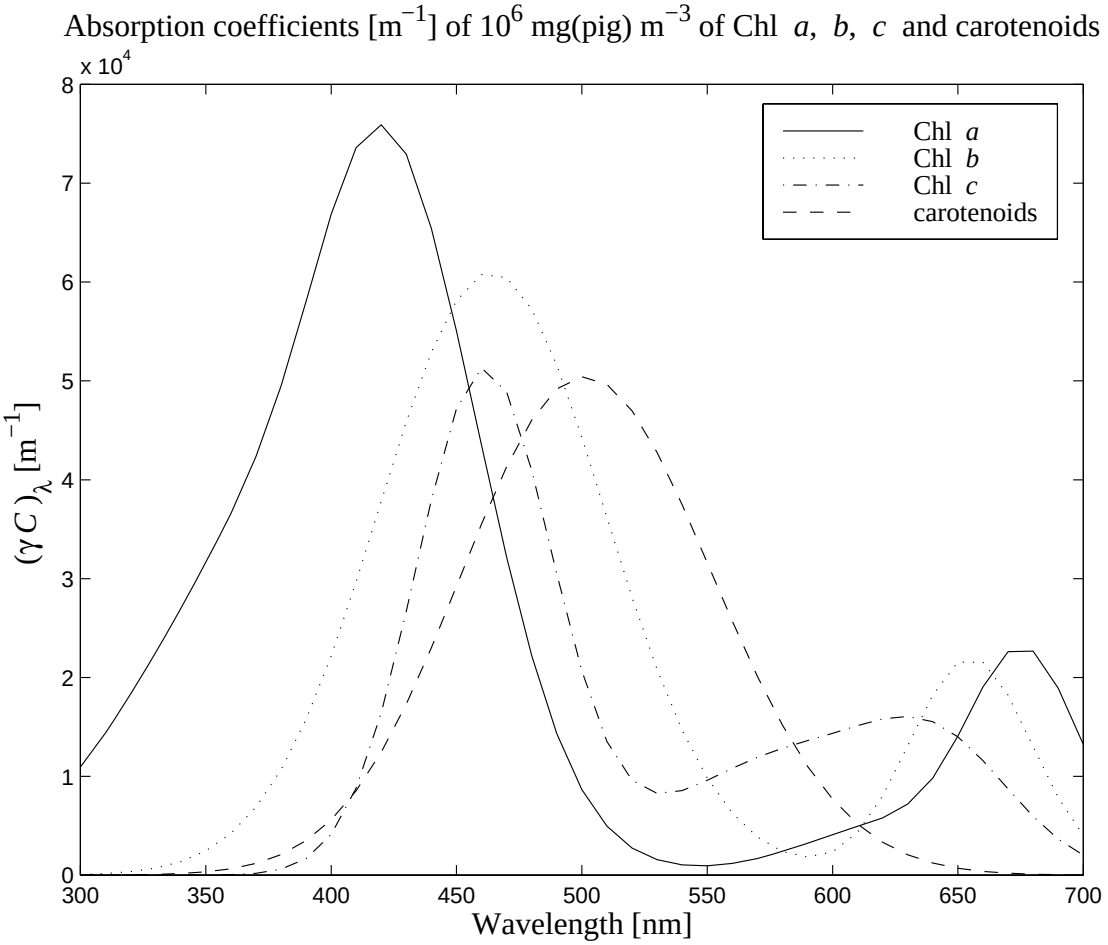

Figure 2.1: Absorption coefficients, $\overline{\gamma C}_\lambda$ [m^{-1}], of 1×10^6 mg(pig) m^{-3} of Chl *a*, Chl *b*, Chl *c* and carotenoids as approximated by Gaussian curves (Hoepffner and Sathyendranath, 1991). Total absorbance is calculated as the sum of the absorption coefficients due to each pigment at each wavelength (Eq. 2.16). The coefficients for the Gaussian curves are given Table A.2

The spectrum of absorption coefficients for a pigment assemblage can be empirically determined by approximating the absorption bands of each pigment as a Gaussian curve (Figure 2.1), and summing the combined absorption of all bands at each wavelength (Hoepffner and Sathyendranath, 1991). The absorption coefficient of phytoplankton

species j at a wavelength λ [nm] due to pigments $\xi = 1, ..., \Upsilon$, $\left(\overline{\gamma C}\right)_{\lambda,j}$[m^{-1}], is given by:

$$\left(\overline{\gamma C}\right)_{\lambda,j} = \sum_{\xi=1}^{\Upsilon} \gamma_\xi C_{\xi,j} \exp\left(-\frac{(\lambda - \lambda_\xi)^2}{2W_\xi^2}\right) \tag{2.16}$$

where $C_{\xi,j}$ is the concentration of pigment ξ, in species j [mg(pig) m^{-3}]; γ_ξ is the peak specific absorption coefficient of pigment ξ [m^2 mg(pig) $^{-1}$]; λ_ξ is the wavelength of maximum absorption for pigment ξ [nm] and W_ξ is the halfwidth of the ξth Gaussian band [nm].

The pathlength (and therefore light attenuated) of a light beam through a cell is a function of cell shape, and orientation with respect to the direction of the beam propagation (Figure 2.2). The light attenuated by one cell of phytoplankton species j at wavelength λ, $(I_{j,\lambda})_{light\ attenuated}$, is given by (Kirk, 1975a):

$$(I_{j,\lambda})_{light\ attenuated} = a_{j,\lambda} A_j \, (I_\lambda)_{incident\ on\ j} \tag{2.17}$$

where $(I_\lambda)_{incident\ on\ j}$ is the incident radiation at wavelength λ on cell j [mol(quanta) m^{-2} s^{-1} nm^{-1}]; A_j is the projected area of a cell of species j on a plane perpendicular to incident light [m^2]; and $a_{j,\lambda}$ is the fraction of light absorbed by a cell of species j, at wavelength λ [-], and is a function of pathlength and $\left(\overline{\gamma C}\right)_{j,\lambda}$. The product, $a_{j,\lambda}A_j$ is the absorption cross-section of cell j at wavelength λ [m^2]. Since both $a_{j,\lambda}$ and A_j vary with shape and orientation, it is simplest to determine the product, $\overline{aA}_{j,\lambda}$ for different cells and orientations. $\overline{aA}_{j,\lambda}$ can be measured in the laboratory for a particular species adapted to a particular light regime (Lewis *et al.*, 1988), or solved geometrically as a function of shape, pigment concentration, and orientation. For the geometric solution, small phytoplankton cells in a turbulent environment cannot control their orientation, so a random orientation with respect to the incident light is assumed. $\overline{aA}_{j,\lambda}$ is determined by considering the light attenuated in each infinitesimally small area of the projected area perpendicular to the beam (in the XZ plane in Figure 2.2) for all orientations (θ, φ in Figure 2.2) (Table 2.3). Geometric solution of $\overline{aA}_{j,\lambda}$, allows theoretical investigation

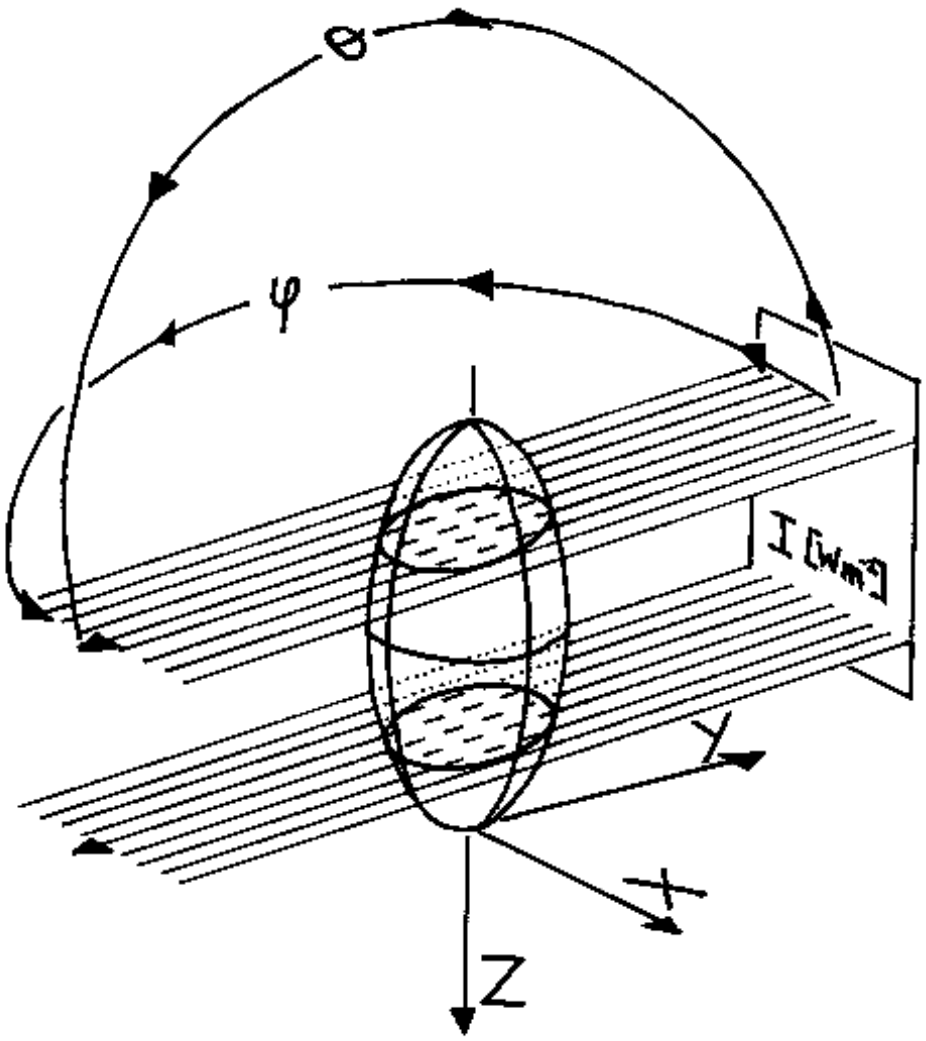

Figure 2.2: The pathlength of a two planes of light beams through a prolate spheroid. (—, $\cdots$) light beam travelling through fluid, in view and behind the spheroid respectively; (- - -) light beam travelling through the cell. Calculation of the light absorbed by a randomly oriented shape requires determination of the pathlength of light through the cell for all orientations (θ, φ) to the light field, and at each infinitesimally small area of the projected area perpendicular to the beam (in the XZ plane) (Kirk, 1975a,b, 1976). In the case of a surface of revolution such as the above prolate spheroid, integration with respect to angle through which the shape has been revolved (φ above) is not required (Table 2.3).

Shape	Absorption cross-section for random orientation, $\overline{aA}$ [m^2]
Sphere	$\pi r_1^2 \left(1 - \dfrac{2\left(1 - \left(1 + 2\overline{\gamma C} r_1\right) e^{-2\overline{\gamma C} r_1}\right)}{\left(2\overline{\gamma C} r_1\right)^2}\right)$
Spheroid	$\displaystyle\int_0^{\pi/2} \pi L v \cos\theta \left(1 - \frac{4}{\pi L v} \int_0^s \int_0^L e^{-2\overline{\gamma C} R \sqrt{1 - \frac{Z^2}{s^2}}} dX dZ\right) d\theta$
$r_1 \geq r_2 \geq r_3$	$L = \sqrt{w^2 \cos^2\theta + v^2 \sin^2\theta}$
	$s = v\sqrt{1 - \dfrac{X^2}{L^2}}$
	$R = \dfrac{wv\sqrt{v^2 + w^2 \cot^2\theta - X^2 \csc^2\theta}}{\sin\theta\left(v^2 + w^2 \cot^2\theta\right)}$
	prolate spheroid $r_1 = w, \quad r_2 = r_3 = v$
	oblate spheroid $r_1 = r_2 = v, \quad r_3 = w$
Cylinder	$\displaystyle\int_0^{\pi/2} 2 r_1 h \cos^2\theta \left(1 - \frac{1}{r_1} \int_0^{r_1} e^{-2\overline{\gamma C} r_1 \sec\theta \sqrt{\left(1 - \frac{Z^2}{r_1^2}\right)}} dZ\right) d\theta$

Table 2.3: Absorption cross-section of randomly orientated phytoplankton cells of a given shape (Kirk, 1976, 1975b). A = projected area of the cell perpendicular to the light beam [m^2]; a = fraction of light absorbed by the cell [dimensionless]; γ = pigment specific absorbance [m^2 mg(pig)$^{-1}$]; C = pigment concentration [mg(pig) m^{-3}]; $\overline{\gamma C}$ = the absorption coefficient of all pigments [m^{-1}]; $\overline{aA}$ = average absorption cross-section for a randomly orientated cell [m^2]; $r_{1,2,3}$ = orthogonal radii of sphere, ellipsoid or cylinder [m]; h = height of cylinder [m]. For a weakly absorbing particle of any shape, $\overline{aA} = \overline{\gamma C} V$, where V = volume [m^3].

of the effect of varying pigment concentrations and shape on light capture.

The incident light on cell j, $I_{incident\ on\ j}$, required in Eq. 2.17 is a function of incident light on the top (at depth z [m]) of the medium, $I_{z,\lambda}$ [mol(quanta m^{-2} s^{-1} nm^{-1}], the effect of all attenuating components in the medium, and the pathlength through the medium to reach cell j. To solve for $(I_{j,\lambda})_{light\ attenuated}$ a well-mixed medium in which all attenuating components are evenly distributed (which for a cell means it has equal probability of being at any depth in the medium) is assumed. Beer's law (Kirk, 1975a) can now be used to calculate the radiation at the bottom (depth $z - M$ [m]) of the medium, $I_{z-M,\lambda}$ [mol(quanta) m^{-2} s^{-1} nm^{-1}]:

$$I_{z-M,\lambda} = I_{z,\lambda} e^{(-\sum_{x=1}^{X} k_{x,\lambda}) M_{path,\lambda}} \tag{2.18}$$

where $I_{z-M,\lambda}$ is the radiation at depth $z - M$ [m] after travelling M_{path} [m] through the medium, and $\sum_{x=1}^{X} k$ is the sum of all (X in number) absorbing components of the medium. For water containing humic substances and phytoplankton species, $P_j, j = 1, ..., p$, Eq. 2.18 becomes:

$$I_{z-M,\lambda} = I_{z,\lambda} e^{-\left(k_{w,\lambda} + k_{g,\lambda} + \sum_{j=1}^{p} A_v P_j \overline{aA}_{j,\lambda}\right) M_{path,\lambda}} \tag{2.19}$$

where $k_{w,\lambda}$ is the partial attenuation coefficient due to pure water at wavelength λ [m^{-1}] (Figure 2.3); $k_{g,\lambda}$ is the partial attenuation coefficient due to the presence of gilvin or humic substances at wavelength λ [m^{-1}] (Figure 2.3); and $A_v P_j\ \overline{aA}_{j,\lambda}$ is the partial attenuation of species j at wavelength λ [m^{-1}] (Kirk, 1975a); Avogadro constant, $A_v = 6.02214 \times 10^{23}$ mol^{-1} (Atkins, 1994); p is the number of phytoplankton species [-]; P_j is the concentration of phytoplankton species j [mol m^{-3}] and $M_{path,\lambda}$ is the average pathlength of a photon through a layer at wavelength λ [m]. If there is no scattering or backscattering of light within the medium, $M_{path,\lambda} = M \sec\theta$, where θ is the azimuth angle [rad], and M_{path} is independent of wavelength.

To determine the fraction of light absorbed by each attenuating component of the medium, we rewrite Beer's law (Eq. 2.18) as:

$$I_{z-M,\lambda} = I_{z,\lambda} \prod_{x=1}^{X} e^{-k_{x,\lambda}} \tag{2.20}$$

In a well-mixed medium, with attenuating components spread evenly throughout the medium, the fraction attenuated by one component, $x = \zeta$, out of X components is given by:

$$\frac{e^{-k_{\zeta,\lambda}}}{\sum_{x=1}^{X} e^{-k_{x,\lambda}}} = \frac{-k_{\zeta,\lambda}}{\sum_{x=1}^{X} -k_{x,\lambda}} \tag{2.21}$$

Combining Eqs. 2.19 and 2.21 the light attenuated by one cell of species j in a layer with a top depth of z, and bottom depth $z - M$, is given by:

$$(I_{j,\lambda})_{light\ attenuated} = \frac{A_v P_j \overline{aA}_{j,\lambda}}{k_{w,\lambda} + k_{g,\lambda} + \sum_{j\prime=1}^{p} A_v P_{j\prime} \overline{aA}_{j\prime,\lambda}} \frac{(I_{z,\lambda} - I_{z-M,\lambda})}{A_v P_j M} \tag{2.22}$$

Light scattering has the potential to change the trajectory and pathlength, $M_{path,\lambda}$, of each photon. The effect of scattering on the light field is a function of wavelength, angle of incidence into the layer, and the ratio of scattering coefficients and absorption coefficients (Kirk, 1994). Monte Carlo techniques (Kirk, 1981) can be used to track a large number of individual photons, to determine the average effect of scattering on $M_{path,\lambda}$. It has been found (Kirk, 1984) that the average effect of scattering on the pathlength of a photon at wavelength λ, $M_{path,\lambda}$, can be approximated for a water body with a given ratio of the total scattering coefficient, $b_{T,\lambda}$ [m^{-1}], to total absorption coefficient, $a_{T,\lambda}$ [m^{-1}], by:

$$M_{path,\lambda} = (M \sec\theta) \sqrt{1 + G(\theta) \frac{b_{T,\lambda}}{a_{T,\lambda}}} \tag{2.23}$$

where

$$G(\theta) = g_1 \cos\theta - g_2 \tag{2.24}$$

$$a_{T,\lambda} = k_{w,\lambda} + k_{g,\lambda} + \sum_{j=1}^{p} A_v P_j \overline{aA}_{j,\lambda} \tag{2.25}$$

$$b_{T,\lambda} = b_{w,\lambda} + \sum_{j=1}^{p} b_{j,\lambda} A_v C_{\text{Chl } a,j} V_j P_j \tag{2.26}$$

G, g_1 and g_2 are dimensionless scattering constants characteristic of a water body (Table 2.13); $b_{w,\lambda}$ is the scattering coefficient of sea water and its non-phytoplankton constituents at wavelength λ [m^{-1}] (Table 2.13); $b_{j,\lambda}$ is the chlorophyll a specific scattering coefficient of cell j at wavelength λ [m^2 mg(Chl a)$^{-1}$] (Table 2.7); V_j is the volume of cell j [m^3] (Table 2.8); and $C_{\text{Chl } a,j}$ is the concentration of chlorophyll a in phytoplankton species j [mol m^{-3}] (Table 2.7).

Experiments (Figure 2.4) show that high levels of radiation reduce the efficiency of use of light attenuated by pigments. This has been heuristically modelled using a changing internal cell reservoir of energy, q_j, similar to that used for nutrients (Eq. 2.10) such that:

$$I_{light\ captured} = I_{attenuated} \left(\frac{q_j^{max} - q_j}{q_j^{max}} \right) \tag{2.27}$$

where q_j^{max} is the maximum energy in photons stored in phytoplankton species j [mol cell^{-1}]. Although photochemical energy is not stored as photons, but rather as ATP and NADPH, energy storage will still be counted in photons for simplicity. Considering all photons between 300 nm and 700 nm to be equivalent in photosynthetic reactions, the change in internal reservoir of energy of species j due to light capture is given by:

$$\left(\frac{dq_j}{dt} \right)_{light\ capture} = \int_{PAR} \frac{\overline{aA}_{j,\lambda} \left(I_{z,\lambda} - I_{z-M,\lambda} \right)}{k_{w,\lambda} + k_{g,\lambda} + \sum_{j\prime=1}^{p} A_v P_{j\prime}\, \overline{aA}_{j\prime,\lambda}} \frac{1}{M} \left(\frac{q_j^{max} - q_j}{q_j^{max}} \right) d\lambda \tag{2.28}$$

2.3.4 Growth rate of photosynthetic cells

The growth rate of photosynthetic cells is modelled using methodology employed in the study of chemical kinetics. Describing chemical reaction dynamics mechanistically using quantum theory is a major new field (Clary, 1998), but is not sufficiently developed to describe complex biochemical reactions. As a result, empirical chemical kinetics methodology must be used. The reproduction of phytoplankton of species j,

P_j, is assumed to be fully described by a simple chemical reaction: the reactants are a phytoplankton cell (including the molecules and energy it took to make it), and the molecules and energy required to make another phytoplankton cell; the products are two phytoplankton cells less inefficiencies, waste molecules and heat. The balanced chemical reaction becomes:

$$\overbrace{P_j + \left(\underbrace{\sum_{i=1}^{n} m_{i,j} Q_{i,j}}_{molecules} + \underbrace{(m_{I,j} q_j)}_{energy} \right)}^{1 \text{ phytoplankton+molecules and energy}} \longrightarrow \overbrace{2\alpha_j P_j + 2(1-\alpha_j) \left(\underbrace{\sum_{i=1}^{n} m_{i,j} Q_{i,j}}_{waste} + \underbrace{(m_{I,j} q_j)}_{heat} \right)}^{2 \text{ phytoplankton less inefficiencies+waste molecules+heat}} \tag{2.29}$$

where $m_{i,j}$ is the stoichiometric coefficient for nutrient i, phytoplankton j [mol mol^{-1}]; $m_{I,j}$ is the stoichiometric coefficient for energy (in photons), phytoplankton species j [mol mol^{-1}]; and α_j is the growth efficiency of phytoplankton species j [-] Eq. 2.29 assumes that phytoplankton cells have a fixed stoichiometry, which could be, for example, the Redfield ratio (Table 2.11). Under the rules of balancing chemical reactions, Eq. 2.29 can be used to describe population growth of sexually or asexually reproducing populations: the stoichiometry of Eq. 2.29 remains the same, but the growth rate of the population, k_j (defined below), will be seen to vary according to the parent to offspring ratio.

Based on Eq. 2.29, using chemical kinetic methodologies (Atkins, 1994), and assuming a first-order reaction rate of growth with respect with each reactant, the rates of change of P_j, $Q_{i,j}$ and q_j can be written as follows:

$$\frac{dP_j}{dt} = \alpha_j k_j q_j \left(\prod_{i=1}^{n} Q_{i,j} \right) P_j = \mu_j P_j \tag{2.30}$$

where k_j is the reaction rate constant for species j [s^{-1} mol$^{-(n+1)}$] and μ_j is the growth rate of phytoplankton species j [s^{-1}]. k_j can be determined at the maximum observed growth rate, $\mu_j^{max\ ob}$, which is assumed to occur at an ideal temperature, with the max-

imum concentration of stored nutrient and energy:

$$k_j = \frac{\mu_j^{max}}{\alpha_j q_j^{max} \prod_{i=1}^{n} Q_{i,j}^{max}} \tag{2.31}$$

where $\mu_j^{max} = \mu_j^{max\ ob.}/\alpha_j$. The rates of reaction of the different reactants can be equated:

$$\left(\frac{dP_j}{dt}\right)_{growth} = -\frac{A_v}{\alpha_j \left(m_{i,j} + Q_{i,j}\right) P_j} \left(\frac{dQ_{i,j}}{dt}\right)_{growth} = -\frac{A_v}{\alpha_j \left(m_{I,j} + q_j\right) P_j} \left(\frac{dq_j}{dt}\right)_{growth} \tag{2.32}$$

so that:

$$\left(\frac{dQ_{i,j}}{dt}\right)_{growth} = \overbrace{-k_j \frac{m_{i,j}}{A_v} q_j \prod_{il=1}^{n} Q_{il,j}}^{formation\ of\ organic\ matter} \underbrace{-k_j \frac{Q_{i,j}}{A_v} q_j \prod_{il=1}^{n} Q_{il,j}}_{division\ amomgst\ offspring} \tag{2.33}$$

$$\left(\frac{dq_j}{dt}\right)_{growth} = \overbrace{-k_j \frac{m_{I,j}}{A_v} q_j \prod_{il=1}^{n} Q_{il,j}}^{formation\ of\ organic\ matter} \underbrace{-k_j \frac{q_j}{A_v} q_j \prod_{il=1}^{n} Q_{il,j}}_{division\ amomgst\ offspring} \tag{2.34}$$

The average internal cell properties of a population, Q and q, are changed as a result of the formation of organic matter, and the sharing of internal reserves amongst offspring. Later, we shall see how internal reservoirs can also be changed by the mixing of cells with different light and nutrient histories (Eq 2.56). The inefficiency of phytoplankton growth results in a return of nutrients to the extracellular nutrient pool at the rate of:

$$\left(\frac{dN_i}{dt}\right)_{recycled} = \sum_{j=1}^{p} (1 - \alpha_j)\, k_j m_{i,j} q_j \left(\prod_{il=1}^{n} Q_{il,j}\right) P_j \tag{2.35}$$

The term "recycled" has been used to distinguish the process in Eq. 2.35 from nutrient regeneration or remineralisation, which usually imply the breakdown of organic material (Libes, 1992). Recycled nutrient is better thought of as nutrient which has been taken into the cell, but then lost before it is turned into organic matter. Eq. 2.35 represents nutrient that leaks or is excreted as a result of growth inefficiencies. Another source of recycled nutrient is the internal reservoirs of phytoplankton cells which have been

consumed by herbivore grazing. The mathematical form for this is introduced later (Eq. 2.52), once grazing rates have been calculated. This model includes no breakdown of organic matter once it has been formed.

The above growth equations are re-derived in Chapter 3 for the specific cases of batch, continuous and semi-continuous cultures. The reader may find this case study approach easier to follow.

2.3.5 Temperature dependence of growth rates

Temperature dependence of biochemical reactions is commonly fitted (Geider *et al.*, 1997; Raven and Geider, 1988) to the Arrhenius equation: an empirical formula based on an exponential change in reaction rate with temperature. The Arrhenius equation is given by (Atkins, 1994):

$$k = Ae^{\frac{-E_a}{RT}} \tag{2.36}$$

where k is a reaction rate [s^{-1}]; A is the experimentally-determined constant for Arrhenius equation [s^{-1}]; E_a is the activation energy [J mol^{-1}]; universal gas constant, R = 8.31451 J K^{-1} mol^{-1} and T is the temperature [K]. Eq. 2.36 is used to determine the growth rate constant at all temperatures, given the experimentally determined maximum growth rate at an ideal temperature, T_{ref}. The temperature dependence of k_j becomes:

$$k_j(T) = \frac{\left(\mu_j^{max}\right)_{T_{ref,j}}}{\alpha_j q_j^{max} \prod_{i=1}^{n} Q_{i,j}^{max}} \exp\left[\frac{-E_{a,j}}{R}\left(\frac{1}{T} - \frac{1}{T_{ref,j}}\right)\right] \tag{2.37}$$

where $T_{ref,j}$ is the temperature at which the reaction rate constant, k_j, is at a maximum [K]; and $E_{a,j}$ can be determined experimentally (Table 2.11).

2.3.6 Sinking rates of plankton

A force balance on a particle in suspension determines the terminal vertical velocity, U_{sink} [m s^{-1}], of a cell due to a density difference between the fluid and the cell:

$$\underbrace{gV\left(\rho_{cell}-\rho_{water}\right)}_{gravitational\ force} = \underbrace{C_D\eta U_{sink}}_{frictional\ force} \tag{2.38}$$

where g is the acceleration due to gravity [m s^{-2}]; V is the cell volume [m^3]; ρ_{cell} and ρ_{water} are the density of the cell and surrounding water respectively [kg m^{-3}]; C_D is the drag coefficient [m], which is shape and orientation dependent [Table 2.4]; and η is the dynamic viscosity [kg m^{-1} s^{-1}]. The removal rate of phytoplankton species j due to sinking from a well-mixed layer of thickness M [m] is given by:

$$\left(\frac{dP_j}{dt}\right)_{sinking} = -\frac{gV_j\left(\rho_j-\rho_{water}\right)}{C_{D,j}\eta M}P_j \tag{2.39}$$

A similar force balance is used to determine the sinking rate of herbivore species.

Shape	Random	Axial	Normal
Sphere	$6\pi r_1$	$6\pi r_1$	$6\pi r_1$
Oblate	$\dfrac{6\pi r_1\sqrt{1-r_a^2}}{\cos^{-1} r_a}$	$\dfrac{8\pi r_1\left(1-r_a^2\right)}{\frac{\left(1-2r_a^2\right)\cos^{-1} r_a}{\sqrt{1-r_a^2}}+r_a}$	$\dfrac{16\pi r_1\left(1-r_a^2\right)}{\frac{\left(3-2r_a^2\right)\cos^{-1} r_a}{\sqrt{1-r_a^2}}-r_a}$
Prolate	$\dfrac{6\pi r_2\sqrt{r_a^2-1}}{\ln\left(r_a+\sqrt{r_a^2-1}\right)}$	$\dfrac{8\pi r_2\left(r_a^2-1\right)}{\frac{\left(2r_a^2-1\right)\ \ln\left(r_a+\sqrt{r_a^2-1}\right)}{\sqrt{r_a^2-1}}-r_a}$	$\dfrac{16\pi r_2\left(r_a^2-1\right)}{\frac{\left(2r_a^2-3\right)\ \ln\left(r_a+\sqrt{r_a^2-1}\right)}{\sqrt{r_a^2-1}}+r_a}$

Table 2.4: Drag coefficients, C_D [m], of various shapes and orientation (Clift *et al.*, 1978). C_D is used to calculate terminal sinking velocity of cells (Eq. 2.38) and Sherwood numbers in a uniform flow (Table 2.2). r_a = aspect ratio = axial dimension / normal dimension; $r_{1,2}$ = orthogonal radii [m] where $r_1 > r_2$.

2.3.7 Plankton grazing

The process of a predator assimilating a prey can be divided into a series of events, such as searching, encounter, attack, capture, and ingestion (for review of the large body of work on these processes see Dower *et al.* (1997)). This chapter considers only small herbivores, which are assumed to have no search or attack behaviours. Encounter occurs passively due to relative fluid motion between the predator and prey. Under this simplification, the grazing rate of a predator is dependent on its encounter, capture and

ingestion rates of the prey (Shimeta *et al.*, 1995). Assuming these three rates to be independent, the grazing rate is determined by the slowest of encounter, capture and ingestion rates. Without sufficient theoretical understanding of plankton capture mechanisms, capture rates are assumed unlimiting (although Shimeta *et al.* (1995) suggests that capture may become limiting under high shear). Plankton grazing rates therefore becomes the minimum of the encounter rate (a function of shear, swimming and sinking velocities) and the species-specific ingestion rate.

Encounter rates. Two different approaches have been used to estimate the encounter rate of particles. The first involves considering the velocities of all possible sources of relative motion between particles (swimming, sinking, turbulent motion, diffusion, feeding currents etc.), to calculate an approximate relative velocity between particles, on which an encounter rate can be calculated (Gerritsen and Strickler, 1977; Rothschild and Osborn, 1988). An alternative approach, called coagulation theory (Jackson, 1995), calculates the encounter rate as the sum of encounter rates due to each source of relative motion. We have chosen to sum the relative velocities due to sinking and swimming of both predator and prey (Gerritsen and Strickler, 1977) to determine an encounter rate due to sinking and swimming, which is then added to the encounter rates calculated due to diffusion and turbulent motions following coagulation theory.

To calculate the relative velocity of the predator species k, and prey species j, due to their respective sinking and swimming velocities, $U_{j,k}$ [m s^{-1}], firstly their differential sinking (which is always along the vertical) rate is determined:

$$U_{sink,j,k} = U_{sink,j} - U_{sink,k} \tag{2.40}$$

The relative swimming velocities (addition of random swimming velocities of the predator and prey) is given by (Gerritsen and Strickler, 1977):

$$U_{swim,j,k} = \frac{U_{slow}^2 + 3U_{fast}^2}{3U_{fast}} \quad \text{where} \quad \begin{array}{l} U_{slow} = \min\left[U_{swim,j}, U_{swim,k}\right] \\ U_{fast} = \max\left[U_{swim,j}, U_{swim,k}\right] \end{array} \tag{2.41}$$

Assuming that the relative swimming direction of predator and prey is random, the relative velocity due to sinking and swimming, $U_{j,k}$ [m s^{-1}], is given by:

$$U_{j,k} = \frac{U_{slow}^2 + 3U_{fast}^2}{3U_{fast}} \quad \text{where} \quad \begin{array}{l} U_{slow} = \min\left[U_{swim,j,k}, U_{sink,j,k}\right] \\ U_{fast} = \max\left[U_{swim,j,k}, U_{sink,j,k}\right] \end{array} \tag{2.42}$$

Coagulation theory. Coagulation theory predicts that the encounter rate of a particle, say a predator, with other particles in a fluid, say the prey, P_j, can be given by:

$$\text{Encounter rate} = \phi_{j,k} P_j \tag{2.43}$$

where $\phi_{j,k}$ is the encounter rate coefficient of species j with species k [m^3 s^{-1}]; and P_j is the concentration of phytoplankton species j [mol m^{-3}]. $\phi_{j,k}$ is determined for encounter rates as a result of diffusion, relative velocity ($U_{j,k}$ from Eq. 2.42) and turbulent shear (Table 2.5) using (Jackson, 1995):

$$\phi_{j,k} = \phi_{j,k,diffusion} + \phi_{j,k,relative\,velocity} + \phi_{j,k,turbulent\,shear} \tag{2.44}$$

When calculating the encounter rate coefficient for relative velocity and turbulent shear, two types of solutions are used:

- Rectilinear solution - assumes that the presence of a larger organism does not change the velocity of smaller organisms. Filter-feeder contact rates are solved this way.
- Curvilinear solution - assumes that smaller organisms follow streamlines around larger organisms, the two organisms only coming into contact if the streamline the smaller organism follows is within 1 smaller organism's radii of the larger organism. The most basic heterotrophs are solved this way.

The rectilinear and curvilinear solutions of the encounter rate coefficient given for spherical cells are given in Table 2.5. The encounter rate of non-spherical cells has been briefly analysed by Hill (1992), who used the same encounter rate formulations for spherical cells, but included a contact efficacy to correct for the non-spherical. Further work by

Mechanism	Rectilinear encounter ϕ_r [m^3 s^{-1}]	Curvilinear encounter ϕ_c [m^3 s^{-1}]
Diffusion	$\frac{2k_BT}{3\eta}\left(\frac{1}{r_1}+\frac{1}{r_2}\right)(r_1+r_2)$	$\frac{2k_BT}{3\mu}\left(\frac{1}{r_1}+\frac{1}{r_2}\right)(r_1+r_2)$
Relative velocity	$\pi\left(r_1+r_2\right)^2 U_{1,2}$	$0.5\pi r_1^2 U_{1,2}$
Turbulent Shear	$1.3\left(\frac{\epsilon}{\upsilon}\right)^{0.5}(r_1+r_2)^3$	$9.8\frac{p^2}{(1+2p)^2}\left(\frac{\epsilon}{\upsilon}\right)^{0.5}(r_1+r_2)^3$

Table 2.5: Encounter rate coefficients for spherical cells. $\phi_{1,2}$ = encounter rate coefficient [m^3 s^{-1}] of two spheres, radii r_1 and r_2 where $r_2 > r_1$ [m]. Rectilinear formulae assumes the path of the cells are uninterrupted by the presence of other cells. Curvilinear formulae correct for the influence of large cells on the path of smaller cells. $p = r_1$ / r_2; Boltzmann constant, $k_B = 1.38066 \times 10^{-23}$ J K^{-1}; T = temperature [K]; η = dynamic viscosity [kg s^{-1} m^{-1}]; ϵ = mean rate of dissipation of turbulent kinetic energy [m^2 s^{-3}]; and υ = kinematic viscosity [m^2 s^{-1}] (Jackson, 1995).

Loyalka and Griffin (1994) involved more direct calculations on motion of non-spherical particles, including rotation and encounter rates amongst other things. Given, the complexity of these calculations, however, encounter rates have been based on the spherical coefficients only. The encounter rate coefficient for non-spherical shapes have been calculated based on an average spherical radius for the predator and prey when using the rectilinear solution, and the predator for the curvilinear solution. To account for the rotation due to shear of the prey as it passes around the predator, the prey's largest radius is used for the curvilinear solution.

To obtain the encounter rate for a population of H_k cells with a population of P_j cells, Eq. 2.43 becomes:

$$\text{Encounter rate} = A_v \phi_{j,k} P_j H_k \tag{2.45}$$

where Avogadro constant, A_v, is required to retain units of mol m^{-3} s^{-1}.

Ingestion rates. Herbivore maximum ingestion rates are reported (Hansen *et al.*, 1997), or can be calculated, given a maximum growth rate at unlimiting prey density, μ_k^{max}, and the yield of predator cells per prey, $Y_{j,k}$ (Eccleston-Parry and Leadbeater,

1994). The maximum ingestion rate of prey is then given by $\mu_k^{max} Y_{j,k}^{-1}$.

2.3.8 Growth rate of herbivore cells

Herbivore growth rate is a function of temperature, the encounter rate of phytoplankton and herbivore cells, and the maximum herbivore ingestion rate of phytoplankton. It is assumed that the growth of herbivore species k can be described by a series of chemical reactions, one for the assimilation of each prey species $P_j, j = 1, ..., p$ such that:

$$\begin{aligned} H_k + Y_{1,k}^{-1}\, P_1 &\rightarrow 2H_k \\ H_k + Y_{2,k}^{-1}\, P_2 &\rightarrow 2H_k \\ \vdots \qquad\qquad &\quad \vdots \\ H_k + Y_{p,k}^{-1}\, P_p &\rightarrow 2H_k \end{aligned} \tag{2.46}$$

Like Eq. 2.29, Eq. 2.46 is a balanced chemical reaction, describing sexually or asexually reproducing populations of variable parent to offspring ratios. Herbivore growth rate in unlimiting prey concentrations is assumed to be exponential. The change in herbivore species k with time due to grazing on phytoplankton species $j = 1, ..., p$ is assumed to be proportional to the minimum of the prey saturated growth rate, μ_k^{max} [s^{-1}], and the product of the encounter rate per predator, $A_v \sum_{j=1}^{p} \phi_{j,k} P_j$, and the yield of predator per prey, $Y_{j,k}$:

$$\left(\frac{dH_k}{dt}\right)_{grazing\ uptake} = \min\left[\mu_k^{max}, \quad A_v \sum_{j=1}^{p} \phi_{j,k} P_j Y_{j,k}\right] H_k \tag{2.47}$$

If predator k is not ingestion rate limited, the resultant grazing loss in phytoplankton species j is given by:

$$\left(\frac{dP_j}{dt}\right)_{grazing\ loss\ to\ H_k} = A_v \phi_{j,k} P_j H_k \tag{2.48}$$

If a predator k is ingestion rate limited, all phytoplankton grazing loss terms of k will be a function of the population of the predator, and the predator preference for each prey species. Assuming that the predator k has an equal preference for all prey, the grazing loss of phytoplankton species j becomes a function of the population of the predator k, and the fraction of encounters of species j with k in a diet of $1, ..., j\prime$. Therefore, the loss term for population P_j in a diet of $P_{j\prime}$, $j\prime = 1, ..., p$, for ingestion rate limited predator k with no prey preference is given by:

$$\left(\frac{dP_j}{dt}\right)_{grazing\ loss\ to\ H_k} = \frac{\phi_{j,k}P_j}{\sum_{j\prime=1}^{p}\phi_{j\prime,k}P_{j\prime}}\mu_k^{max}Y_{j,k}^{-1}H_k \tag{2.49}$$

Combining Eqs. 2.48 and 2.49, the grazing loss term of phytoplankton species j in an assemblage of $j\prime = 1, ..., p$ to grazers H_k, $k = 1, ..., h$ is given by:

$$\left(\frac{dP_j}{dt}\right)_{grazing} = \sum_{k=1}^{h}\begin{cases} -A_v\phi_{j,k}P_jH_k & \text{if} \quad A_v\sum_{j\prime=1}^{p}\phi_{j\prime,k}P_{j\prime}Y_{j\prime,k} \leq \mu_k^{max} \\ -\dfrac{\phi_{j,k}P_j}{\sum_{j\prime=1}^{p}\phi_{j\prime,k}P_{j\prime}}\mu_k^{max}Y_{j,k}^{-1}H_k & \text{if} \quad \mu_k^{max} \leq A_v\sum_{j\prime=1}^{p}\phi_{j\prime,k}P_{j\prime}Y_{j\prime,k} \end{cases} \tag{2.50}$$

Eq. 2.50 implies that the grazing loss to an ingestion rate limited predator is less than the loss to an encounter rate limited predator for the same prey species concentration. For two competing prey species, P_1 and P_2, the bloom of species P_1, if it results in the ingestion limitation of a common predator, will reduce the grazing pressure on P_2.

The temperature dependence of herbivore growth rates can be fitted to the Arrhenius equation (Eq. 2.36) in a similar manner to phytoplankton (Eq. 2.37):

$$\mu_k^{max}(T) = (\mu_k^{max})_{T_{ref,k}} \exp\left[\frac{-E_{a,k}}{R}\left(\frac{1}{T} - \frac{1}{T_{ref,k}}\right)\right] \tag{2.51}$$

where $T_{ref,k}$ is the temperature at which the prey saturated growth rate, μ_k^{max}, is a maximum [K]; $E_{a,k}$ can be determined experimentally (Table 2.12); yield, $Y_{j,k}$ is assumed to be unaffected by temperature, and the encounter rate coefficient, $\phi_{j,k}$, is a known function of temperature (Table 2.5).

The above treatment of herbivore growth rate considers all phytoplankton cells from one species, independent of their internal nutrient reservoirs, to be of the same nutritional value to the herbivores. Since herbivores maintain a similar C:N:P ratio as the structural material of the phytoplankton they consume, this is not an unreasonable assumption. The internal nutrient of the grazed cells, however, must be allocated to another state variable, since the grazed phytoplankton cells they resided in are now non-existent. It is assumed that this excess nitrogen is recycled instantaneously to the extracellular nutrient pool, N, at a rate given by the sum over all phytoplankton and herbivores species of the the ingestion rate (Eq. 2.50) multiplied by the size of the internal nutrient reservoir :

$$\left(\frac{dN_i}{dt}\right)_{recycled} = \sum_{j=1}^{p}\sum_{k=1}^{h}\begin{cases} A_v^2\phi_{j,k}P_jH_kQ_{i,j} & \text{if} \quad A_v\sum_{j\prime=1}^{p}\phi_{j\prime,k}P_{j\prime}Y_{j\prime,k} \leq \mu_k^{max} \\ \dfrac{\phi_{j,k}P_j}{\sum_{j\prime=1}^{p}\phi_{j\prime,k}P_{j\prime}}A_vQ_{i,j}\mu_k^{max}\dfrac{H_k}{Y_{j,k}} & \text{if} \quad \mu_k^{max} \leq A_v\sum_{j\prime=1}^{p}\phi_{j\prime,k}P_{j\prime}Y_{j\prime,k} \end{cases} \tag{2.52}$$

2.3.9 Mixing

In addition to the interactions described by the ODEs above, plankton populations are also affected by fluid mixing, which is best described using partial differential equations (PDEs). Mixing of scalars such as nutrient, salinity, and cells, here simplified to mixing in the vertical (z) direction only, takes the form (Sharples and Tett, 1994):

$$\frac{\partial S_z}{\partial t} = \frac{\partial}{\partial z}\left(K_z\frac{\partial S_z}{\partial z}\right) + \left(\frac{dS_z}{dt}\right)_{\text{loss and gain at depth } z} \tag{2.53}$$

where S_z is the concentration of a scalar at depth z [mol m^{-3}]; and K_z is the vertical eddy diffusivity at depth z [m^2 s^{-1}]. The mixing rate of the properties of a cell, such as stored nutrient, Q, is given by:

$$\frac{\partial Q_z}{\partial t} = \frac{\partial}{\partial z}\left(\frac{K_z}{P_z}\frac{\partial\left(P_zQ_z\right)}{\partial z}\right) + \left(\frac{dQ_z}{dt}\right)_{\text{loss and gain at depth } z} \tag{2.54}$$

To integrate PDEs forward in time, a variety of differencing schemes can be used. To illustrate the mixing of the properties of a cell, the forward-time centred-space (FTCS)

(Hoffman, 1992) differencing scheme is used:

$$P_i^{n+1} = P_i^n + K_z \left(P_{i+1}^n - 2P_i^n + P_{i-1}^n \right) \tag{2.55}$$

where P_i^n represents is the phytoplankton cell numbers at time n, position i. The mixing for internal properties becomes:

$$P_i^{n+1}Q_i^{n+1} = P_i^n Q_i^n + K_z \left(\overbrace{+P_{i+1}^n Q_{i+1}^n}^{\text{nutrient from above}} \quad \underbrace{-2P_i^n Q_i^n}_{\text{lost to above and below}} \quad \overbrace{+P_{i-1}^n Q_{i-1}^n}^{\text{nutrient from below}} \right) \tag{2.56}$$

It should be noted that in Eq. 2.54, and its numerical approximation Eq. 2.56, the direction of the flux of the stored internal nutrient , Q, is dependent on the gradient in Q only, but the magnitude is a function of the gradient of both P and Q, as would be expected.

Instead of tracking individual molecules and their internal physiological states (Lagrangian formulation), Eq. 2.56 mixes the average internal properties (Eulerian formulation). Errors resulting from using an Eulerian approximation (of, at the scale of the plankton, the Lagrangian reality) should be small if, for an individual, the time to move between layers is large compared to the time to reach the average value of the layer from gains and losses at that depth. A comparison between Lagrangian and Eulerian models of phytoplankton growth found only a small (20 %) difference in phytoplankton growth (McGillicuddy Jr., 1995).

2.3.10 The model equations

Including the effects of mixing, the model equations are given in Table 2.6. The equations contain n nutrient species, p phytoplankton species and h herbivore species. Phytoplankton species are differentiated on the basis of pigment assemblages (Table 2.7) and shape (Table 2.8). Herbivores are differentiated by shape, swimming velocity, feeding mechanism (Table 2.10), and yield of prey per herbivore (Table 2.9). Other biological parameters required, but not routinely measured in laboratory experiments, include the

ability to store nutrients, cell stoichiometry, maximum growth rate, density, swimming velocity and growth efficiency of phytoplankton, and the density of zooplankton. These values have been obtained from general size-dependent relationships found in the literature (Tables 2.11 and 2.12).

$$\frac{\partial N_i}{\partial t} = \underbrace{\frac{\partial}{\partial z}\left(K_z \frac{\partial N_i}{\partial z}\right)}_{mixing} - \underbrace{\sum_{j=1}^{p} \psi_j D_i N_i P_j A_v Sh_{i,j} \left(\frac{Q_{i,j}^{max} - Q_{i,j}}{Q_{i,j}^{max}}\right)}_{uptake\,by\,phytoplankton} + \underbrace{\sum_{j=1}^{p}\sum_{k=1}^{h} \begin{cases} A_v^2 \phi_{j,k} P_j H_k Q_{i,j} & \text{if} \quad A_v \sum_{j\prime=1}^{p} \phi_{j\prime,k} P_{j\prime} Y_{j\prime,k} \leq \mu_k^{max} \\ \frac{\phi_{j,k} P_j}{\sum_{j\prime=1}^{p} \phi_{j\prime,k} P_{j\prime}} A_v Q_{i,j} \mu_k^{max} H_k Y_{j,k}^{-1} & \text{if} \quad \mu_k^{max} \leq A_v \sum_{j\prime=1}^{p} \phi_{j\prime,k} P_{j\prime} Y_{j\prime,k} \end{cases}}_{recycled\ nutrient\ from\ herbivore\ grazing}$$

$$\frac{\partial Q_{i,j}}{\partial t} = \underbrace{\frac{\partial}{\partial z}\left(\frac{K_z}{P_j}\frac{\partial (Q_{i,j} P_j)}{\partial z}\right)}_{mixing} + \underbrace{\psi_j D_i N_i Sh_{i,j} \left(\frac{Q_{i,j}^{max} - Q_{i,j}}{Q_{i,j}^{max}}\right)}_{uptake} - \underbrace{\frac{k_j}{A_v} q_j \left(m_{i,j} + Q_{i,j}\right) \prod_{i\prime=1}^{n} Q_{i\prime,j}}_{consumption\ for\ growth}$$

$$\frac{\partial q_j}{\partial t} = \underbrace{\frac{\partial}{\partial z}\left(\frac{K_z}{P_j}\frac{\partial (q_j P_j)}{\partial z}\right)}_{mixing} - \underbrace{\frac{k_j}{A_v} q_j \left(m_{I,j} + q_j\right) \prod_{i=1}^{n} Q_{i,j}}_{consumption\ for\ growth} + \underbrace{\int_{PAR} \frac{\overline{aA}_{j,\lambda}}{k_{w,\lambda} + k_{g,\lambda} + \sum_{j\prime=1}^{p} A_v P_{j\prime} \overline{aA}_{j\prime,\lambda}} \frac{(I_{z-M,\lambda} - I_{z,\lambda})}{M} \left(\frac{q_j^{max} - q_j}{q_j^{max}}\right) d\lambda}_{light\ captured\ and\ stored}$$

$$\frac{\partial P_j}{\partial t} = \underbrace{\frac{\partial}{\partial z}\left(K_z \frac{\partial P_j}{\partial z}\right)}_{mixing} \underbrace{+\alpha_j k_j P_j q_j \prod_{i=1}^{n} Q_{i,j}}_{growth} \underbrace{-\frac{g V_j \left(\rho_j - \rho_{water}\right)}{C_{D,j}\,\eta} \frac{\partial P_j}{\partial z}}_{sinking} \underbrace{- \sum_{k=1}^{h} \begin{cases} A_v \phi_{j,k} P_j H_k & \text{if} \quad A_v \sum_{j\prime=1}^{p} \phi_{j\prime,k} P_{j\prime} Y_{j\prime,k} \leq \mu_k^{max} \\ \frac{\phi_{j,k} P_j}{\sum_{j\prime=1}^{p} \phi_{j\prime,k} P_{j\prime}} \mu_k^{max} Y_{j,k}^{-1} H_k & \text{if} \quad \mu_k^{max} \leq A_v \sum_{j\prime=1}^{p} \phi_{j\prime,k} P_{j\prime} Y_{j\prime,k} \end{cases}}_{grazing\ loss}$$

$$\frac{\partial H_k}{\partial t} = \underbrace{\frac{\partial}{\partial z}\left(K_z \frac{\partial H_k}{\partial z}\right)}_{mixing} + \underbrace{\min\left[\mu_k^{max}, \quad A_v \sum_{j=1}^{p} \phi_{j,k} P_j Y_{j,k}\right] H_k}_{grazing\ uptake} \underbrace{- \frac{g V_k \left(\rho_k - \rho_{water}\right)}{C_{D,k}\,\eta} \frac{\partial H_k}{\partial z}}_{sinking}$$

Table 2.6: The model equations. Units for state variables are: N_i -[mol(N_i) m^{-3}]; $Q_{i,j}$ - [mol(Q_i) cell(P_j)$^{-1}$]; q_j - [mol(q) cell(P_j)$^{-1}$]; P_j - [mol(P_j) m^{-3}]; H_k - [mol(H_k) m^{-3}].

Phytoplankton species	b	Pigment Concentrations $[10^6 \text{mg(pig)m}^{-3}]$				References
	$[\text{m}^2\ \text{mg(Chl } a)^{-1}]$	Chl a	Chl b	Chl c	Carot.	
Skeletonema costatum	0.535	6.0	-	1.9	4.3	NS93,BDC96[1,2]
Phaeodactylum tricornutum	0.5	4.8	-	1.2	9.7	GOR85,K94[1,2]
Isochrysis galbana	0.066	4.3	-	1.3	5.1	FDW85,JW94[2]
Dictylum brightwelli	0.5	0.088	-	0.029	0.037	JW94[1,3]
Emiliania huxleyi	0.587	0.22	-	0.083	0.33	JW94[1]
Stephanopyxis palmeriana	0.5	0.30	-	0.064	ND	GHD92,JW94[4]
Synechococcus sp.	0.2	3.0	-	-	2.0	MAPVC93
Prochlorococcus marinus	0.2	9.4	8.2	-	3.6	MAPVC93

Table 2.7: Scattering coefficient, b, and pigment concentrations in phyto plankton species. NS93 - Nielsen and Sakshaug (1993), BDC96 - Brunet *et al.* (1996), GOR85 - Geider *et al.* (1985), K94 - Kirk (1994), FDW85 - Falkowski *et al.* (1985), JW94 - Jeffery and Wright (1994), GHD92 - Goldman *et al.* (1992), MAPVC93 - Morel *et al.* (1993), ND - no data. Scattering coefficients from Morel and Bicaud (1986). If b for a species was unknown, diatoms were assumed to have $b = 0.5\ \text{m}^2\ \text{mg(Chl } a)^{-1}$ based on *S. costatum*, and cyanobacteria $b = 0.2\ \text{m}^2\ \text{mg(Chl } a)^{-1}$ based on *Synechocystis* sp. Notes: [1]Concentrations reported in mg(pig) cell^{-1}, and converted to mg(pig) m^{-3} using cell volume calculated from dimensions given in Table 2.8. [2]Accessory pigment concentration calculated from separate study giving ratio of concentration of Chl a to accessory pigment. [3]Using ratios of the molecular weight of Chl a and Chl c from Geider and Osbourne (1992) [4]Using *Stepanopyxis turris* to determine Chl c concentration.

Phytoplankton species	Taxa	Shape	r_1, r_2, r_3 [μm]	References
S. costatum	diatom	Prolate	4, 2, 2	PG75[2],SKA89
P. tricornutum	diatom	Ellipsoid	12.5, 1.5, 1	WR97[2]
I. galbana	haptophyte	Prolate	3.5, 1.9, 1.9	FDW85,PCC[3]
D. brightwelli	diatom	Prolate	75, 25, 25	PG75[2]
E. huxleyi	haptophyte	Sphere	5, 5, 5	PCC[4]
S. palmeriana	diatom	Sphere	80, 32, 32	GHD92,BW85[3]
Synechococcus sp.	cyanobacteria	Prolate	1.35, 0.27, 0.27	MAPVC93,BW85[3]
P. marinus	cyanobacteria	Prolate	0.83, 0.17, 0.17	MAPVC93[5]

Table 2.8: Taxa, shape and dimensions of phytoplankton species. PG75 - Pasciak and Gavis (1975), SKA89 - Sakshaug *et al.* (1989), WR97 - Wolf-Gladrow and Riebesell (1997), FDW85 - Falkowski *et al.* (1985), PCC - Plymouth Marine Laboratory (1990b), GHD92 - Goldman *et al.* (1992), BW85 - Bold and Wynne (1985), MAPVC93 - Morel *et al.* (1993). Dimensions were obtained by: [1]Measurement of images from electron microscope, [2]All dimensions given in reference, [3]Equivalent spherical diameter or volume given by 1st reference dimensions inferred by image in 2nd reference, [4]Equivalent spherical diameter given by reference, and without further information, shape assumed to be sphere, [5] Ratio of radii assumed to be in direct proportion to *Synechococcus* sp.

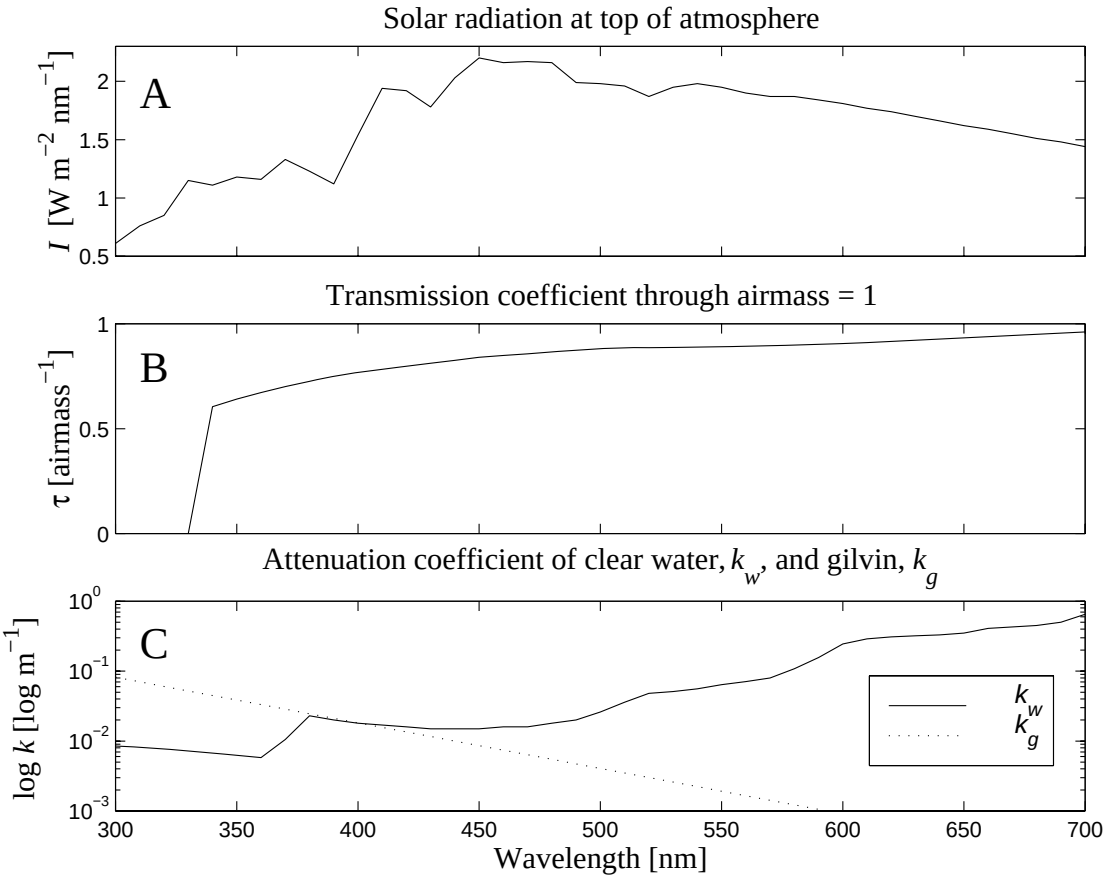

Figure 2.3: Spectrally resolved optical properties of the atmosphere and water. A. Solar radiation at the top of the atmosphere, I [$\mathrm{Wm^{-2}\,nm^{-1}} = 8.3525 \times 10^{-9}\lambda$ mol(photons) $\mathrm{s^{-1}\,m^{-2}\,nm^{-1}}$] (Koller, 1965). B. Transmission coefficient, τ [$\mathrm{airmass^{-1}}$], of a cloudless atmosphere, zenith sun (airmass = 1) (Koller, 1965), and C. Attenuation coefficient of (—) clear water, k_w [$\mathrm{m^{-1}}$] and ($\cdots$) gilvin (humic substances), k_g [$\mathrm{m^{-1}}$], at typical open ocean concentrations. Spectrally-resolved k_g has been calculated using $k_{g,\lambda} = k_{g,\lambda_o}\exp(-S(\lambda - \lambda_o))$ (Bricaud *et al.*, 1981), based on values typical of open ocean environments of $k_{g,440\,\mathrm{nm}} = 0.01$ $\mathrm{m^{-1}}$, $S = 0.015$ $\mathrm{nm^{-1}}$ (Kirk, 1994).

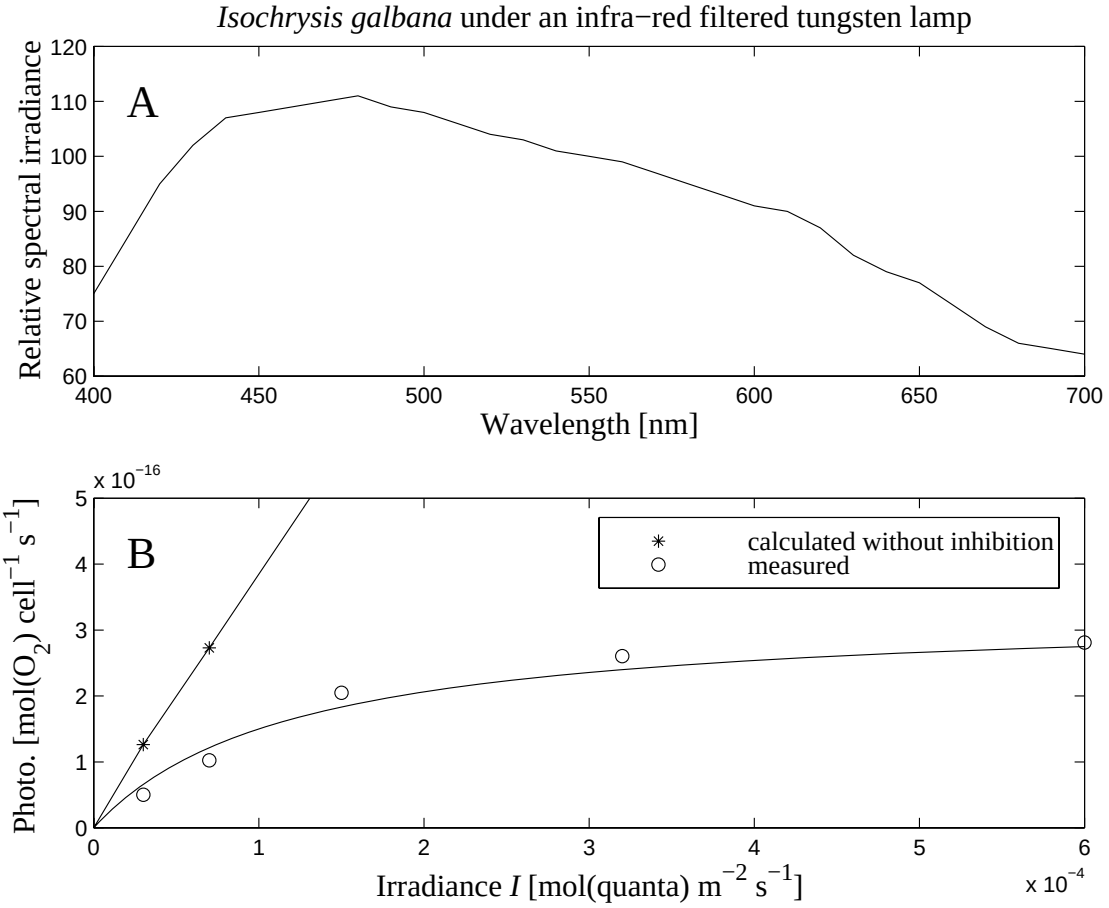

Figure 2.4: Gross photosynthesis rate of *Isochrysis galbana* under an infra-red tungsten lamp. A. The relative spectral irradiance of a tungsten-iodine lamp with filter (Driscoll and Vaughan, 1978) between 400 and 700 nm. B. (o) Measured photosynthesis rate and (∗) calculated based on uninhibited light capture in units of oxygen evolved for the prolate spheroid (aspect ratio = 1.84) *Isochrysis galbana* (Falkowski *et al.*, 1985). Calculated uninhibited light capture ($\overline{aA}_\lambda\,(I_\lambda)_{incident\,on\,j}$ (Eq. 2.17)) where $m_{O_2} = 10.4$, $\overline{aA}_{I.\,galbana}$ is calculated from formulae in Table 2.3 using cell geometry in Table 2.8, pigment ratios from Table 2.7, and absorbance according to Eq. 2.16.

$Y_{j,k}^{-1}$	B1	B2	*P.tricornutum*	*I.galbana*
Monosiga sp.[1]	ND	300	X	X
Ciliophrys marina[1]	ND	ND	X	X
Codosiga gracilis[2]	3,989	ND	X	X
Favella sp.[1]	ND	ND	ND	ND
Paraphysomonas imperforata[1,2]	208	ND	78	34
Stepanoeca diplocostata[2]	733	ND	X	X
Bodo designis[2]	693	ND	X	X
Jakoba libera[2]	96	ND	X	X

Table 2.9: Species-specific herbivore grazing yields. $Y_{j,k}^{-1}$ - reciprocal of the grazing stoichiometry coefficient [cells(P_j) cells(H_k)$^{-1}$] calculated during exponential growth in batch culture. ND - no data; X - outside food range; B1 - Unidentified Gram-negative, motile, rod-shaped bacterium (0.8 x 1.4 x 1.8 μm) with a volume of approx. 0.67 μm^3; B2 - *Escherichia coli* strain χ-1488, with assumed dimensions (0.6 x 0.6 x 0.6 μm) and volume 0.13 μm^3; References: [1] Shimeta *et al.* (1995); [2] Eccleston-Parry and Leadbeater (1994).

Herbivore species	Shape	r_1, r_2, r_3 [μm]	Growth rate [d^{-1}]	Enc. mech.	Swim speed [μm s^{-1}]	Prey range [μm]
Monosiga sp.	sphere	3 3 3	1.6	FF	30	bacteria
C. marina	sphere	65 65 65	1.1†	RW	0	bacteria
Favella sp.	oblate	175 175 100	0.82	FF	1000	any algae
P. imperforata	sphere	4 4 4	5.0	DI	42	0.5 - 200
S. diplocostata	cone	10 5* 5*	0.84	FF	178	bacteria
B. designis	prolate	5 1.6 1.6	3.8	DI	80	bacteria
J. libera	prolate	6 1.7 1.7	0.86	DI	19	bacteria
C. gracilis	prolate	4 2.2* 2.2*	1.2	FF	215	bacteria

Table 2.10: Constants used to describe herbivore species from Shimeta *et al.* (1995) and Eccleston-Parry and Leadbeater (1994). Encounter mechanisms (Enc. Mech.): RW - random walk, or diffusion; DI - direct interception, solved using rectilinear encounter rate coefficient; FF - filter feeder, solved using curvilinear encounter rate coefficient. Dimensions include any organic envelope (lorica) surrounding the cell. Dimensions were obtained by: [1]All dimensions given in reference, [2]Equivalent spherical diameter or volume given by 1st reference dimensions inferred by image in 2nd reference.[3]Equivalent spherical diameter given by reference, and without further information, shape assumed to be sphere. For FF, a volume clearance rate [m^3 s^{-1}] given in literature is converted to a product of a filter cross sectional area [m^2] (based on marked (*) dimensions) and a swimming velocity [m s^{-1}], and the swimming velocity is then used in the rectilinear coagulation formulae. (†) - growth rate based on *Ciliophrys infusionum* (Hansen *et al.*, 1997).

General Relationship for Phytoplankton	Units	Reference
$Q_{C,j}^{max} = 9.14 \times 10^3 V_j$	mol(Q_N) cell^{-1}	Straile (1997)
$q_j^{max} = \frac{m_I}{m_N} Q_N^{max}$	mol(q) cell^{-1}	-
$\rho_j = \rho_{water} + 0.0369 V_j^{-0.28}$	kg m^{-3}	Kiørboe (1993)
$U_{swim,j} = 3.57 \times 10^{-3} V_j^{0.26/3}$ $r^2 = 0.38$	m s^{-1}	Sommer (1988)
$\mu_j^{maxob.} = 8.06 \times 10^{-8} V_j^{-0.15}$ $r^2 = 0.34$ $n = 126$	s^{-1}	Tang (1995)
$E_{a,j} = 5.4 \times 10^4$ ($Q_{10} = 2.1$)	J mol^{-1}	RG88
$T_{ref,j} = T$	K	(Table 2.13)
$\alpha_j = 0.75$	-	-
$m_I : m_C : m_N : m_P = 848 : 106 : 16 : 1$	-	Kirk (1994)
$m_{i,j} = A_v Q_{i,j}^{max}$	mol cell^{-1}	-
$(\mathrm{C} : \mathrm{Chl}\, a)_j = 50$	-	F90

Table 2.11: General relationships used to calculate size-dependent phytoplankton parameter values. V_j = volume of species j [m^3]; $Q_{C,j}^{max}$ = maximum internal concentration of carbon in species j; q_j^{max} = maximum internal concentration of energy in species j; ρ_j = absolute density of species j; $U_{swim,j}$ = swimming velocity of species j; $\mu_j^{max\ ob}$ = maximum observed growth rate of species j; $E_{a,j}$ = activation energy of species j converted (Raven and Geider, 1988) from literature values of Q_{10} = ratio of reaction rates at $T + 10$ and T; $T_{ref,j}$ = temperature of maximum growth rate of species j; α_j = growth efficiency of species j; $m_{i,j}$ = stoichiometric ratio of reactant i in growth of species j, assumed to fit the Redfield ratio; $(\mathrm{C} : \mathrm{Chl}\, a)_j$ = weight ratio of carbon to Chl a of species j. RG88 - Raven and Geider (1988); F90 - Fasham *et al.* (1990). Note that the maximum growth rate of species j, μ^{max}, is given by its maximum observed growth rate, $\mu^{max\ ob}$ divided by the growth efficiency, α_j.

General Relationship for Herbivores	Units	Reference
$\rho_k = \rho_{water}$	kg m^{-3}	-
$\mu_k^m = 2.40 \times 10^{-8}\ V_k^{-0.21}\ r^2 = 0.69$ n = 69	s^{-1}	Hansen *et al.* (1997)
$Y_{j,k} = 0.33\dfrac{V_j}{V_k} \pm 0.032$ SE n = 33	predator prey^{-1}	Hansen *et al.* (1997)
$U_{k,swim} = 1.97 \times 10^{-2}\ V_k^{0.20}$ n = 39	m s^{-1}	Hansen *et al.* (1997)
$E_{a,k} = 7.1 \times 10^4\ (Q_{10} = 2.8)$	J mol^{-1}	Hansen *et al.* (1997)
$T_{ref,k} = T$	K	(Table 2.13)

Table 2.12: General relationships used to calculate size-dependent herbivore parameter values. V_k = volume of species k [m^3]; $U_{swim,k}$ = swimming velocity of species k; μ_k^m = maximum growth rate of species k; $E_{a,k}$ = activation energy of species k converted (Raven and Geider, 1988) from literature values of Q_{10} = ratio of reaction rates at $T + 10$ and T; $T_{ref,k}$ = temperature of maximum growth rate of species k; ρ_k = density of species k.

2.4 Experimental validation of functional forms

Published laboratory experiments involving plankton populations can be used to assess the performance of the presented mechanistic functional forms, based on individual plankton cells, to describe population dynamics.

Nutrient uptake. Eq. 2.14 is a function of extracellular nutrient concentration, fluid motion, phytoplankton shape, internal nutrient concentration (or physiological state), and the saturation and maximum activity of internal uptake processes. No published experimental studies have investigated all of these variables. However, experiments on populations of a single species of cyanobacterium (Mierle, 1985a), a diatom (Pasciak and Gavis, 1975), and a macroalgae (Smith and Walker, 1980) have been conducted to test the validity of the Hill-Whittington equation (Hill and Whittingham, 1955):

$$\frac{J^2}{\psi DSh} - \left(K + C_b + \frac{V}{\psi DSh}\right) J + VC_b = 0 \tag{2.57}$$

The functional form for nutrient uptake proposed earlier, Eq. 2.14, is based on Eq. 2.57, with the addition of the heuristically determined function for enzyme activity, K, on the internal cell processes (Eq. 2.12). Using parameter values for a cyanobacterium (Figure 2.5) and a diatom (Figure 2.6), the approximation of Eq. 2.14 given earlier, Eq. 2.15, is found to be $\pm 50\%$ in all regions except those where there is both high C_b and low Q (Figures 2.5 and 2.6). However conditions of both high C_b and low Q are unlikely to be present in natural environments, or numerical models of phytoplankton growth. Furthermore, Eq. 2.15 has a dependence on internal nutrient concentration, Q, similar to that used by other authors (Sharples and Tett, 1994), and does not require determination of V, or K_o, which is problematic (see above).

Light capture. Figure 2.7 compares the measured spectrally-resolved Chl *a* specific absorbance of pigments extracted from two species of cyanobacteria with the calculated value, assuming the pigment assemblage is made up of Chl *a*, Chl *b*, Chl *c* and carotenoids (Table 2.7) with absorbances described by Gaussian curves (Eq. 2.16). Errors are a result of using only 4 pigment types, and the lack of fit of the true pigment absorbances to Gaussian curves. These errors could be avoided by using measured spectrally-resolved absorbances.

The equations used to determine $\overline{aA}$ (Table 2.3) are exact for particular shapes with evenly distributed pigment, but are only as good as the approximation of the phytoplankton shape. The initial slope of a photosynthesis versus. irradiance curve should be approximated by $\overline{aA}\, m_{O_2}$, where $m_{O_2} = 10.4$. Figure 2.4 compares measured values of *Isochrysis galbana* with those calculated using cell geometry in Table 2.8, pigment ratios from Table 2.7, and absorbance according to Eq. 2.16.

Grazing rates. The ingestion rate of 6 protozoan species has been investigated in a stagnant fluid (swimming only) and in shear flows (Shimeta *et al.*, 1995). In a stagnant fluid, coagulation theory satisfactorily predicted the slope of ingestion rate versus. prey concentration (Figure 2.8) for a number of protozoan species. The growth kinetics of 6 heterotrophic flagellates has been studied under stagnant conditions, at higher prey

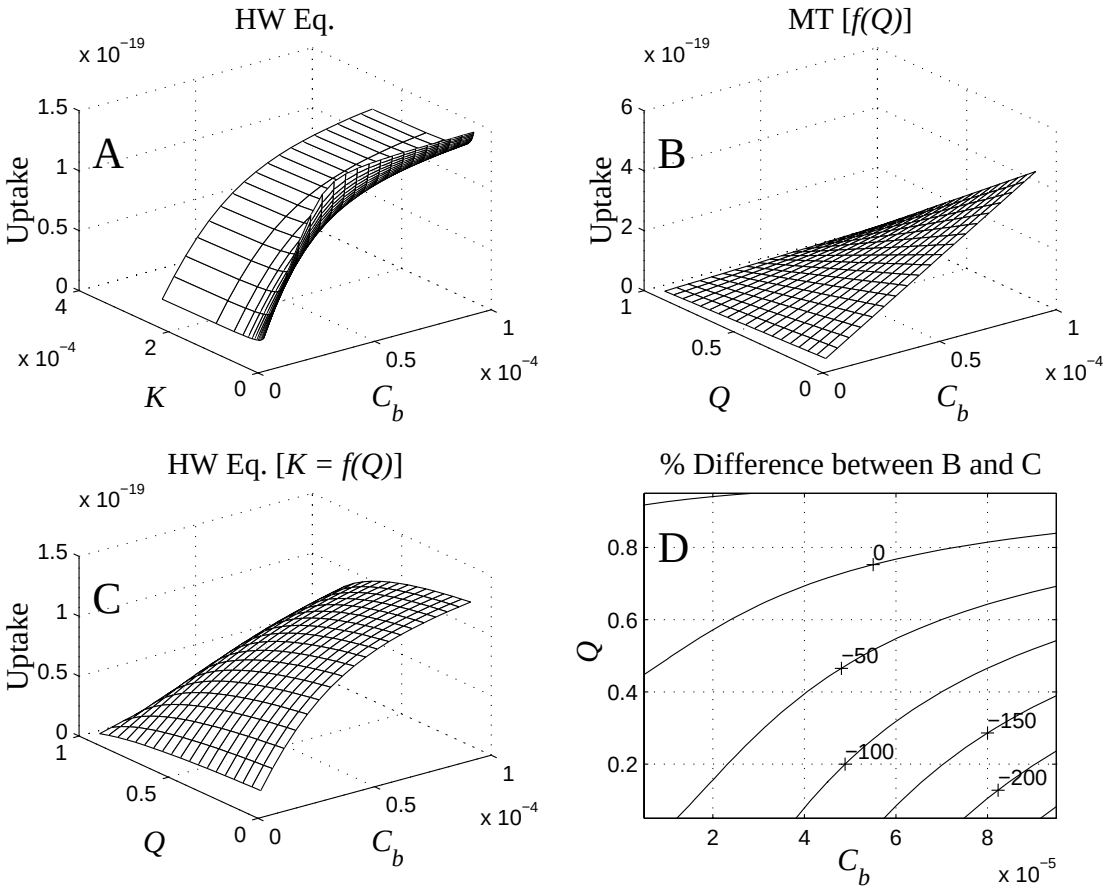

Figure 2.5: Analysis of nutrient uptake functional forms (Eqs. 2.14 and 2.15) using parameters (K, V) determined from laboratory experiments of phosphate uptake rates to the cyanobacterium *Synechococcus leopoliensis* (Mierle, 1985b), as a function of extracellular concentration and internal nutrient concentration of nitrate. A. Uptake determined using the Hill-Whittingham equation (HW) (Eq. 2.57). B. Uptake determined using mass transfer (MT) formulation dependent on internal nutrient concentration, Q (Eq. 2.15). C. Uptake determined using HW, with K a function of Q (HW Eq. $[K = f(Q)]$) (Eq. 2.14). D. Percentage difference between B. and C. (HW Eq. $[K = f(Q)]$) is the most theoretically justifiable functional form, but MT has been preferred because of lack of experimental determinations of K_o and V.

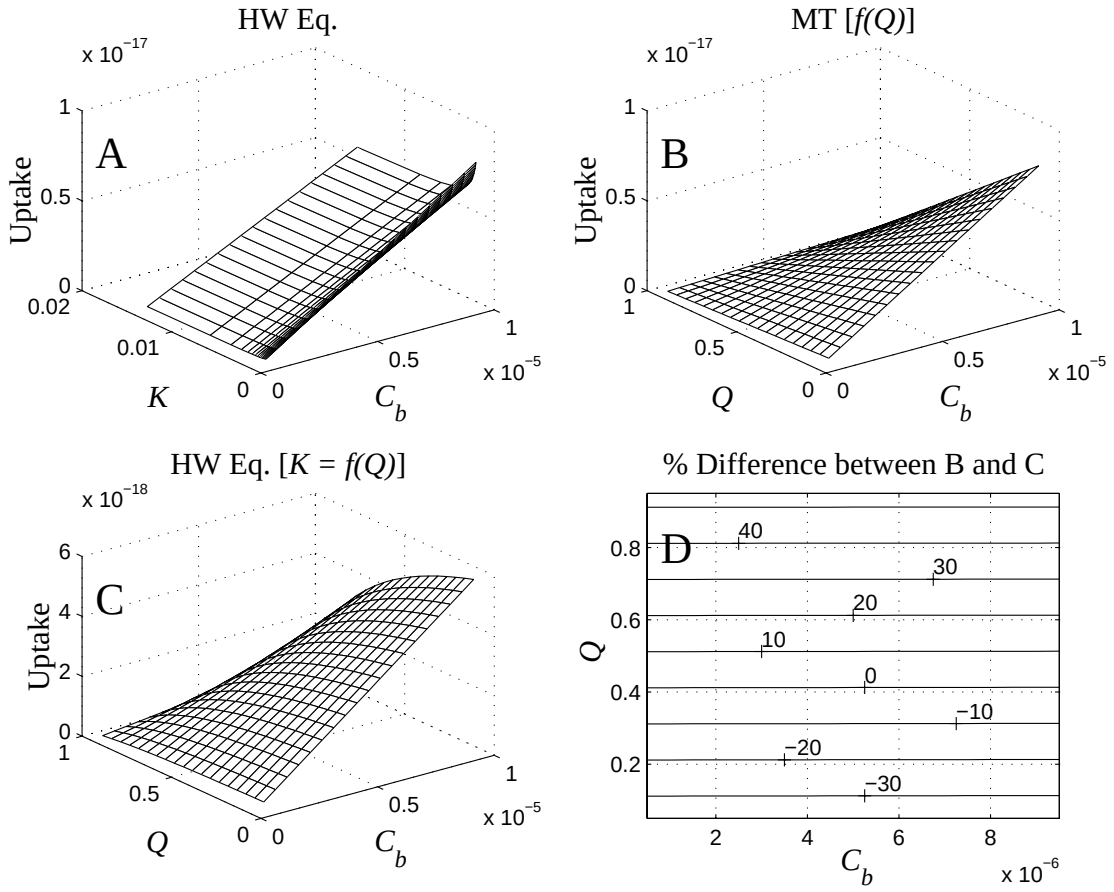

Figure 2.6: Analysis of nutrient uptake functional forms (Eqs. 2.14 and 2.15) using parameters (K, V) determined from laboratory experiments of nitrate uptake to the diatom *Dictylum brightwelli* (Pasciak and Gavis, 1975), as a function of extracellular concentration and internal nutrient concentration of nitrate. See Figure 2.5.

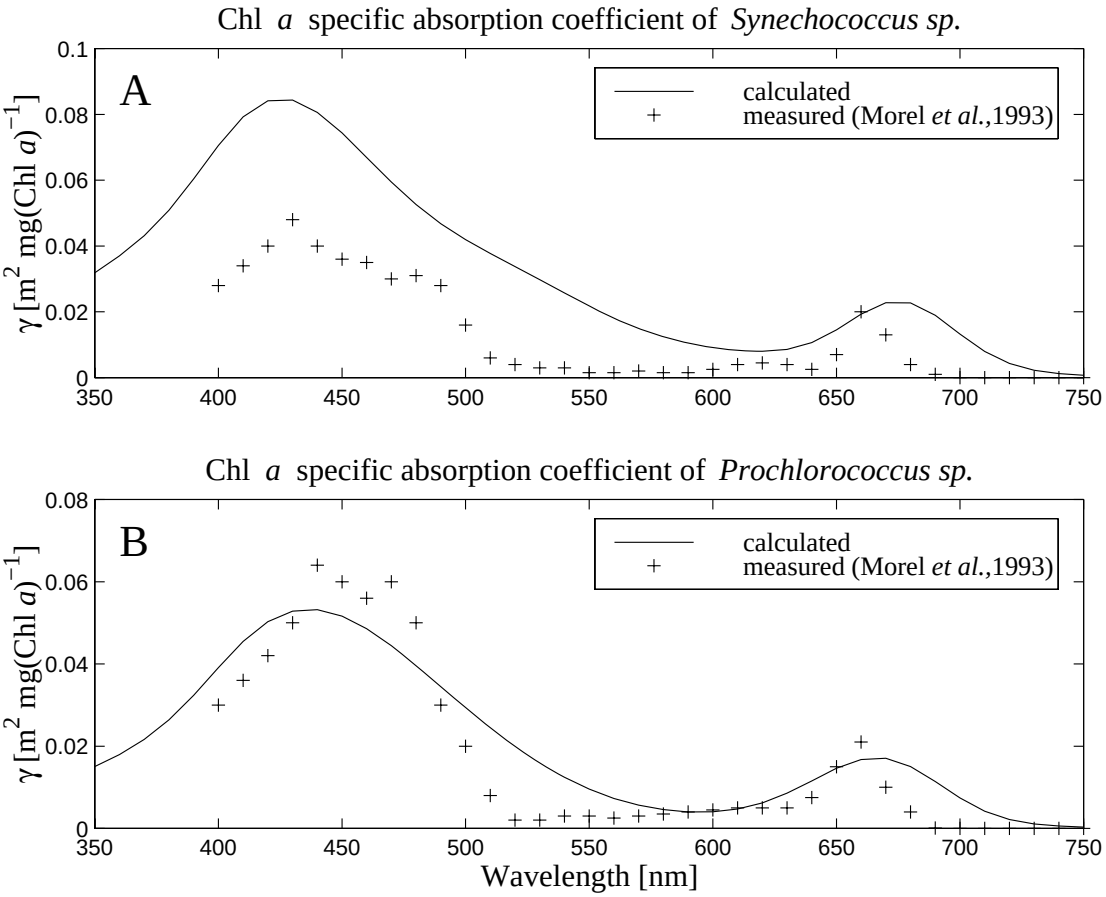

Figure 2.7: (+) Measured and (—) calculated Chl *a* specific absorbance [m^2 mg(Chl *a*)$^{-1}$] based on absorption coefficients calculated using Eq. 2.16, W_ξ, λ_ξ and γ_ξ from Hoepffner and Sathyendranath (1991), and pigment concentrations, C_ξ, from Table 2.7 of *Synechococcus* sp. and *Prochlorococcus* sp.

concentration (Eccleston-Parry and Leadbeater, 1994). Although the encounter rate coefficient still predicted the initial slope of the growth rate versus. prey concentration curve, a deviation from this line was observed for *Codosiga gracilis* before ingestion rate limitation is reached (Figure 2.9). This may be explained by a reduced swimming velocity at higher prey concentrations, although such an effect was not included in the model as presented.

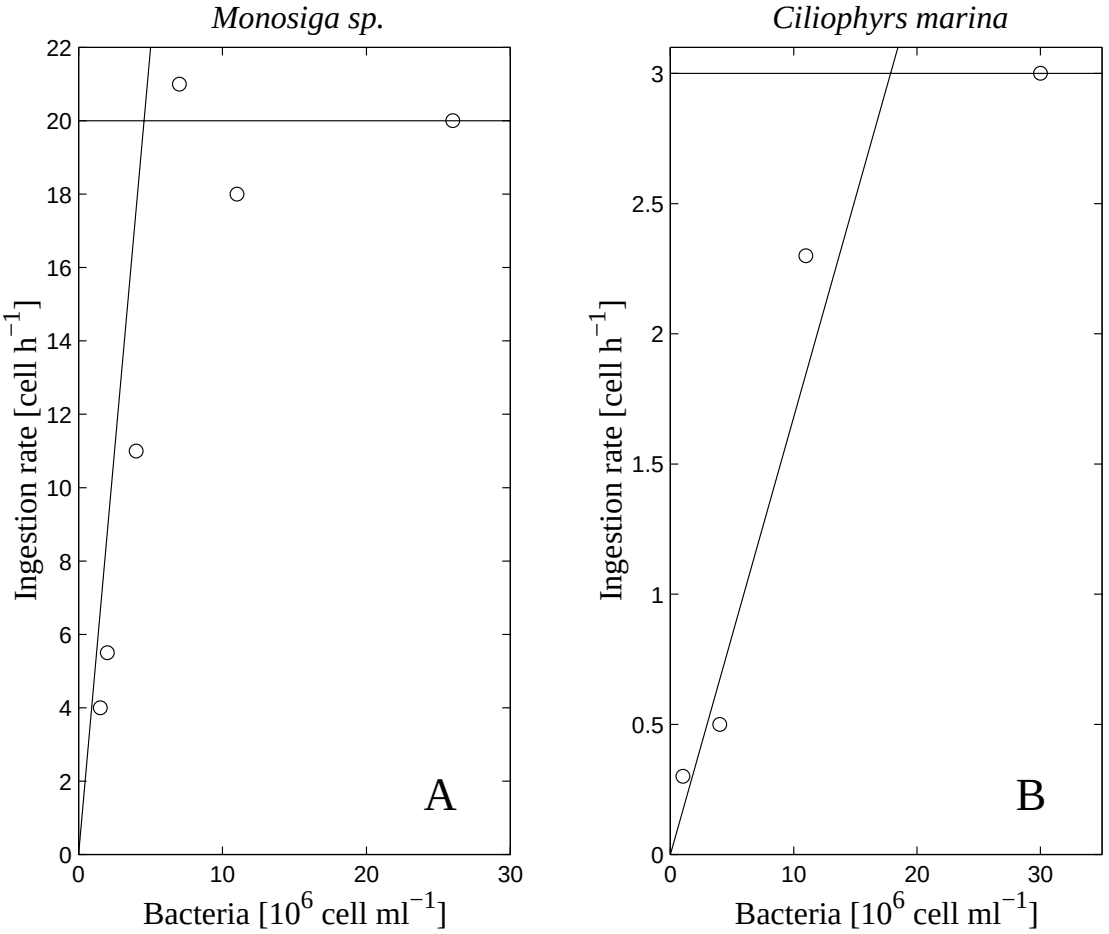

Figure 2.8: (∘) Measured ingestion rate of *Monosiga* sp. and *Ciliophyrs marina* (Shimeta *et al.*, 1995) and (—) predicted ingestion rate using coagulation theory. For *Monosiga* sp.: dimensions $3 \times 3 \times 3$ μm, $U_{swim,pred} = 30$ μm s^{-1} and non-motile bacteria $0.6 \times 0.6 \times 0.6$ μm, $\epsilon = 0$ m^2 s^{-3}, rectilinear encounter rate coefficient $\phi = 4.4 \times 10^{-12}$ m^3 hr^{-1}. For C. marina: dimensions $30 \times 30 \times 30$ μm, $U_{swim,pred} = 0$ μm s^{-1} and non-motile bacteria $2 \times 2 \times 2$ μm, $\epsilon = 0$ m^2 s^{-3}, encounter rate coefficient for diffusion, $\phi = 168 \times 10^{-15}$ m^3 hr^{-1}. The horizontal line represents the ingestion rate limit used in Table 2.9.

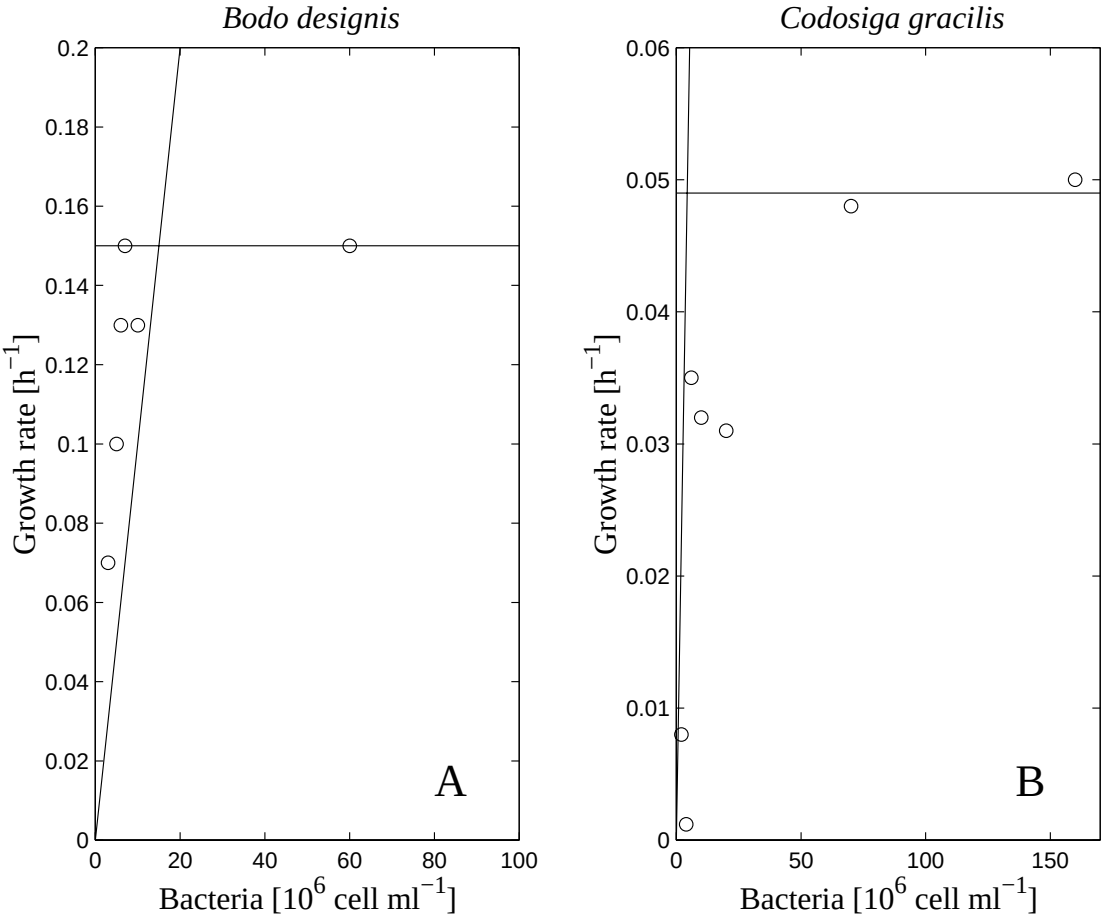

Figure 2.9: (∘) Measured growth rate of *Bodo designis* (Eccleston-Parry and Leadbeater, 1994) and (—) predicted growth rate using coagulation theory, and assuming exponential growth. For *Bodo designis*: dimensions 2.7 × 2.7 × 2.7 μm, $U_{swim,pred} = 80$ μm s^{-1} and non-motile bacteria 1.5 × 1.5 × 1.5 μm, $\epsilon = 0$ m^2 s^{-3}, rectilinear encounter rate coefficient $\phi = 16 \times 10^{-12}$, yield $\gamma = 1/693$ prey predator^{-1}; For *Codosiga gracilis*: dimensions 2.8 × 2.8 × 2.8 μm, $U_{swim,pred} = 215$ μm s^{-1} and non-motile bacteria 1.5 × 1.5 × 1.5 μm, $\epsilon = 0$ m^2 s^{-3}, rectilinear encounter rate coefficient $\phi = 45 \times 10^{-12}$ m^3 hr^{-1}, yield $\gamma = 1/3990$ prey predator $^{-1}$. The horizontal line represents the ingestion rate limit used in Table 2.9.

Sinking rates. The force balance for particle sinking, Eq. 2.38, is well known (Atkins, 1994). Measurement of sedimentation rates in the open ocean suggests that Eq. 2.38 underestimates the sinking velocities for small phytoplankton cells (radius < 5 μm) by 1-3 orders of magnitude (Kennett, 1982). For a long time this anomaly, of increased sedimentation rates, has been explained by the formation of aggregates (Lohmann, 1902). The understanding of the mechanisms of aggregation formation, or coagulation, has been well studied at the individual scale (Jackson, 1995). However, due to increasing the simulation time, coagulation will not be included in the presented model. In open ocean environments, where plankton are dilute, growth, grazing and mixing are probably more important terms than sinking, even including coagulation. In coastal regions, however, coagulation can result in sinking becoming the dominant phytoplankton loss term, and has been used to explain the ending of phytoplankton blooms (Kiørboe *et al.*, 1996).

The chemical reaction of phytoplankton growth. The behaviour of the "chemical reaction" describing phytoplankton growth (Eq. 2.29) (CR) can be simplified at steady-state, assuming only an internal reservoir for one nutrient, Q, and energy, q, to two simultaneous non-linear equations:

$$k_1 \frac{Q^{max} - Q}{Q^{max}} = k_3 Q q \left(m_Q + Q\right) \tag{2.58}$$

$$k_2 \frac{q^{max} - q}{q^{max}} = k_3 Q q \left(m_q + q\right) \tag{2.59}$$

where $k_1 = \psi D N S h$ [mol(Q) s^{-1}]; $k_2 = \overline{aA}I$ [mol(q) s^{-1}]; and $k_3 = k_j / A_v$ [mol s^{-1} mol(Q)$^{-1}$ mol(q)$^{-1}$] are respectively the nutrient uptake, light capture and growth rate constants for an individual cell. These equations have been solved for growth rate, $k_3 Q q$, at $m_Q = m_q = 1$ (Figure 2.10). Numerical solutions were obtained using MATLAB software, by applying Newton's method for solving systems of non-linear equations, truncating the Taylor series approximation to one term, and using Gaussian elimination to solve the intermediate linear simultaneous equations, until successive approximations were within 10^{-9} (Hoffman, 1992).

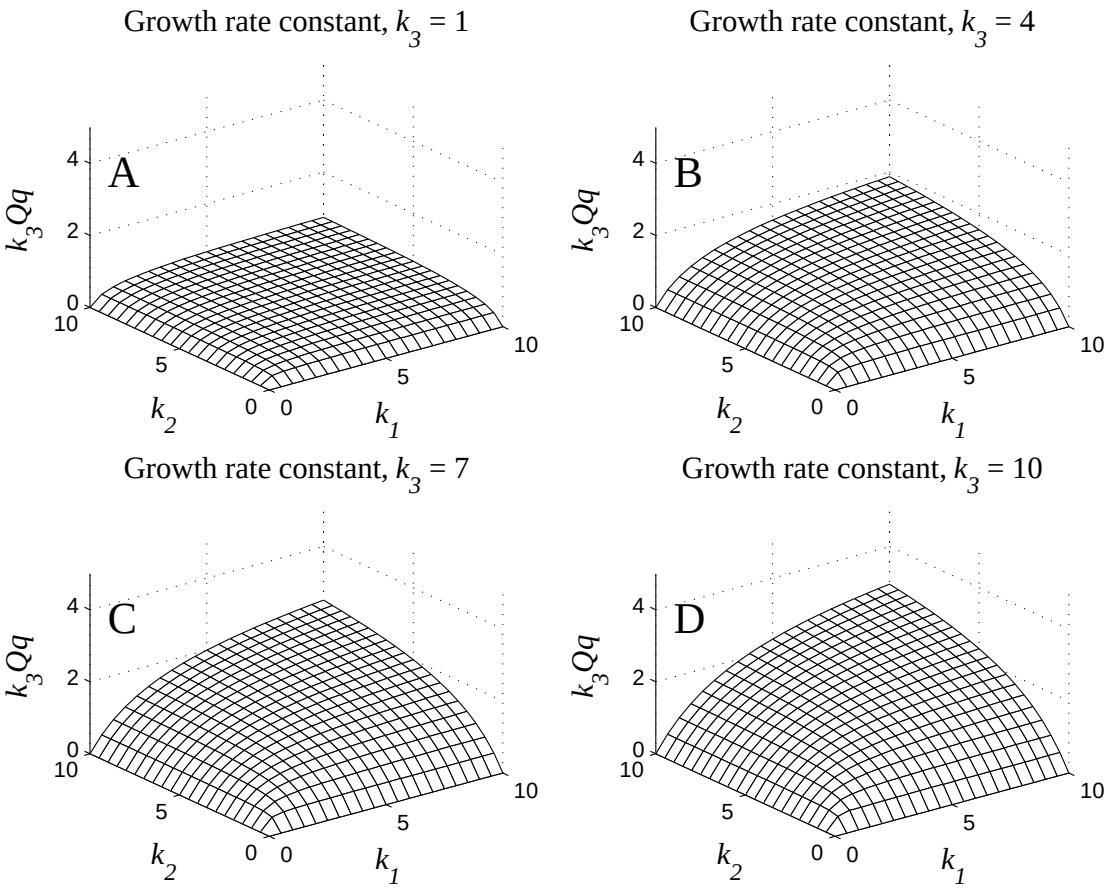

Figure 2.10: Steady-state analysis of non-linear simultaneous Eqs. 2.58 and 2.59 using Newton's method for non-linear equations (Hoffman, 1992). A. $k_3 = 1$; B. $k_3 = 4$; C. $k_3 = 7$. D. $k_3 = 10$. In the limit of one rate (k_1, k_2 or k_3) being much smaller than the other two, the growth rate k_3Qq, becomes proportional to the smallest rate only. This behaviour is similar to the "Law of the Minimum" (von Liebig, 1840)

The growth functional forms most commonly used in plankton population models are: either the multiplicative form (MP)(Steele and Henderson, 1981; Fasham *et al.*, 1990; Taylor and Stephens, 1993), which can be written as:

$$(\text{growth rate})_{\text{MP}} = k_1 k_2 k_3 \tag{2.60}$$

or the threshold or "Law of the Minimum" form (LM) (de Baar, 1994), in which the growth rate is dependent on the slowest uptake rate and the growth rate constant:

$$(\text{growth rate})_{\text{LM}} = (\min[k_1,\ k_2])k_3 \tag{2.61}$$

A comparison of the temperature dependence of growth rates obtained using CR, MP and LM functional forms has been made for a variety of values of k_1, k_2 and k_3 (Figure 2.11) based on the assumptions: k_1 is proportional to extracellular concentration and experiences a linear increase of 0.87 every 10 K (based on molecular diffusivity of nitrate), k_2 is proportional to irradiance, and k_3 doubles every 10 K.

The CR form was chosen because: (1) chemical kinetics methodology is used in many applications; (2) the internal reservoirs of Q and q take into account the light and nutrient histories of the cells; (3) the non-linear characteristics of the Eqs. 2.58 and 2.59 fitted laboratory experiments with a minimum of parameters (i.e. it did not require the addition of half saturation constants for nutrient and energy uptake); and (4) the CR form fits observed temperature dependencies of algal growth rate at low nutrient and low light conditions. For example, laboratory experiments at unlimiting nutrient concentrations ($k_1 = 10$) and low light conditions show that algal growth rate is independent of temperature (Kirk, 1994). This is also the case for the CR form (Figure 2.11A), but both the MP (Figure 2.11C) and LP (Figure 2.11E) forms are at least linear functions of temperature for all light conditions. At unlimiting light ($k_3 = 10$) and low nutrients conditions nutrient uptake is a positive function of temperature (Raven and Geider, 1988), which the CR form also predicts (Figure 2.11B).

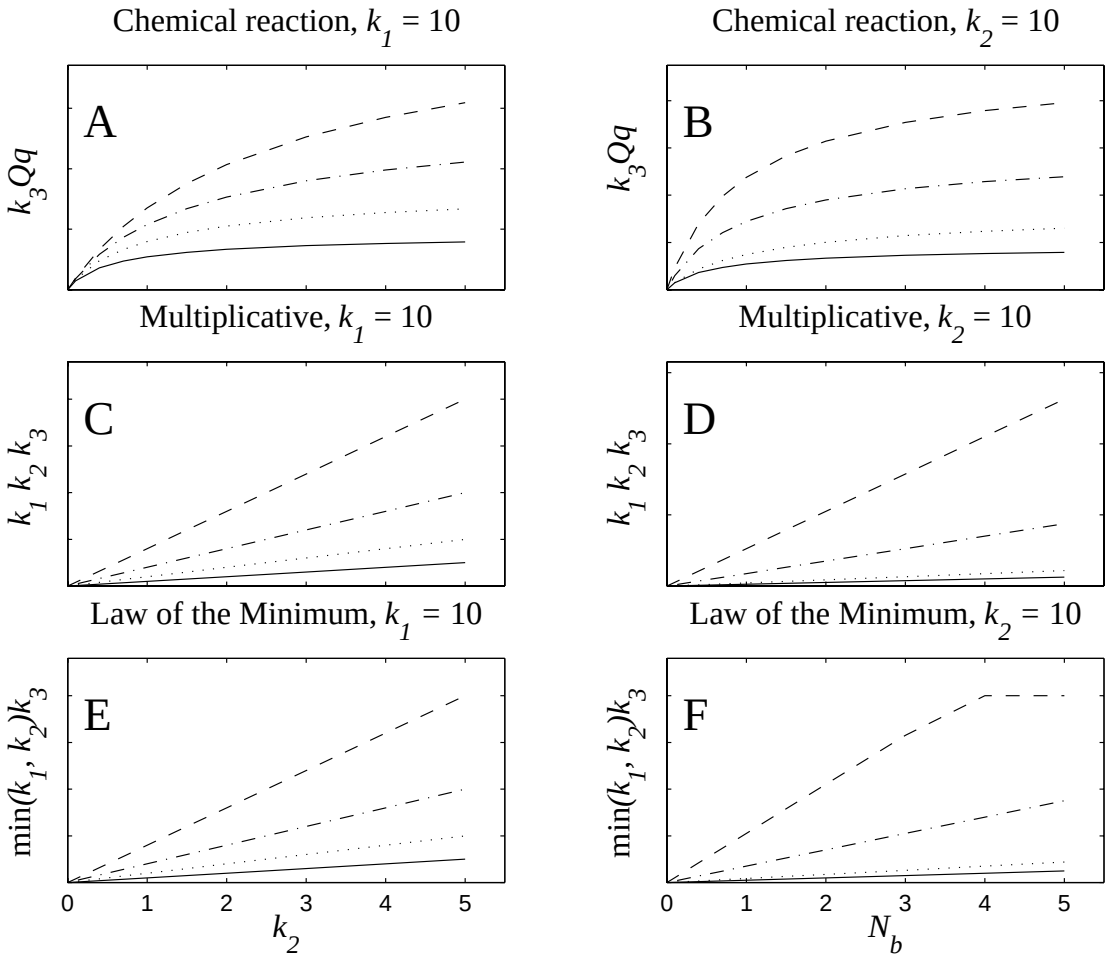

Figure 2.11: A comparison of phytoplankton growth functional forms (CR, MP and LM) at 4 different temperatures in low light (left column) and low nutrient (right column) conditions. The four different temperatures, 10 K apart correspond to a doubling a k_3, and are solved using: (-) $k_3 = 0.5$; $(\cdots)$ $k_3 = 1$; (- ·) $k_3 = 2$; (- -) $k_3 = 4$.

Mathematically, the CR form shares similar characteristics to both alternate functional forms. The CR growth term is a multiplicative form, albeit based on internal reservoirs of nutrient and energy rather than extracellular quantities, and for a nutrient with a much slower supply rate CR approximates the "Law of the Minimum":

$$\frac{\frac{\partial(k_3 Qq)}{\partial k_1}}{\frac{\partial(k_3 Qq)}{\partial k_2}} \longrightarrow \infty \text{ as } \frac{k_2}{k_1} \to \infty \text{ and } \frac{k_3}{k_1} \to \infty \tag{2.62}$$

where the symmetry of Eqs. 2.58 and 2.59 allows the interchanging of k_1 and k_2 in Eq. 2.62. Using the CR form satisfies the need for a dynamic balance of multiple growth and loss terms, with the observation in many natural environments of phytoplankton populations which are well approximated by the "Law of the Minimum" (de Baar, 1994). A further examination of the phytoplankton growth model is undertaken in Chapter 3.

2.5 Model simulation

The model was run to simulate plankton population dynamics in the oceanic mixed layer at Bermuda Station 'S' (32°10′ N, 65°30′ W) and OWS 'India' (59° N, 19° W). Depth and seasonally changing mixing rates (K_z) were simplified to a seasonally varying mixed layer depth (determined using climatic monthly averages (Fasham *et al.*, 1990)), and a fixed exchange rate, D_e [m s^{-1}], with the bottom water. Light was assumed to consist of 41 discrete wavelengths, at 10 nm intervals, from 300 to 700 nm. The spectrally-resolved incoming solar radiation at the top of the atmosphere (Figure 2.3) was attenuated through the atmosphere by the sum of a spectrally-resolved cloudless atmosphere transmission coefficient, τ [airmass^{-1}] (Figure 2.3), and an average attenuation rate characteristic of short-wave radiation through 4 otkas of cloud (Smith and Dobson, 1984). Azimuth angle is a function of latitude, day and hour (Brock, 1981), and is used to determine the intensity of solar radiation at the top of the atmosphere, and the angle (and hence pathlength) of light through the atmosphere. Light scattering in the atmosphere is not considered. At the sea surface, a fraction of the light is reflected, and the rest refracted (Kirk, 1994). The pathlength of the beam through the water

medium is calculated from the refracted angle, and a correction made (Eqs. 2.23-2.26) to account for scattering within the water. Nitrate was assumed to be the only limiting nutrient species, with a concentration below the mixed layer of $N_b = 2$ and 12 mol m^{-3} at Bermuda and OWS 'India' respectively. A summary of all the parameters used to specify environmental conditions appear in Table 2.13.

Pigment concentrations and dimensions of 8 phytoplankton species, and the dimensions, swimming velocity and feeding strategies of 8 herbivores species are summarised in Tables 2.7, 2.8 and Table 2.10 respectively. Size dependent general relationships are also given (Tables 2.11 and 2.12). The model was run with just two phytoplankton species, *Skeletonema costatum* and *Phaeodactylum tricornutum*, and two spherical ($r = 10$ & $20\,\mu$m) herbivores based on general relationships. The phytoplankton species were chosen because of their common use in plankton studies. The cyanobacteria species were not chosen because of the order of magnitude increase in computational time resulting from the very dynamic behaviour of their internal reservoirs of nutrients: a result of having a large surface area to volume ratio. Herbivores based on general relationships were used because of the lack of data on yield and growth rates.

By simplifying K_z to a seasonally varying mixed layer and a fixed exchange rate with the water below the mixed layer, the model equations reduced to a system of ODEs (Fasham *et al.*, 1990). Importantly, the internal properties are not mixed or diluted with the bottom water. Dilution removes cells (changing the number of cells), but not the average property of those cells (for further discussion, see the Chapter 3 continuous culture simulation, which has a similar behaviour).

The ODEs are integrated forward in time using MATLAB with an adaptive step-size, 4th-5th Order Runge-Kutta-Fehlberg integration scheme (Hoffman, 1992) requiring an

Parameter	Symbol	Units	Bermuda	OWS India	Oceanic Range
Mean dissipation of turbulent KE	ϵ	10^3 W m^{-3} = m^2 s^{-3}	10^{-7}		10^{-6} - 10^{-9}
Nitrate below	N_b	mol m^{-3}	2×10^{-3}	14×10^{-3}	$2 - 15 \times 10^{-3}$
Gravity	g	m s^{-2}	9.80665		$\pm$ 0.02
Salinity	S	‰	35		33-37
Cloud fraction	C	otkas	4		0-8
Scattering coef. of water	b_w	m^{-1}	0.05		0.02-0.3
Scattering	g_1	-	0.5		0.29 - 0.58
coefficients	g_2	-	0.2		0.13 - 0.23
Eddy Diffusivity	D_e	m s^{-1}	6.66×10^{-6}		$0.6 - 20 \times 10^{-6}$
Temperature	T	K	293	278	273-298
Molecular diffusivity of NO_3^{-1}	D_N	m^2 s^{-1}	17.27×10^{-10}	13.44×10^{-10}	$9.8 - 19 \times 10^{-10}$
Kinematic viscosity	υ	m^2 s^{-1}	1.085×10^{-6}	1.394×10^{-6}	$1.8 - 0.8 \times 10^{-6}$
Density of water	ρ_{water}	kg m^{-3}	1024.4	1026.6	1030-1000

Table 2.13: Environmental parameters values and range for simulation of Bermuda Station 'S', 32° N and OWS India, 59° N. KE = kinetic energy. References: ϵ (Lazier and Mann, 1989); D_e, N_b (Taylor *et al.*, 1997; Strass and Woods, 1991); υ, D_N (Li and Gregory, 1974); ρ_{water} (Pond and Pickard, 1983); b_w (Kirk, 1994); g_1, g_2 (Kirk, 1991). Refractive index of air/water interface = 1.341 (Kirk, 1994). Fundamental physical constants used (Atkins, 1994): Avogadro constant $A_v = 6.02214 \times 10^{23}$ mol^{-1}; Boltzmann constant $k_B = 1.38066 \times 10^{-23}$ J K^{-1}; Planck constant $h = 6.62608 \times 10^{-34}$ J s; Universal gas constant $R = 8.31451$ J K^{-1} mol^{-1}.

accuracy on all state variables of:

$$\text{Error} < 0.1 \ \min \begin{bmatrix} Q_{1,1}^{max} & \dots & Q_{1,p}^{max} \\ \vdots & \dots & \vdots \\ Q_{n,1}^{max} & \dots & Q_{n,p}^{max} \end{bmatrix} \tag{2.63}$$

Phytoplankton populations were converted to units of mg(pig) m^{-3} by:

$$C_{T,b} = \sum_{j=1}^{p} C_{j,b} A_v P_j V_j \tag{2.64}$$

where $C_{T,b}$ is the total concentration of pigment b due to all phytoplankton cells.

A Bermuda simulation was run for 10 years at which point it had reached a stable annual cycle, and results graphed for years 8, 9 and 10 (Figure 2.12). An India simulation was run for 40 years, without reaching a stable annual cycle. Years 18, 19 and 20 are graphed (Figure 2.13), as they are representative of the small amount of inter-annual variability that persisted throughout the simulation. In both simulations, the populations of *S. costatum* and the 10 μm herbivore persisted, while *P. tricornutum* and the 20 μm herbivore populations became vanishingly small. Interestingly, an India simulation run with only one phytoplankton species, *P. tricornutum* produced a chaotic (or periodicity $>$ 40 years) output, but retained strong annual trends such as the spring bloom.

2.6 Discussion

2.6.1 Choice of plankton interactions

The model equations (Table 2.6) do not contain a number of processes that are typically included in plankton population studies. Fasham *et al.*, (1990), for example, have detrital, dissolved organic nitrogen and bacteria state variables, and include processes of respiration, regeneration and mortality in their description of phytoplankton and zooplankton. Furthermore, theoretically-analysed plankton processes described in the literature, but not utilised in this chapter include: sinking of biological populations, as a function of formation rates of "marine snow" (Jackson, 1995); intra-species interac-

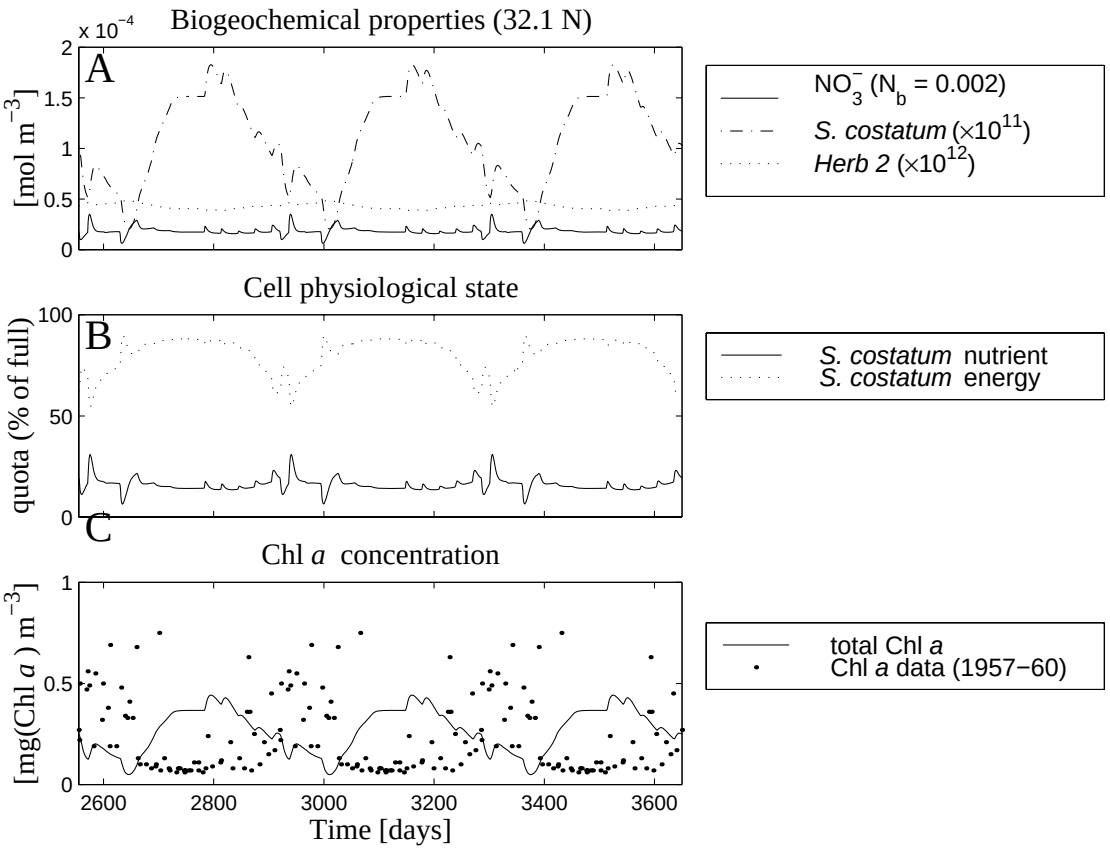

Figure 2.12: Simulation of plankton population dynamics in the oceanic mixed layer at Bermuda (32°N, 65°W), graphing years 8, 9 and 10. A. Nutrient and population dynamics: Nitrate [mol(NO_3^-) m^{-3}]; Phytoplankton [mol(cells) m^{-3}]; Herbivores [mol(cells) m^{-3}]. B. Dynamics of physiological state of organisms, graphing internal nutrient concentration, Q [% of Q^{max}], and energy, q [% of q^{max}]. C. Chl a concentration dynamics (Eq. 2.64). Note from B. that nutrient is always more limiting than light.

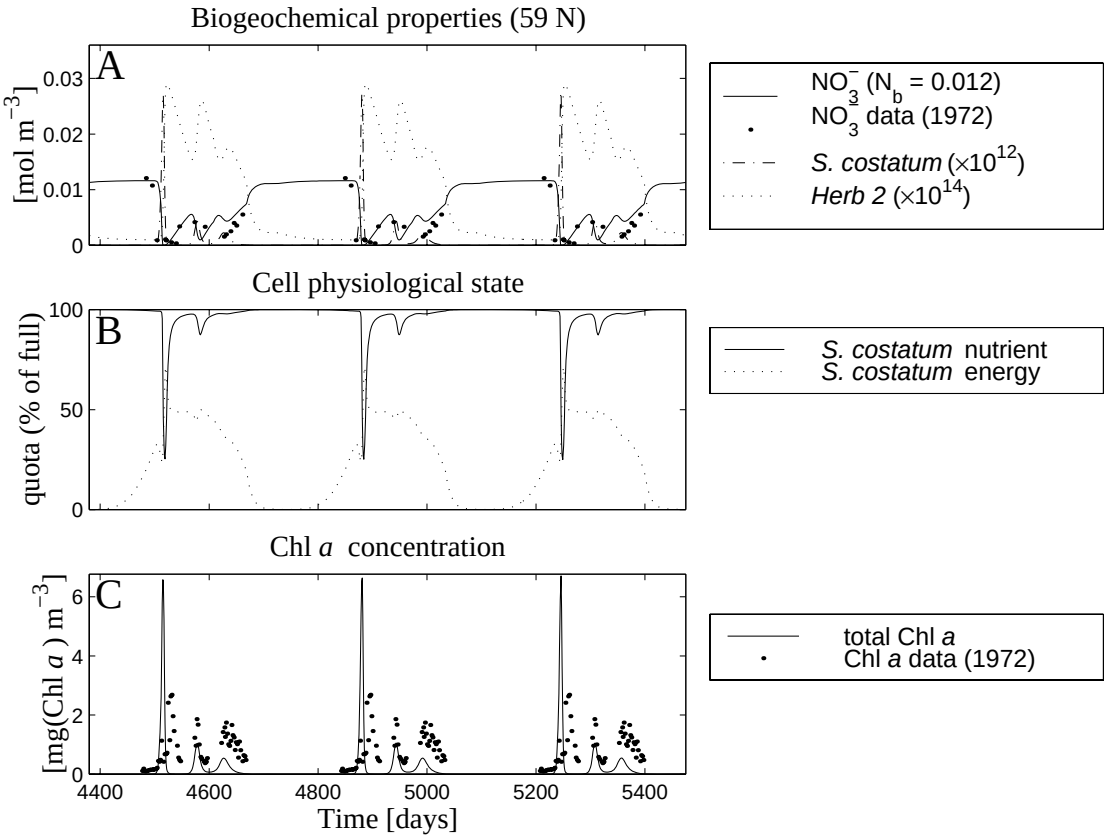

Figure 2.13: Simulation of plankton population dynamics in the oceanic mixed layer at OWS 'India' (59°N, 19°W), graphing years 12, 13 and 14. A. Nutrient and population dynamics: Nitrate [mol(NO_3^-) m^{-3}]; Phytoplankton [mol(cells) m^{-3}]; Herbivores [mol(cells) m^{-3}]. B. Dynamics of physiological state of organisms, graphing internal nutrient concentration, Q [% of Q^{max}], and energy, q [% of q^{max}]. C. Chl a concentration dynamics (Eq. 2.64). Note from B. that light is always more limiting than nutrient, except during the spring bloom.

tions, behaviours, histories or adaptations (McGillicuddy Jr., 1995); action of pathogens (Suttle *et al.*, 1990) or chemical toxicity (Sunda and Huntsman, 1996) on biological populations; scavenging of microscopic organisms by aeration, and transport to the atmosphere (Blanchard, 1989); spatial heterogeneity of plankton populations (Piontkovski *et al.*, 1997); more complicated food chains including carnivores and cannibals (Fasham *et al.*, 1990) or mixotrophs (Raven, 1997); organisation of fluid mixing such as Langmuir cells (Bees *et al.*, 1998); and internal cell processes (Flynn *et al.*, 1997).

Simply, it was decided to include only the most basic and well understood processes required to formulate a plankton population model. Inclusion of processes which could not be constrained by physical laws would make it difficult to assess the value of the theoretical approach adopted in this chapter. For example, a theoretical understanding of mixing and grazing processes allows a reasonable estimate of resulting phytoplankton loss terms. However, estimates of another phytoplankton loss term, cell mortality, is poorly constrained. By not including poorly estimated processes, the simulations assess whether the present theoretical understanding of plankton processes is sufficient to model plankton population dynamics.

2.6.2 Considerations of scale

The model equations have been formulated at the scale of the individual plankton cells. It is not possible to use the theoretical approach of this chapter on larger scales such as phytoplankton biomass. Of course, there are a variety of scales smaller than the cell that could have been chosen (i.e. cell organelles, molecules, atoms ...). A quick comparison follows of the outputs of some of the mechanistic functional forms based on the individual, to the output from functional forms based on a variety of smaller scales.

For light capture, the packaging of pigments into chloroplasts within cells has the potential to decrease light capture compared to the assumed uniform concentration of pigment within the cell. To test this, a hypothetical cell, A, of uniform pigment concentration can be compared to another cell, B, with the same quantity of pigment packaged

into only 1/3 of the cell volume, although this 1/3 is spread evenly throughout the cell. Taking a sphere ($r = 5\ \mu$m) with average Chl a concentration 10^6 mg(Chl a) m^{-3}, analysing a light beam of $\lambda = 435$ nm (Chl a's peak absorbance) and intensity $I_{incident}$ = 100 W m^{-2}: $\overline{\gamma C}_{A,435} = 7.59 \times 10^4$ m^{-1} (Eq. 2.16); $\overline{aA}_{A,435} = 3.04 \times 10^{-11}$ m^{-2} (Table 2.3), so $I_{A,attenuated} = 3.04 \times 10^{-9}$ W (Eq. 2.17). For cell B (which would attenuate light at the same rate as a sphere $r = 5\ \sqrt[3]{1/3}\ \mu$m, average Chl a concentration = 3×10^6 mg(Chl a) m^{-3}), $\overline{\gamma C}_{B,435} = 2.28 \times 10^5$ m^{-1}; $\overline{aA}_{B,435} = 2.36 \times 10^{-11}$ m^{-2} and $I_{B,attenuated} = 2.36 \times 10^{-9}$ W, a 30 % difference. For a sphere, $r = 1\ \mu$m, but otherwise the same parameters as above the difference is only 6 %. The larger, more spherical, more concentrated pigments are within the cell, and the higher $\overline{\gamma C}$, the worse the approximation of uniform pigment distribution becomes. For the purposes of this study, using primarily small phytoplankton cells, and considering light absorbed over the whole photosynthetic band, the choice of the individual as the scale of light capture is sufficient.

For nutrient uptake by diffusion, it has been shown (Berg and Purcell, 1977) that number and distribution of nutrient uptake sites on a cell surface is such that the assumption of uniform cell wall concentration (and hence the individual as the smallest necessary scale) used in calculating nutrient flux is justified for algal cells. For convective fluxes, the correlations used (Table 2.2) are based on whole particles, and can only be used to determine the average convective flux to the whole cell surface.

Choosing the individual as the scale for the "chemical reaction" of growth cannot be verified in as simple manner as for the mechanistic functional forms above. Nonetheless, it allows use of internal reservoirs with mechanistic uptake rates, and appears to capture much of the behaviour of cell populations. Mechanistic functional forms for encounter and sinking rates are clearly based on the assumption that the individual is the relevant scale, and cannot be easily formulated on a different scale. A significant disadvantage of choosing the scale of the individual is that the processes modelled occur at small time scales. For example, it can take only minutes for a phytoplankton cell to become nutrient

saturated, so the maximum time step in the numerical integration must be an equivalent size. Despite the resulting increase in computation time, the individual appears to be a good choice of scale for modelling plankton population dynamics.

2.6.3 The mechanistic functions.

Functions which describe underlying physical mechanisms should provide better estimates of the rates of plankton interactions. Parameters determined in controlled laboratory environments are likely to be both more accurate and more precise than field estimations and, in general, physical parameters can be estimated more accurately and more precisely than biological parameters. When compared to non-mechanistic functional forms, mechanistic functional forms are typically based on a higher proportion of physical parameters than biological parameters. Furthermore, at the chosen scale of the individual cell, the source of parameter values inevitably becomes the laboratory. Since the laboratory environment (such as a chemostat) is still large compared to the organism, laboratory constants for use in mechanistic functional forms are applicable to field environments. This is not necessarily true of physical processes in the ocean, such as mixing, which occurs on a range of scales, some many orders of magnitude bigger than laboratory flows. Ironically, it may turn out that the modelling strategy of using mechanistic functional forms and laboratory-determined constants is better suited to biological models than physical models of the oceans.

From the above arguments, it should be expected that mechanistic functional forms will be more constrained than non-mechanistic functional forms. As an example, the nutrient uptake term (Eq. 2.15) contains three laboratory-determined physical constants (ψ, D and Sh) and one laboratory-determined biological parameter (Q^{max}), while the more commonly applied Michaelis-Menton uptake term (Eq. 2.11) has two field-determined biological parameters (V and K). D is known to three decimal places (Li and Gregory, 1974), ψ is exact for a known cell geometry, and cell geometries for which Sh has been measured or theoretically derived Sh is $\pm$ 10 %. Laboratory measurements of Q^{max} are also likely to be within 10 %. Non-mechanistic, biomass models rely on field estimates

of V and K which have literature values varying by a factor of 5 and 10^4 respectively (Yool, 1997).

Much of the variation in field determined biological parameters such as V is a result of the inability of non-mechanistic functional forms to include explicitly the affects of environmental conditions on the processes they describe (the other main source of uncertainty being sampling logistics). Mechanistic functions allow a more complete description of the effects of environmental factors on plankton than would a biomass model. Examples of this include, (1) the effect of small-scale turbulence being incorporated into nutrient uptake and grazing using Sh and ϕ respectively; (2) the variation in "particle effect" (Kirk, 1994) due to different wavelengths of light in the environment; and (3) the effect of temperature on molecular diffusivity and viscosity being included in nutrient uptake and encounter rates.

Realising the advantages of mechanistic functions relies on the correct application of physical laws, and significantly increased computing power. While computing power is expected to continue to increase, few mechanistic forms have been tailored specifically for plankton population dynamics, and gaps exist in the presented mechanistic model. In particular, the presented mechanistic theory of plankton interaction rates is incomplete for: determination of the encounter rate coefficient, ϕ for non-spherical plankter; Sherwood numbers, Sh, for non-spherical plankter in shear and turbulent flows, and consideration of the effect of swimming methods on the local flow field.

2.6.4 Comparison with data, Fasham *et al.* (1990) and Fasham (1993).

The model presented has similar solar irradiance (albeit spectrally resolved) and mixing functions as Fasham *et al.* (1990) and Fasham (1993). However, while the Fasham models use empirical function forms based on field measured (or estimated) parameters to describe plankton interactions, the presented model uses primarily mechanistic functional forms based on laboratory-determined parameters, sourced from studies performed independently of the modelling exercise. The simplification of the mixing equa-

tions (Eqs. 2.53 and 2.54) to ODEs resulted in a single environment. Given a single environment, it is not surprising that only one species of phytoplankton and herbivore persisted. In the real ocean, light, nutrient and turbulence vary in both the horizontal and vertical directions. The world's oceans contains thousands of plankton species. Simulations with space resolved at least vertically will be required to assess whether a mechanistic model such as the one presented can sustain a large variety of plankton species. Interestingly, another result of using a zero dimensional model was that light capture by phytoplankton cells became independent of either the angle of light propagation through the water column, or the scattering characteristics. This is due to light being 'limiting' only in the winter, when light out of the mixed-layer is small compared to the incident light on the upper surface of the layer, and is only negligibly decreased by an increase in pathlength due to scattering or azimuth angle.

OWS India simulation. The Fasham (1993) model OWS India simulation was compared to data from 1972 (Figure 10 in Fasham (1993)), part of a 5 year time-series (Plymouth Marine Laboratory, 1990a). The 5 year data set showed considerable yearly variation in the size and frequencies of plankton blooms. The presented model (Figure 2.13) and Fasham (1993) appeared to capture much of the behaviour of phytoplankton and nutrient dynamics, although only the simulation run using only one phytoplankton species, *P. tricornutum*, showed significant yearly changes in size and frequency of plankton blooms.

Bermuda simulation. The Fasham *et al.* (1990) model Bermuda simulation was compared to data from 1958-60 (Figure 5 in Fasham *et al.* (1990)). Neither the presented model (Figure 2.12) or the Fasham *et al.* (1990) model captured the seasonal variation in nitrate or phytoplankton population. Both models overestimated the summer chlorophyll concentrations. This may be a result of the existence of a deep-chlorophyll maxima in low latitudes, or horizontal advection associated with the Gulf Stream, phenomena which cannot be modelled with a zero-dimensional model. A change in the Chl *a* :biomass ratio (Taylor *et al.*, 1997) may also be responsible. At Bermuda, where loss

of scalars such as herbivores is less than at OWS India, introduction of an additional loss term to herbivores, such as cell mortality, sinking or vertical migration may improve the simulation. Introduction of such terms into a mechanistic model, however, would require a better understanding of the underlying processes involved.

For the oceanic mixed layer at Bermuda and OWS India the presented model performance was similar to the Fasham models. This result was achieved with a model based on primarily laboratory-determined constants, and a small number of well constrained environmental parameters (Table 2.13). Of the environmental parameters, only the deep water nutrient concentration, $N_{i,b}$, would not be an output of a 3 dimensional coupled atmospheric-ocean turbulent closure mixing model forced by a spectrally-resolved solar radiation algorithm. Considering the variety of oceanic environments, and the costs of field sampling programs, a model based almost entirely on laboratory-determined constants rather than field-determined parameters may be able to justify the significant number of laboratory experiments (to obtain parameters from a wider variety of marine plankton species) and computational overheads (required to run 3 dimensional models), which make such a 3 dimensional mechanistic model simulation more costly than a simple empirical plankton population model simulation.

In conclusion, this chapter has worked towards a plankton population model constructed using mechanistic functional forms only. The mechanistic approach necessitated the modelling of plankton interactions on the scale of individual plankton cells, and inevitably led to the use of laboratory-determined constants. This appears to provide a way around the problem of uncertainties in field-determined parameters and arbitrary choices of functional forms that reduce the predictive power of many plankton models. The model is ideally suited to being coupled to a multi-layer turbulent closure mixing model. Such a coupled model, though computationally intensive, would only require inputs of deep water nutrient concentrations, laboratory-determined constants and an initial variety of plankton species.

Chapter 3

Verification of a phytoplankton growth model using population dynamics and carbon isotope fractionation

---

All this is a dream. Still, examine it with a few experiments.

Michael Faraday

3.1 Abstract

The behaviour of a model of phytoplankton growth developed by analogy with chemical kinetics is investigated. Simulations of populations in batch and diluting mediums exhibit conservation of mass, and give confidence to the model's applicability to describe phytoplankton growth in a variety of environments. A process-based description of the fractionation of stable isotopes of carbon in marine phytoplankton is incorporated into the growth model. Published data from laboratory experiments are used to assess the performance of the growth model at predicting population dynamics and stable isotope fractionation rates. Finally, the growth model is discussed in terms of being a set of governing equations describing phytoplankton growth in a variety of environments and the fractionation of stable isotope as a process-based verification technique.

3.2 Introduction

A variety of models have been used to describe phytoplankton growth in natural environments. Examples include equations based on the multiple of extracellular properties and phytoplankton concentration (Steele and Henderson, 1981; Fasham *et al.*, 1990; Edwards and Brindley, 1996; Taylor and Stephens, 1993; Doney *et al.*, 1996), the extracellular concentration of the most limiting nutrient multiplied by the phytoplankton concentration (Hurtt and Armstrong, 1999; Oschlies and Garçon, 1999), the multiple of internal properties and the phytoplankton concentration (Sharples and Tett, 1994) and the intracellular concentration of the most limiting nutrient multiplied by the phytoplankton concentration (Legovic and Cruzado, 1997; Bissett *et al.*, 1999b). This disagreement over the equations of phytoplankton growth contrasts with the universal agreement over the governing equations of fluid motion (the Navier-Stokes equations) used in ocean circulation models (Denman and Gargett, 1995). Could a set of equations governing all phytoplankton growth behaviour exist ?

Chapter 2 introduced a growth equation based on an analogy with a chemical reaction in a finite volume. This model has the advantage of being derived from fundamental considerations such as conservation of mass, in a similar manner to which the equations of fluid motion are derived. In this paper, the behaviour of the growth model based on chemical kinetics is investigated for use as a set of governing equations of phytoplankton growth in natural environments. Verification will involve investigating population dynamics and carbon isotope fractionation of phytoplankton cells.

It is difficult to verify a phytoplankton growth model directly from field measurements of population size. Estimates of field growth rates based on changing population size (or biomass, concentration etc.) need to consider mechanisms other than growth which change population size. These include turbulent mixing (Sharples and Tett, 1994), aggregation and sinking (Kiørboe *et al.*, 1996), grazing (Dower *et al.*, 1997), viral cell death (Suttle *et al.*, 1990) and natural mortality (Fasham *et al.*, 1990). Considering the uncertainty in estimating these mechanisms in field environments, verification of

phytoplankton growth based on population dynamics is limited to laboratory environments. In experimental cultures, mixing rates are controlled, grazing, viral death and sinking are eliminated, and the growth rate is much greater than the mortality rate. The comparison of the growth model behaviour and population dynamics in laboratory environments (batch, semi-continuous and continuous cultures) is an important technique of model verification. Such techniques, however, have not resolved the disagreement over the governing equations of phytoplankton growth in natural environments.

The fractionation of stable isotopes can also be used to verify a phytoplankton growth model. Stable isotopes fractionate at different rates during phytoplankton growth, depending on the environmental conditions. This results from the interaction of a variety of processes (such as diffusion and biochemical reactions) with different fractionating rates. Laboratory studies of carbon isotope fractionation during phytoplankton growth, both empirical (Laws *et al.*, 1995, 1997; Popp *et al.*, 1998b,a) and mechanistic (Rau *et al.*, 1996; Wolf-Gladrow and Riebesell, 1997), have been relatively successful at predicting carbon isotope fractionation at constant growth rates (i.e. in continuously diluting mediums).

The fractionation of stable isotopes during phytoplankton growth is independent of the mode of death of a phytoplankton cell. Fractionation depends only on the conditions that determine growth (i.e. light, nutrients, temperature, etc.), and the mixing rate of populations with different growth histories. It is therefore more straight forward to verify the performance of the growth equations in the field environment using the fractionation of stable isotopes than measurements of population size.

This paper has two goals: Firstly, to verify as far as possible the growth model based on chemical kinetics (see Chapter 2) by using laboratory population dynamics. Secondly, to include the process of stable isotope fractionation in the growth model, and investigate, with the potential future use of field studies in the back of our minds, the growth model's ability to predict stable isotope fractionation in laboratory studies.

3.3 Model derivation and verification

3.3.1 The growth model revisited

In the hope of making it clearer by less notation, it is worth restating the growth model developed in Chapter 2, assuming light, carbon and nitrogen are the only potentially limiting resources. The equation describing growth becomes:

$$P + m_C Q_C + m_N Q_N + m_I q \xrightarrow{k_p} 2P \tag{3.1}$$

where P is the concentration of phytoplankton cells, Q_C, Q_N and q are the internal concentrations of carbon, nitrogen and energy, and m_C, m_N and m_I are the number of carbon and nitrogen atoms and photons (energy) respectively required to make another phytoplankton cell. The growth model considers four interacting rates: the maximum supply rate of carbon, k_C; the maximum supply rate of nitrogen, k_N; the maximum absorption rate of light, k_I; and a reaction rate of the construction of organic matter, k_p [k_j in Chapter 2]. The actual growth rate of the phytoplankton cell, μ_p, is calculated by the product of the internal reservoirs of the energy, q, carbon, Q_C, and nitrogen Q_N, such that:

$$\mu_p = k_p Q_C Q_N q \tag{3.2}$$

The value of k_p can be calculated from the maximum growth rate of the phytoplankton cell, μ_p^{max}, divided by the maximum internal reservoirs of carbon, Q_C^{max}, nitrogen, Q_N^{max}, and energy, q^{max}:

$$k_p = \frac{\mu_p^{max}}{Q_C^{max} Q_N^{max} q^{max}} \tag{3.3}$$

The supply rate of nutrients (carbon, nitrate etc.,) and light are assumed to be determined by the maximum supply rate (k_C for carbon), and a measure of depletion of nutrients within the cell. The simplest such form gives the overall uptake rate (in this case for carbon) as:

$$\left(\frac{dC}{dt}\right)_{uptake} = k_C \frac{Q_C^{max} - Q_C}{Q_C^{max}} \tag{3.4}$$

and similarly for nitrogen and energy. More complicated functions might include uptake rate being a function (perhaps non-linear) of internal concentrations of other nutrients.

3.3.2 Batch cultures

The simplest application of the growth model is a batch culture, where there are no gains or losses to the system. With $k_N = \psi D_N Sh_N N_N$, $k_C = \psi D_C Sh_C N_C$ and $k_I = \overline{aA}I$ as determined in Chapter 2, the differential equations describing phytoplankton growth in a batch culture become:

$$\frac{dN}{dt} = \underbrace{-k_N \left(\frac{Q_N^{max} - Q_N}{Q_N^{max}} \right) P}_{N\ uptake\ by\ phytoplankton} \tag{3.5}$$

$$\frac{dC}{dt} = \underbrace{-k_C \left(\frac{Q_C^{max} - Q_C}{Q_C^{max}} \right) P}_{C\ uptake\ by\ phytoplankton} \tag{3.6}$$

$$\frac{dQ_N}{dt} = \underbrace{+k_N \left(\frac{Q_N^{max} - Q_N}{Q_N^{max}} \right)}_{N\ uptake} - \underbrace{k_p Q_N Q_C q \left(m_N + Q_N \right)}_{consumption\ for\ growth} \tag{3.7}$$

$$\frac{dQ_C}{dt} = \underbrace{+k_C \left(\frac{Q_C^{max} - Q_C}{Q_C^{max}} \right)}_{C\ uptake} - \underbrace{k_p Q_N Q_C q \left(m_C + Q_C \right)}_{consumption\ for\ growth} \tag{3.8}$$

$$\frac{dQ_q}{dt} = \underbrace{+k_I \left(\frac{q^{max} - q}{q^{max}} \right)}_{light\ capture} - \underbrace{k_p Q_N Q_C q \left(m_I + q \right)}_{consumption\ for\ growth} \tag{3.9}$$

$$\frac{dP}{dt} = \underbrace{+k_p P_j q_j Q_N Q_C}_{growth} \tag{3.10}$$

A simulation of a simple batch culture using Eqs. 3.5 - 3.10 is given in Fig. 3.1. A fundamental requirement of any description of a batch culture is that the total amount of nitrogen in the culture does not change. Fig. 3.1 shows that as nitrogen moves from the extracellular fluid, N, into cell reservoirs, Q, and then into phytoplankton organic matter, P, the total amount of nitrogen in the system does not change. Assuming unlimiting

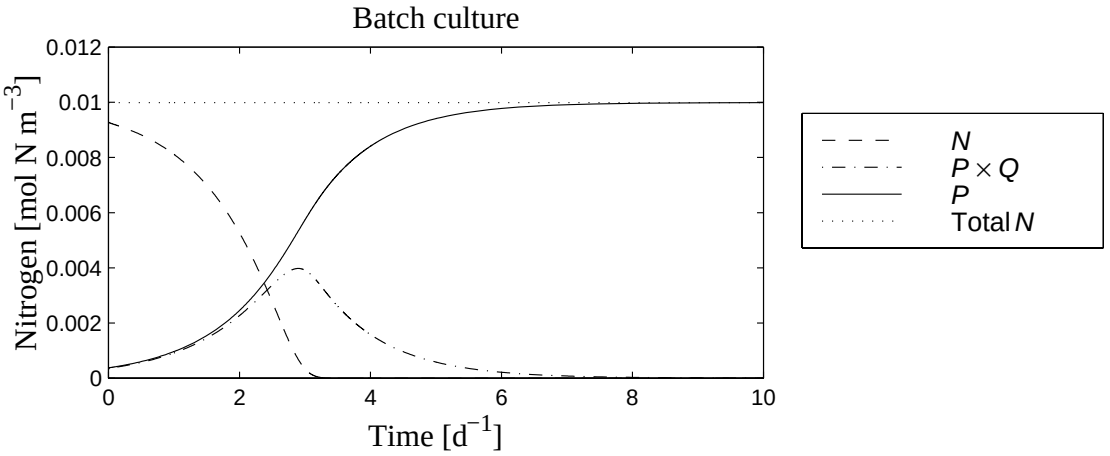

Figure 3.1: Simulation of a batch culture (Eqs. 3.5 - 3.10), assuming unlimiting carbon ($Q_C = Q_C^{max}$) and light ($q = q^{max}$). Extracellular nutrient, N, total intracellular nutrient, $Q \times P$, and total organic nitrogen, P. The total nitrogen in the batch culture, Total $N = N + QP + P = 0.01$, is conserved.

light, the final population size is limited by the nutrient whose initial concentration divided by its stoichiometry coefficient, m, is the least:

$$\text{final population} = \min\left[\frac{N_{in}}{m_N}, \quad \frac{C_{in}}{m_C}\right] \tag{3.11}$$

The rate at which it reaches the final population is determined by the interaction of rates k_N, k_C, k_I and k_p.

3.3.3 Continuous cultures

In a continuously diluting medium, nutrient is added at a rate of:

$$\left(\frac{dN}{dt}\right)_{dilution} = \mathcal{D}\left(N_{in} - N\right) \tag{3.12}$$

and phytoplankton removed at a rate of:

$$\left(\frac{dP}{dt}\right)_{dilution} = -\mathcal{D}P \tag{3.13}$$

where $\mathcal{D}$ is the dilution rate [s^{-1}] and N_{in} is the concentration of N in the dilutant [mol m^{-3}]. In Chapter 2 it was proposed that the mixing of internal reservoirs of nutrients in all environments occurs according to the product of the population size and internal reservoir concentration. Using the forward-time space-centred (FTSC) integration scheme, where 1 is the water body concerned, and 0 and 2 are the water with which it mixes, n is the present time, and $n+1$ one time step forward, this becomes:

$$P_1^{n+1}Q_1^{n+1} = P_1^nQ_1^n + K_z\left(\overbrace{+P_0^nQ_0^n}^{\text{into 1 from 0}} \underbrace{-2P_1^nQ_1^n}_{\text{lost to 0 and 2}} \overbrace{+P_2^nQ_2^n}^{\text{into 1 from 2}}\right) \tag{3.14}$$

where K_z is the mixing rate. In a continuous culture, where 0 is the dilutant, and 2 is the out flow, there is no exchange of fluid from 2 to 1, or 1 to 0. Furthermore, the dilutant (0) contains no phytoplankton. With the mixing rate, K_z, replaced by the dilution rate, $\mathcal{D}$, Eq. 3.14 reduces to:

$$P_1^{n+1}Q_1^{n+1} = P_1^nQ_1^n + \mathcal{D}\left(\underbrace{-P_1^nQ_1^n}_{\text{lost to 2}}\right) \tag{3.15}$$

which reduces to:

$$Q_1^{n+1} = (1-\mathcal{D})P_1^nQ_1^n/P_1^{n+1} \tag{3.16}$$

but since $P_1^{n+1} = (1-\mathcal{D})P_1^n$, $Q^{n+1} = Q^n$. So there is no change in internal reservoirs as a result of dilution. Conceptually this must be the case: if you have a population of cells in a diluting medium, all with the same internal properties, dilution will change the total number of cells, but not the average internal properties.

The total concentration of a nutrient in a continuous culture at steady-state is determined by the concentration of the nutrient in the source fluid, N_{in}, only:

$$N_{in} = N + PQ + P \tag{3.17}$$

The sharing of nutrient amongst the extracellular fluid, N, stored internal nutrient, Q, and phytoplankton organic matter, P, depends on the interaction of supply and

consumption rates. So, for example, in a continuous culture with low light levels, the majority of the nitrogen will be in the extracellular fluid. For a nitrogen limited culture, the majority will be held as organic matter.

A simulation of two continuous culture using Eqs. 3.5 - 3.10, 3.12 and 3.13 is shown in Fig 3.2. The simulations are based on phytoplankton cells with the same rates of nutrient uptake, light capture, and phytoplankton growth rate, but with different initial conditions. Nonetheless, both simulations reached the same steady-state, as would be expected.

3.3.4 Semi-continuous cultures

A third laboratory environment to test the growth equation on is a semi-continuous culture: dilution occurs like in a continuous culture, but the dilution rate varies periodically. The equations are same as for a continuous culture, but with a time varying dilution rate, $\mathcal{D}$. The experiments of Caperon (Caperon, 1968, 1969) (Fig. 3.3) for a semi-continuous culture show the presented model captures much of the behaviour of phytoplankton growth under varying growth conditions.

3.3.5 Fractionation of stable isotopes of carbon

The model presented above uses the interaction of the rates of nutrient uptake, light capture and organic matter construction to predict growth rate. Another phenomena that is influenced by these interacting rates is stable isotope fractionation. Stable isotope fractionation may therefore provide a good tool for the verification of the presented growth model.

Isotope compositions are specified as δ values (Farquhar *et al.*, 1982):

$$\delta(‰) = (\mathrm{R_{sample}}/\mathrm{R_{standard}} - 1) \times 1000 \tag{3.18}$$

where $\mathrm{R_{sample}}$ and $\mathrm{R_{standard}}$ are the abundance ratios of the heavier to lighter isotope of the sample and the standard (usually PDB) respectively. The isotopic fractionation of

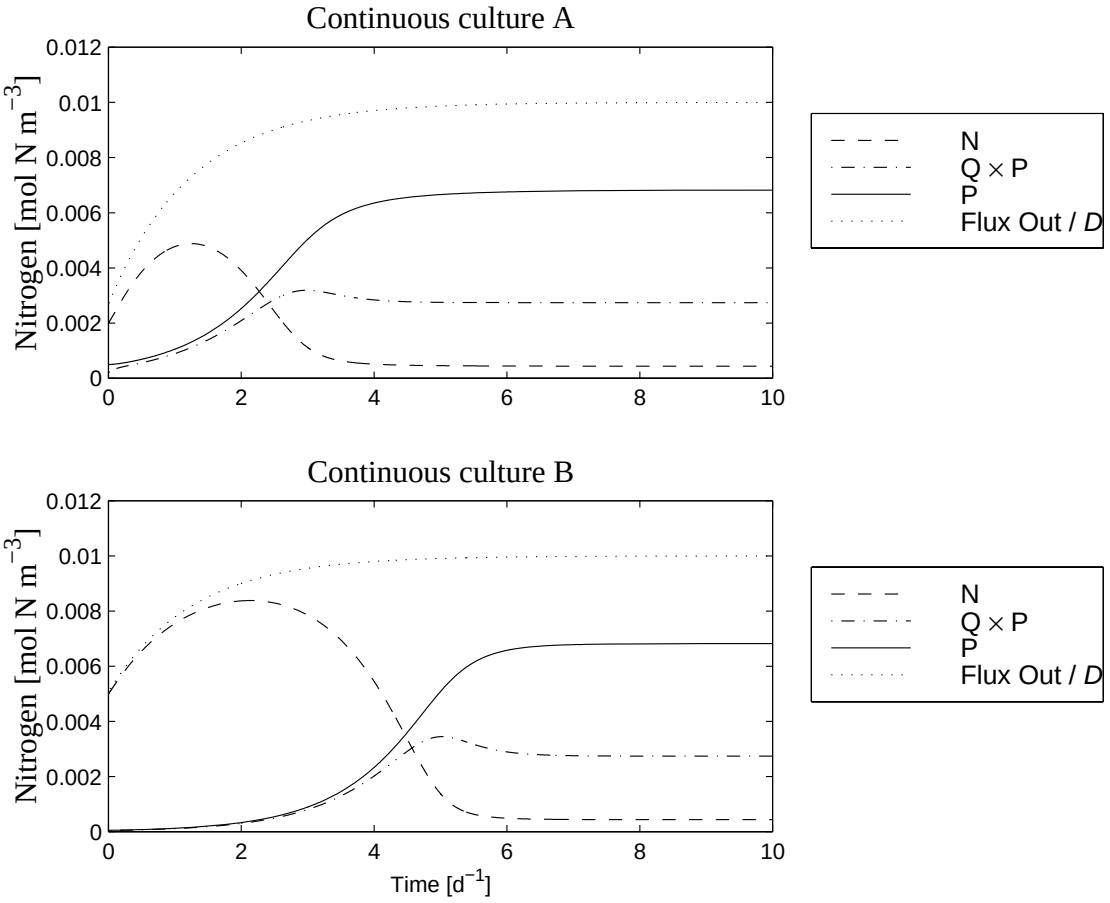

Figure 3.2: Two simulations of continuous cultures using the same equations as for the batch simulation (Eqs. 3.5 - 3.10), and including the dilution of N (Eq. 3.12) and P (Eq. 3.13), assuming unlimiting carbon (i.e. $Q_C = Q_C^{max}$). N - Extracellular nutrient, Q_N - intracellular nutrient, P - population. Initial conditions of culture A were: $N = 0.02$ mol N m^{-3}, $Q = 2 \times 10^{-13}$ mol cell^{-1}, $P = 10^9$ cell m^{-3}; and of culture B: $N = 0.05$ mol N m^{-3}, $Q = 2 \times 10^{-13}$ mol cell^{-1}, $P = 10^8$ cell m^{-3}. The flux of nitrogen into the culture is equal to $N_{in}\mathcal{D}$. Note how both simulations reach the same steady-state with a flux out equal to the flux in.

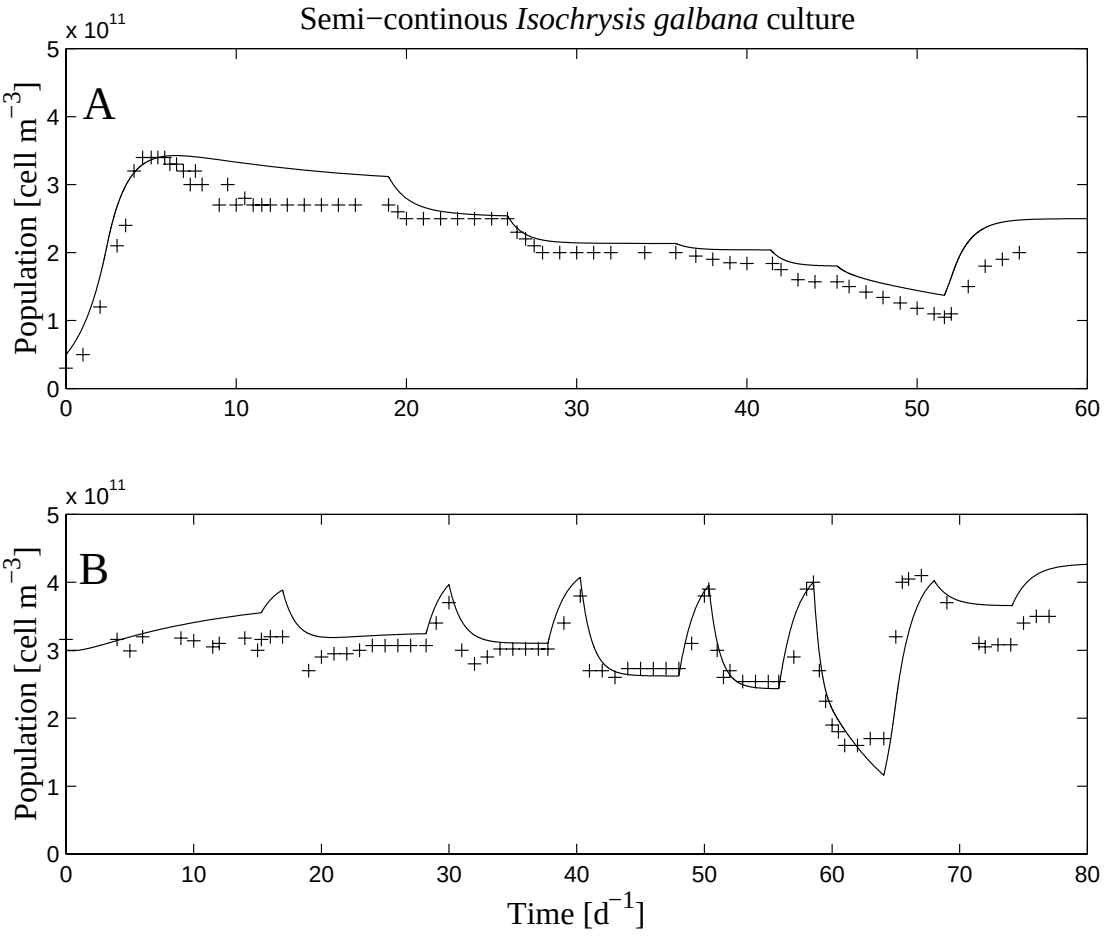

Figure 3.3: Comparison of laboratory data of *Isochrysis galbana* grown in a semi-continuous culture conditions (Caperon, 1968, 1969) with that predicted by Eqs. 3.5 - 3.14, assuming unlimiting carbon and light ($Q_C = Q_C^{max}$, $q = q^{max}$). In his experiments, Caperon varied the dilution rate, resulting in the observed changes in cell numbers. Although the cells were obtain from a common culture, Caperon tuned his model by varying the growth rate, maximum internal and minimum internal nitrate concentrations. No such 'tuning' was undertaken in the model results given above. *Isochrysis galbana* was assumed to be a prolate ellipsoid (radii $= 3.5 \times 1.9 \times 1.9 \mu$m, $\mu^{max} = 0.7$ d^{-1}, $Q_N^{max} = 2.55 \times 10^{-4}$ mol N cell^{-1}), and $k_N = 2.7236 \times 10^{-14}$ m^3 s^{-1} (see Chapter 2). (A) $N_{in} = 8.65 \times 10^{-3}$ mol m^{-3}, and initial conditions of $Q_N = 2.55 \times 10^{-4}$ mol N cell^{-1}, $N = 8.65 \times 10^{-3}$ mol m^{-3} and $P = 50 \times 10^9$ cell m^{-3}; (B) $N_{in} = 8.65 \times 10^{-3}$ mol m^{-3}, and initial conditions of $Q_N = 0.255 \times 10^{-4}$ mol N cell^{-1}, $N = 10.9 \times 10^{-3}$ mol m^{-3} and $P = 300 \times 10^9$ cell m^{-3}.

a process, $\epsilon_{process}$, is defined by:

$$\epsilon_{process} = 1000 \times (1 - \mathrm{R_{product}}/\mathrm{R_{source}}) = \frac{\delta_{\mathrm{source}} - \delta_{\mathrm{product}}}{1 + \delta_{\mathrm{source}}/1000} \tag{3.19}$$

Phytoplankton growth involves processes with different isotopic fractionation. With a knowledge of the fractionation rate of individual processes, and their position in the chain of reactions that describe phytoplankton growth, the total fractionation rate of phytoplankton growth can be calculated.

Fractionation by molecular diffusion. The heavier, ^{13}C isotope diffuses slower than ^{12}C. Along a concentration gradient from a non-zero concentration to a zero concentration, the rate of isotopic fractionation in seawater is $\epsilon_d = 0.7$ °/₀₀. That is, the molecular diffusivity flux of ^{12}C is 0.07 % faster than ^{13}C. For a steady concentration gradient from c_e to c_i (where $c_e > c_i$), the flux is determined by the interaction of the rate removing molecules at c_i, and the diffusion rates of both isotopes. Now only a component of the flux is dependent on the diffusion rate, and the resulting isotopic fractionation is given by (Farquhar *et al.*, 1982):

$$\epsilon_{c_e \to c_i} = \frac{c_e - c_i}{c_e} \epsilon_d \tag{3.20}$$

Fractionation by Rubisco. Photosynthetic cells convert CO_2 into glucose. The glucose is then used, with other atoms like nitrogen, phosphorus and iron, to create organic molecules. The process of converting CO_2 into glucose, facilitated by the enzyme Rubisco, proceeds faster for ^{12}C than ^{13}C. The resulting fractionation, ϵ_{Ru}, varies with algal species. For Rubisco isolated from marine eukaryotic algae $\epsilon_{Ru} = 25 - 29$ °/₀₀ (Korb *et al.*, 1998), while for Rubisco isolated from the cyanobacteria *Synechococcus* sp., $\epsilon_{Ru} = 21.5$ °/₀₀ (Popp *et al.*, 1998b). Assuming equal concentrations of $^{13}CO_2$ and $^{12}CO_2$ within a cell (i.e. diffusion to the enzyme site is unlimiting), the flux of ^{12}C will be $(\epsilon_{Ru}/10)$ % faster than ^{13}C. If transport to the enzyme site does become limiting, the overall fractionation rate for the combined process of transport and enzyme reaction will become a function of the fractionation rate of both processes, and the rate at which they proceed.

Overall fractionation by diffusion followed by Rubisco. The overall fractionation rate of carbon isotopes by phytoplankton cells, ϵ_p, is calculated using the above model of phytoplankton growth, and initially assuming that light and nitrogen are unlimiting ($q = q^{max}$, $Q_N = Q_N^{max}$). A mass balance similar to that used by Farquhar *et al.* (1982) for terrestrial plants, and applied to marine phytoplankton by Rau *et al.* (1996) is used. Since internal reservoirs are used in the growth model, they will be used instead of the internal concentrations used by Farquhar *et al.* (1982) and Rau *et al.* (1996) to determine fractionation rates. The relevant measurement of phytoplankton fractionation is relative to the surrounding fluid. This is most easily obtained by assuming equal abundance of the isotopes in the extracellular fluid.

$$^{13}\mathrm{C} = {}^{12}\mathrm{C} = C \tag{3.21}$$

The maximum supply rate of carbon, k_C, is a function of the diffusion shape factor for the cell, ψ, the molecular diffusivity of the carbon isotope, D, the conversion rate of HCO_3^- to CO_2 in the boundary layer, and, in the case of passive diffusion, the cell wall permeability, $\mathcal{P}$. Since the carbon molecules must diffuse through the boundary layer and then the cell membrane (i.e. not simultaneously), an effective conductance, $\mho$, of carbon transport through the boundary layer and cell membrane can be defined:

$$\frac{1}{\mho} = \frac{1}{\psi(1 + r/r_k)D} + \frac{1}{A_s\mathcal{P}} \tag{3.22}$$

where A_s is the surface area of the cell, r is the radius of a sphere with the same surface area of the cell, and $r_k \approx 2.06 \times 10^{-4}$ m is the reacto-diffusive length for the conversion of HCO_3^- to CO_2 (Rau *et al.*, 1996), and the difference in effective conductance of the ^{13}C and ^{12}C isotopes is given by:

$$^{13}\mho = \left(1 - \frac{\epsilon_d}{1000}\right) {}^{12}\mho \tag{3.23}$$

The supply rate of carbon isotopes ^{13}C and ^{12}C, ^{13}J and ^{12}J respectively, assuming a dependence on nutrient status of the cell given by Eq. 3.4, can be written:

$$^{13}J = {}^{13}\mho^{13}\mathrm{C}\,(1 - Q^*) \tag{3.24}$$

$$^{12}J = {}^{12}\mho^{12}\mathrm{C}\,(1 - Q^*) \tag{3.25}$$

where the $Q^* = Q_C/Q_C^{max}$, and the ratio of $^{13}Q^*/^{12}Q^*$ is only 2 % different (Farquhar *et al.*, 1982) from the ratio of $^{13}\mathrm{C}/^{12}\mathrm{C}$, so Q^* can be considered the internal concentration of both ^{13}C and ^{12}C. As noted above, Q^* was used instead of c_i in Farquhar *et al.* (1982) and Rau *et al.* (1996). In the case of passive diffusion, $Q^* = c_i/c_e$, and there is little difference between using Q^* or c_i.

The conversion of aqueous CO_2 into glucose occurs before the reaction used to describe the formation of organic matter (Eq. 3.1). At this point, the supply rate of other nutrients and light are assumed to be unlimiting. Under these assumptions, the balance between the conversion of aqueous CO_2 into glucose is the same as the balance between rate of organic matter construction and carbon uptake. The fluxes of ^{13}C and ^{12}C can now be calculated as a function of Q^* as:

$$^{13}J = {}^{13}\mu^{max} m_C Q^* \tag{3.26}$$

$$^{12}J = {}^{12}\mu^{max} m_C Q^* \tag{3.27}$$

where m_C is the stoichiometry coefficient for carbon. The difference in biochemical rates of the two isotopes is given by:

$$^{13}\mu^{max} = \left(1 - \frac{\epsilon_{Ru}}{1000}\right) {}^{12}\mu^{max} \tag{3.28}$$

Eqs. 3.26 and 3.27 do not balance loss and gain terms to intracellular reserves. An additional term is required to account for the sharing internal resources amongst offspring. This additional term is small, however, for stored intracellular aqueous car-

bon. For example, using the Rau *et al.* (1996) model's base values, dissolved carbon $= \mu c_i V = 4.85 \times 10^{-20}$ mol C cell^{-1} which is small compared to the carbon held as structural material $= 1.76 \times 10^{-11}$ mol C cell^{-1}. For isotopes of nutrients such as nitrate, which are actively taken up, and are stored at concentrations of the same order of magnitude as they are held in organic matter, the sharing amongst offspring is an important term.

Solving for ^{13}J from Eqs. 3.24 and 3.26, and using the assumption that $^{13}\mathrm{C} = {}^{12}\mathrm{C} = C$:

$$^{13}J = \frac{^{13}\mho C}{1 + \frac{^{13}\mho C}{^{13}\mu^{max} m_C}} \tag{3.29}$$

and similarly for ^{12}J. The overall rate of carbon fractionation for phytoplankton growth, ϵ_p, is given by:

$$\epsilon_p = \frac{^{13}J}{^{12}J} = \frac{^{13}\mho C}{^{12}\mho C\left(1 + \frac{^{13}\mho C}{^{13}\mu^{max} m_C}\right)} + \frac{\frac{^{12}\mho C}{^{12}\mu^{max} m_C}}{^{12}\mho C\left(1 + \frac{^{13}\mho C}{^{13}\mu^{max} m_C}\right)} \tag{3.30}$$

Now:

$$\frac{^{13}\mho C}{^{12}\mho C\left(1 + \frac{^{13}\mho C}{^{13}\mu^{max} m_C}\right)} = \frac{^{13}\mho}{^{12}\mho}(1 - Q^*) = \epsilon_d (1 - Q^*) \tag{3.31}$$

and:

$$+\frac{\frac{^{12}\mho C}{^{12}\mu^{max} m_C}}{^{12}\mho C\left(1 + \frac{^{13}\mho C}{^{13}\mu^{max} m_C}\right)} = \frac{^{13}\mu^{max} m_C}{^{12}\mu^{max} m_C} Q^* = \epsilon_{Ru} Q^* \tag{3.32}$$

So from Eq. 3.30, ϵ_p becomes:

$$\epsilon_p = \epsilon_d (1 - Q^*) + \epsilon_{Ru} Q^* \tag{3.33}$$

As an alternative notation, biochemical fractionation can be denoted by ϵ_b. This is more appropriate than, for example, ϵ_{Ru}, if a Rubiscohas not been shown to the the source of all intracellular fractionation.

Eq. 3.33 is mathematically similar to the formulation presented by Farquhar *et al.* (1982) for carbon fractionation in terrestrial plants, which Rau *et al.* (1996) applied to

marine phytoplankton and can be written:

$$\epsilon_p = \epsilon_d \frac{c_e - c_i}{c_e} + \epsilon_b \frac{c_i}{c_e} \tag{3.34}$$

where c_e and c_i are the partial pressure of CO_2 in the leaf stomata Farquhar *et al.* (1982) or the internal concentration of $CO_{2(aq)}$ in phytoplankton cells Rau *et al.* (1996).

Fractionation in a continuous culture

In a continuous culture at steady-state, the phytoplankton growth rate ($\mu = \mu^{max} Q^*$) is equal to the dilution rate, $\mathcal{D}$. The value of Q^* required in Eq. 3.33 is given by:

$$\mu^{max} Q^* m_C = k_C (1 - Q^*) = \mathcal{D} m_C \tag{3.35}$$

ϵ_p can be found by substituting Q^* into Eq. 3.33. This is numerically the same as the Rau *et al.* (1996). Given that $k_C = \mho C$ (Eq. 3.25), Q^* is given by:

$$Q^* = 1 - \frac{\mathcal{D} m_C}{\mho C} \tag{3.36}$$

Substituting Eq. 3.36 into Eq. 3.33:

$$\epsilon_p = \epsilon_{Ru} - (\epsilon_{Ru} - \epsilon_d) \frac{\mathcal{D} m_C}{\mho C} \tag{3.37}$$

Popp *et al.* (1998b) [1] observed that at low values of μ/C, there was a linear relationship between ϵ_p and μ/C. At steady-state in a continuous culture, $\mu = \mathcal{D}$, so ϵ_p vs. μ/C will be a line beginning at ϵ_{Ru}, with a slope equal to $-(\epsilon_{Ru} - \epsilon_d) m_C/\mho$, where m_C is the stoichiometry coefficient of the carbon in the phytoplankton cell, or cellular carbon, and $\mho$ is the effective conductivity, and is proportional to the surface area (Wolf-Gladrow and Riebesell, 1997). Therefore, Eq. 3.37 would suggest that the slope of ϵ_p vs. μ/C

[1] The Popp *et al.* (1998b) experiments were nitrate limited, although the above definition is based on unlimiting nitrate. Strangely, in a chemostat where the growth rate, or $k_p qQ$, is set, different nutrients and energy supply rates do not interact, so as long as they are sufficient to sustain growth at the dilution rate. This will not be the case in batch and semi-continuous cultures. This behaviour highlights the strengths (and limitations) of the chemostat environment for assessing growth and fractionation models.

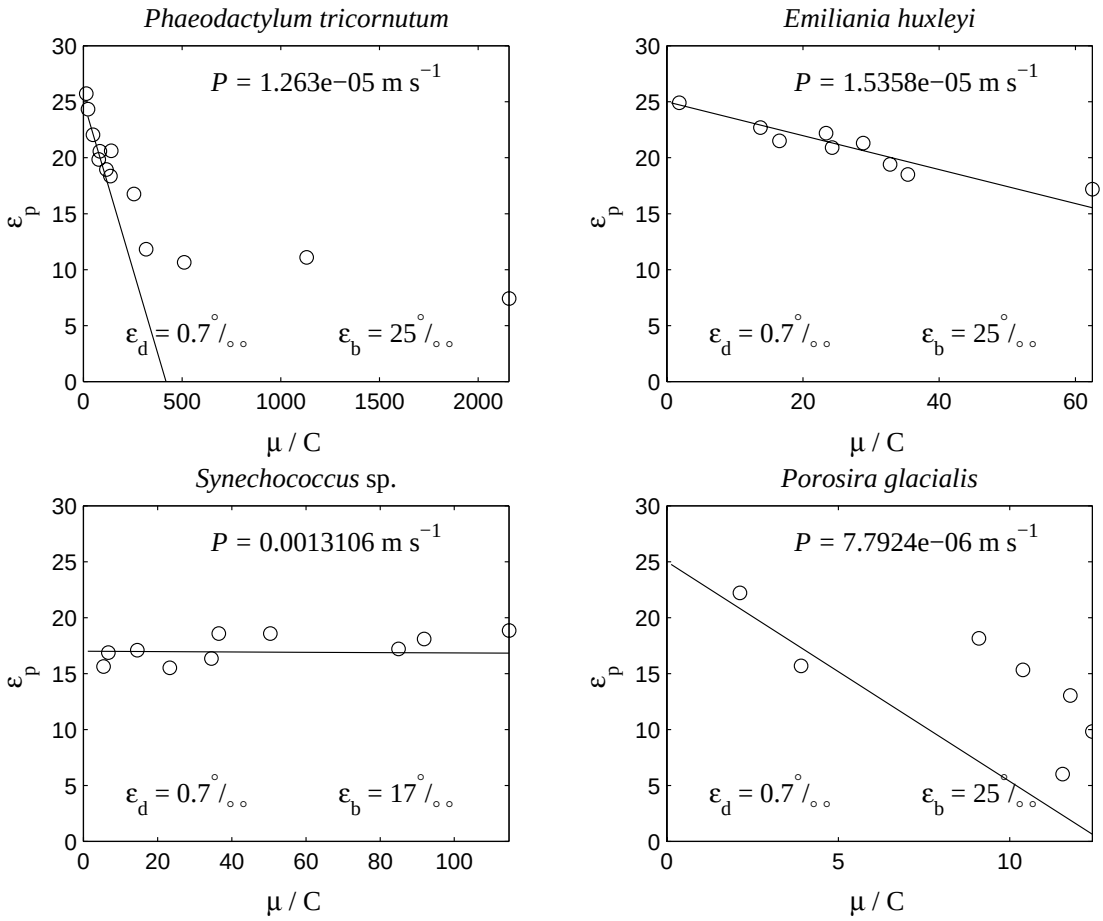

Figure 3.4: Measured (∘) and predicted (-) using Eq. 3.37 carbon isotope fractionation for phytoplankton cells, ϵ_p, at a given μ/CO_2 for *P. tricornutum* (Laws *et al.*, 1997), *E. huxleyi* (Bidigare *et al.*, 1997) *Synechococcus* sp. (Popp *et al.*, 1998b) and *P. glacialis* (Popp *et al.*, 1998b).

should itself be a negative, linear function of cellular carbon to surface area ratio, as has been found to be the case (Popp *et al.* (1998b), Fig. 2c).

The predicted ϵ_p (Eq. 3.37) and slope of ϵ_p vs. μ/C can then be compared to laboratory measured ϵ_p and slope of ϵ_p vs. μ/C (Popp *et al.*, 1998b) of four phytoplankton species (Fig. 3.4). It is difficult, however, to use this comparison to verify the fractionation predicted by the growth model, because the value of the cell wall permeability, $\mathcal{P}$ - an important parameter in the determination of the conductivity, $\mho$ - was not determined during the experimental procedure. To illustrate the behaviour of the model, cell

wall permeability is calculated for each species from the measured slope of ϵ_p vs. μ/C (Fig 3.4). The calculation is given by:

$$\mathcal{P} = \frac{1}{A_s \left[\frac{\frac{d\epsilon_p}{d(\mu/C)}}{-(\epsilon_{Ru} - \epsilon_d)\, m_C} + \frac{1}{\psi\,(1 - r/r_k)\, D} \right]} \tag{3.38}$$

The values of $\mathcal{P}$ calculated for each species, given in Fig. 3.4, appears reasonable (Rau *et al.* (1996) uses a value of 10^{-4} m s^{-1}). A definite test of the above theory, however, would required independent determination of $\mathcal{P}$ for each species.

The Laws *et al.* (1997) experimental investigation of *Phaeodactylum tricornutum* showed a deviation from the linear relationship between ϵ_p and μ/C at higher values of μ/C. As μ/C increases, growth becomes more 'diffusion limited', with the associated decrease on fractionation rates (as $\epsilon_{Ru} > \epsilon_d$). The deviation observed by Laws *et al.* (1997) is towards higher ϵ_p at a particular μ/C than predicted by the linear relationship. One possible explanation for this phenomena is the supply of carbon via a route other than passive CO_2 transport. Two possible mechanisms are the active uptake of CO_2, and the uptake of HCO_3^-, which has been suggested by Korb *et al.* (1998) and Thompson and Calvert (1995) amongst many others. The fractionation rate must be between ϵ_{Ru} and ϵ_d. If Eq. 3.37 gives a value less than ϵ_d, this implies that passive diffusion is not sufficient to supply the demand on growth, and an another mechanism must be responsible for carbon uptake.

Fractionation in a non-continuous culture

In a non-continuous culture, such as a batch environment or the natural environment, the fractionation rate is not steady, and cannot be solved for in the simple manner presented above. Ideally, the changing concentrations of each isotope in the extracellular fluid, intracellular reservoirs and organic matter should be modelled through time (Laws *et al.*, 1998). This involves solving the batch equations for each isotope. The sets of equations are coupled by the dependence of nutrient uptake and growth rate on the

combined internal nutrient of all isotopes.

Unfortunately, no laboratory experiments were found to directly test the growth model using carbon isotope fractionation in a non-continuous medium. Thompson and Calvert (1994, 1995) looked at carbon fractionation in batch cultures at a range of conditions, but only took one sample per experiment, during what they called the late phase of exponential growth. Exponential growth, by definition, is when the population change is proportional to the present population. For exponential growth, the growth model requires that the product Q^*q^* remain constant:

$$\mu = \mu^{max} Q^* q^* = \text{constant} \tag{3.39}$$

or

$$Q^* = \frac{\text{constant}}{\mu^{max} q^*} \tag{3.40}$$

At low irradiance, q^* approaches 0, Q^* approaches 1, and according to Eq. 3.40 and Eq. 3.33 ϵ_p should approach ϵ_d. Thompson and Calvert (1994, 1995), however, find that ϵ_p increases at low irradiance. What assumption in the construction of the theory could account for this discrepancy between theory and measurement ? It may be a result of assuming a single step reaction for the formation of growth (Eq. 3.1). Qualitatively, let's consider construction of organic matter to be a two stage processes: first photons and carbon are combined, and then growth rate is determined from the interaction of the supply rate of fixed carbon (and other nutrients) and the rate of construction of organic matter. Again this results in the conclusion that at low irradiance, ϵ_p should approach ϵ_b, contrary to Thompson and Calvert (1994, 1995). However, considering a third step, the transport of fixed carbon to the site of organic matter construction, low irradiance results in high internal CO_2, but low fixed carbon. Since the transport of fixed carbon to the reaction is by diffusion, the slower the rate, the greater closer the overall fractionation approaches that of the diffusion rate. Hence, low ϵ_p occurs at low irradiance. An understanding of the paths of internal diffusion would be required to test this line of thinking.

Interestingly, although the single-step internal reaction was insufficient to explain carbon fractionation at low light levels, it still explains growth rates. This is consistent with an internal transport limitation. Since transport limitation and growth rate are both a function fixed C, they can be combined as an effective internal reactivity, much in the in same manner in which the processes of diffusion to the cell surface, and then though the cell membrane, are combined into an effective conductance. Therefore, in terms of growth, internal carbon transport limitation and low light levels would look the same, but in terms of isotope fractionation, they would give different results.

3.4 Discussion

3.4.1 The growth model

This paper corrects a mistake made in Baird and Emsley (1999) and a number of other models of phytoplankton growth that include stored nutrients. In all environments, the average internal nutrient and energy reservoirs of a population will be depleted by three effects: (1) stored nutrient being turned into organic matter due to growth; (2) sharing of internal reservoirs of nutrient amongst offspring as a result of division; and (3) mixing of populations of different amounts of stored nutrient. In the case of a continuously diluting medium, (3) is zero. This result has not been clearly presented before. Typically, (2) has been ignored (Caperon, 1969; Sharples and Tett, 1994). The theoretical error has not been picked up before because model verification has been limited to continuously diluting mediums, where (2) has not been taken into account, and internal reserves have erroneously been mixed at the dilution rate, $\mathcal{D}$. Since at steady-state in a continuously diluting medium, growth is equal to the dilution rate, the error in (3) cancels the error of ignoring (2), and the overall description of the population dynamics is quantitatively correct. However, should this same model be applied to an environment with populations of cells with different internal reservoirs and/or varying mixing rates, these errors will not cancel, and the model will contain a mass imbalance. Interestingly, Bissett *et al.* (1999b) avoids the mass imbalance described above by considering internal nutrient as a ratio to cellular carbon (although the Bissett *et al.* (1999b) model does not allow the

carbon per cell ratio to vary).

A stark contrast between the models of ocean circulation and models of plankton population dynamics in natural environments is that, in general, physical oceanographers all use the same basic set of equations, while biological oceanographers do not (Denman and Gargett, 1995). This is not because a simple, easily solved set of equations perfectly describe ocean circulation. Physical oceanographers use an approximation of the full solution of fluid motion (the Navier-Stokes equations). They make two standard approximations (the Boussinesq and hydrostatic approximations), to derive the so-called the primitive equations (Gill, 1982), which are used in virtually all advanced models of ocean circulation. Does this paper present a comparable set of equations based on approximations which could gain universal agreement ?

The growth model developed in Chapter 2 is based on a mass balance, assuming simple reaction dynamics within a finite, well mixed volume (i.e. a cell). To arrive at the Eqs. 3.5 - 3.10, the following approximations were required: (1) 100 % efficiency in the construction of organic matter (for comparison, Chapter 2 relaxes this assumption); (2) a single-step reaction in the formation of organic matter from intracellular reservoirs (Eq. 3.1); (3) the uptake rate is a linear function of the emptiness of the internal reservoirs of that particular nutrient (Eq. 3.4); (4) growth rate is a linear function of the internal light and nutrients (Eq. 3.2); and (5) rate coefficients, such as k_C, k_p and $\overline{aA}$ and properties of the cell such as volume, and maximum internal reservoirs do not change during a life cycle, or across generations. It may turn out that some of these approximations are not sufficient to obtain realistic phytoplankton growth rates in natural environments. In this case, a model based on fewer (or more realistic) assumption will need to be developed from the complete set of equations. In part, this is why the analogy to chemical kinetics is appealing. Physical chemists have been required to describe complex chemical reactions, and have developed methodologies for determining the full set of equations. For example, a more general description of the rate of construction of

organic material (in this case of the potentially light and nitrogen limited) is given by:

$$\mu_p = k_p Q_N^{n_1} q^{n_2} \tag{3.41}$$

where n_1 and n_2 are coefficients. n_1 and n_2 could be found experimentally, or, if an understanding of the biochemical reactions is sufficient, Eq. 3.41 can take the form of a mechanism-based rate expression (Brauner and Shacham, 1996). Given the complexity of evolved processes, it would not be surprising to find n_1 and n_2 in Eq. 3.41 to vary with species and the ecological niche to which they are adapted. Whatever the complexity of Eq. 3.41, it is clearly no more complex than the biochemical reactions that drives it, which are modelled using equations like Eq. 3.41.

The presented growth equation is formulated at the scale of the individual cell, but mass is conserved at the population scale as well. The Navier-Stokes equations used to describing fluid motion can also be formulated on a range of scales. Notably, when used to model ocean circulation, the primitive equations cannot resolve phenomena at scales smaller than the grid size of the simulation. For example, it is only recently that mesoscale eddies have been resolved by using higher resolution ocean circulation models: resolving eddies required improving the resolution, but not changing the equations. In the same way, the growth model applied at the population scale cannot resolve individual cells life cycles, or environmental histories. If the model is applied to one cell, however, initially $P = 1$ cell, and Eq. 3.1 represents the growth of an individual cell. A failing of Eq. 3.1 at the individual (and therefore also the population scale) is that it doesn't consider the growth and division of the cell to be different processes. This could be formulated as:

$$P + m_N Q_N \xrightarrow{k_{p_1}} P + \widetilde{P} \xrightarrow{k_{p_2}} 2P \tag{3.42}$$

where $\widetilde{P}$ is organic matter within a cell that has been constructed and is being stored, k_{p_1} is rate of formation of organic matter within a cell and k_{p_2} is the rate of actual division of a cell. In such a scheme, k_{p_2} would be equal to 0 if $\widetilde{P} < P$, and is large when $\widetilde{P}$ approaches P. Eq. 3.42 is significantly more complicated to use than Eq. 3.1, although

it may not in fact increase the usefulness of the model. In particular, it is anticipated that the formation of organic matter, rather than the actual division processes will be the rate limiting step (i.e. $k_{p_2} >> k_{p_1}$). The dynamics of the growth of a population over a number of generations may be well approximated by the much simpler Eq. 3.1.

The growth model presented can not be considered a complete description of phytoplankton growth. However, its formal derivation does provide a framework upon which agreement on a phytoplankton growth model may be achieved. Specifically, it will be through assessment of the unambiguous assumptions upon which the derivation is undertaken, rather than comparison with a particular data set, that an agreement (or otherwise) on a single set of equations describing growth will be found.

3.4.2 Field verification of process-based ecosystem models

An exciting aspect of developing a growth model that predicts stable isotope fractionation in semi-continuous and batch environments, is its application to verifying process-based models in natural environments. Process-based models quantify the fluxes between state variables, yet the verification of models is often restricted to the change in the state variable (Fasham *et al.*, 1990; Steele and Henderson, 1981). However, the change in state variables (such as phytoplankton concentration) is usually the result of a number of processes. If a mismatch in model and field data is establish, it may still not be possible to determine the model process which was in error. If, instead, the individual processes can be tested, strengths and weaknesses of the model derivation are more effectively identified. An example of testing of an individual process, rather than the state of a model, is given by Bissett *et al.* (1999a). Their simulation of carbon and nitrogen fluxes in surface waters resolved apparent and inherent optical properties. As a result, the performance of the equations describing light capture by the phytoplankton could be assessed directly from field measurement of optical properties, rather than relying on the state variables of carbon and nitrogen, which are only indirectly related to optical properties through the growth of photosynthetic organisms. In the same way, stable isotope fractionation offers a test of the equations describing growth of phytoplankton cells, without being

affected by the other factors that impact on the state of the phytoplankton population, such as mortality, sinking, grazing etc. Eventually, this may lead us to be able to not only verify our growth models using stable isotopes, but to use these verified models to reconstruct from sedimentary isotope records the paleo-environments under which the phytoplankton cells lived.

3.4.3 Conclusion

The growth model presented in Chapter 2, based on theoretical considerations, and a number of basic assumptions, explained many of the features of phytoplankton population dynamics and carbon fractionation in laboratory environments. The inclusion of fractionation in the growth model introduces the possibility of verification in natural environments, and that agreement may be reached on the governing equations of phytoplankton growth.

Chapter 4

Discussion

Hypotheses non fingo [I frame no hypothesis].

Isaac Newton

This thesis makes no hypothesis about plankton population dynamics. Instead, it derives a theoretical framework under which plankton populations dynamics can be studied. The example of models of planetary motion given in Chapter 1 demonstrates that theoretical frameworks can have advantages over those obtain by empirical methods alone. As Albert Einstein wrote (Pais, 1982):

"*We now know that science cannot grow out of empiricism alone, that in the constructions of science, we need to use free invention which only a posteriori can be confronted with experience as to its usefulness ... In the nineteenth century, many still believed that Newton's fundamental rule, 'hypothesis non fingo' should underlie all healthy natural science*".

The model presented in Chapter 2 is full of examples of free invention, obtained from a selection of the physical sciences. They are 'free' in the sense that they were developed independent of the problem they are used to solve. For example, the Laplace equation, used to solve for the diffusion shape factor for nutrient uptake (see Appendix B, Table 2.1 and Eq. 2.7), was originally developed to describe electrostatic problems, and has been

applied to mass and heat transfer phenomena. The derivation of equations independently of any quantitative observations of the phenomena being modelled is fundamental to meet Einstein's requirement that a model's usefulness should be assessed only *a posteriori*, or after, the theoretical work. In today's scientific world, this approach most commonly occurs in multi-disciplinary research.

A biological example of 'free' invention, followed by an assessment of its usefulness, is Darwin's theory on the origin of species by natural selection. It is true that his work was inspired by observation. However, the realisation of the causal link between the chances of survival and the origin of species was not based on empirical methods. In his own words (Darwin, 1859):

"*But the mere existence of individual variability and of some few well-marked varieties, though necessary to as the foundation of this work, helps us but little in understanding how species arise in nature*".

In fact, Darwin came upon his theory by considering the mechanisms of survival:

"*If such [variations] do occur, can we doubt (remembering that many more individuals are born than possible survive) that individuals having any advantage, however slight, over others, would have the best chance of surviving and of procreating their kind ? On the other hand, we may feel sure that any variation in the least degree injurious would be rigidly destroyed. This preservation of favourable variations and the rejection of injurious variations, I call Natural Selection.*".

Darwin's theory is based on the existence of three processes: preservation of favourable variations over injurious ones, the passing on off traits from one generation to the next, and that many more individuals are born than survive. Darwin goes on to use his theory to explain variability within populations, and eventually the origin of new species. So we see the processes of deriving a mechanistic model, and then only after the theoretical derivation is complete testing it's usefulness, has been applied in a number of the natural

sciences.

So why have ecological modellers failed to use a mechanistic modelling approach ? The answer, almost certainly, is illustrated in the length and complexity of Chapter 2. Even for the most mechanistically simple ecological system, the work required to construct a theoretical framework independent of observations is daunting. The rest of this discussion looks first at a number of the descriptions of plankton interactions used in Chapter 2, suggesting where further progress is likely in deriving more exact equations. Secondly, techniques of verifying the model equations are discussed. Thirdly, the discussion looks briefly at some of the non-linear behaviour of the model plankton system. And finally, the use of the model in forecasting biogeochemical cycles is discussed.

4.1 Theoretical discussion of equation derivation

Chapter 2 worked towards a mechanistic model of plankton population dynamics. However, it did not achieve this goal. The presented model contains some empirical approximations, and worse still, some heuristically derived functional forms. The discussion sections of Chapters 2 and 3 assessed the usefulness of the functional forms within the model primarily by comparison to laboratory experiments. This section points out where further understanding of the cell interactions may be applied to develop a more mechanistic model, and from which fields of study this knowledge may be sourced.

4.1.1 Nutrient uptake

Chapter 2 clearly divides the extracellular and intracellular nutrient uptake processes, and solves for the wall concentration of the nutrient which links the two processes. The extracellular transport processes are dealt with in a mechanistic fashion. Intracellular processes, however, are modelled heuristically.

One example of a more complex model of intracellular nutrient transport is provided by Flynn *et al.* (1997). Flynn *et al.* (1997) uses a series of empirical and heuristic equations to describe the biochemical processes involved in the uptake of nitrate and

ammonia. A mechanistic representation of these processes is impractical at the moment, due to our limited knowledge of complex biochemical reactions. Nonetheless, it will be through process-based models, like Flynn *et al.* (1997), that the simplistic representation of intracellular uptake processes used in Chapter 2 can be improved.

4.1.2 Light capture

The model of light capture used in Chapter 2 assumes that the absorbing constituents within a layer of fluid are well mixed, and that the paths of a large number of photons can be described by a single path, which losses photons in proportion to the final destination that photons are found to reach by numerical experimentation. Such numerical experiments are undertaken using Monte Carlo techniques (Kirk, 1981). This appears to be realistic, and the method of following every photon so computationally expensive, that it does not seem that an alternate approach will be used in the near future.

The term $\left(\frac{q_j^{max}-q_j}{q_j^{max}}\right)$ in the light capture equation (Eq. 2.28) determines the interaction of light uptake with the energy, q_j, already in the cell. This does not include photoadaptation or photoinhibition, which have been both described (Geider and Osbourne, 1992), and dynamically modelled (Geider *et al.*, 1996). Since photoadaptation involves the changing of the concentration of pigments within a cell (Geider *et al.*, 1996), it requires an additional state variable (for each pigment), and the absorption cross-section of a cell, $\overline{aA}$, will become a function of photoadaptive state.

4.1.3 The growth equation

The growth equations developed in Chapter 2, and further studied in Chapter 3, simplify complex biochemical reactions to a simple interaction of the supply and consumption of elements and photons. This does not include even a basic approximation of internal enzyme kinetics, found in every plankton model cited in this thesis. I believe many authors have introduced complex processes like enzyme kinetics before a satisfactory framework had been established to capture the interaction of supply and growth processes. Many authors use a rectangular hyperbola to describe the process of nutrient

uptake (Eq. 2.6) based on the assumption that nutrient uptake is the result of a single enzyme reaction, fitting the simplest know mechanistic formulation for an enzyme reaction (Eq. 2.11). This uptake term is then coupled to a multiplicative (MP) or law of the minimum (LM) growth term. But because the MP and LM forms do not consider the interaction of supply and consumption terms, all supply terms must saturate (otherwise the growth rate would be infinite at infinite nutrient concentration). The simple enzyme reaction (Eq. 2.11) does saturate, and is therefore commonly used. However, whether enzyme saturation is the cause of growth limitation is not clear. I suspect that an artificially low saturation level of enzyme reactions is used is fit the growth behaviour of phytoplankton to a structure which assumes simple enzyme kinetics and a unsaturating growth term. In effect, this is using Eq. 2.6 with parameters measured from populations instead of using Eq. 2.11 parameterised from enzyme concentrates.

Including enzyme reactions would make the model more complete. Enzyme (and other biochemical) reactions can be reintroduced into the model presented in Chapter 2 by changing the growth equation (Eq. 2.29) into a multi-step, non-linear reaction. By incorporating biochemical reactions within the growth equation, the interaction between supply and consumption rates is maintained. In fact, the need for this to describe the fractionation of stable isotopes of carbon during phytoplankton growth was suggested in Chapter 3. To construct a more complex set of growth equations will require a better understanding of the biochemistry of phytoplankton cells. Again, Flynn *et al.* (1997) provides an example of a model which has included enzyme reactions, and there is a huge literature describing biochemical reactions (for example, Dixon and Webb (1979)).

One particular assumption used in the derivation of the growth equations that could be relaxed is the assumption that cell volume remains constant during growth. Assuming constant cell volume allows the coefficients used in the calculation of supply rates of nutrient, ψ, and light, $\overline{aA}$, and of encounter rates, ϕ, and sinking rates, C_D, to remain constant. Constant volume also allows the reaction rate of growth to be a function of the number of molecules per cell, rather than per volume (i.e concentration), which is more

commonly used in chemical kinetics. By allowing volume to change during the growth of cell, individual life histories of cells will be more closely modelled.

It would require only a small adaptation of the presented equations to include the change in volume on ψ, $\overline{aA}$, ϕ, and C_D, and to revise the growth equation to account for the changing in volume on intracellular concentrations. However, the increased computations required to recalculate ψ, $\overline{aA}$, ϕ, and C_D for changing volumes, and to have the required resolution of life stages within the population, makes this exercise impractical. The use of subpopulations (i.e. individuals within a populations at different life cycle stages) is limited by computational power, rather than model derivation.

4.1.4 Encounter rate

The modelling of particle, and to a greater extent organism, encounter rates in a fluid is limited by our knowledge of small-scale processes, especially in a turbulent environment. This has been highlighted recently by theoretical work on particle encounter rates (Brunk *et al.*, 1998). The theoretically-derived equations used to calculate the encounter rate induced by turbulent shear (using equations from Jackson (1995) summarised in Table 2.5, and originally from the theory of Saffman and Turner (1956)) are based on the assumption that the turbulent velocity gradient surrounding a particle is persistent, and that the hydrodynamic and inter-particle interactions (van der Waals attraction and electrostatic double-layer repulsion) between particles are small. In a theoretical analysis, supported by experimental evidence, Brunk *et al.* (1998) showed that the assumptions of a persistent turbulent velocity gradient and negligible inter-particle forces could result in an over-estimate of encounter rates. Brunk *et al.* (1998) found that removing the assumption of a persistent turbulent velocity gradient, and instead scaling the turbulent coagulation rate constant with the Kolmogorov time and particle radius, produced a turbulent coagulation rate constant of 8.62 ± 0.02, as opposed to 10.35 found using the Saffman and Turner (1956) theory applied in Table 2.5. Furthermore, Brunk *et al.* (1998) found the inclusion of particle interactions could reduced the coagulation rate constant by an additional 50 %.

4.1.5 Summary of future theoretical work

The presented model can be improved in two main ways. Firstly, processes which are modelled heuristically or empirically or not at all (such as more levels within the model such as viruses, bacteria, carnivores etc.), need to be modelled mechanistically. In some cases, such as aggregation of particles (Kiørboe *et al.*, 1996) and the transfer of viral particles (Murray and Jackson, 1992), this derivation is already well developed. For other processes, such as internal biochemical reactions, or the swimming behaviour of organisms, this seems a long way off. In this thesis, we have provided mechanisation as an end goal, to which we have headed as far as possible. The field or plankton population modelling, and more particularly biogeochemical modelling, is looking for predictive models. That a complete mechanistic model may seem impossible, does not detract from the increased predictive capabilities likely to be achieved by pursuing such a goal.

Secondly, mechanistically-derived equations with simplistic assumptions can be re-derived with more realistic assumptions. As an example, the calculation of the coagulation rate illustrates that mechanistically derived equations can have different levels of complexity. Using the definitions in Chapter 1, both the Saffman and Turner (1956) theory used in (Table 2.5) and the Brunk *et al.* (1998) theory are mechanistically derived. So why do they give different answers ? Simply, the Saffman and Turner (1956) theory assumes environmental conditions which, being an approximation of the environmental reality, introduce error. Future theoretically work, even on those equations which seem well grounded in physical principles, may improve the model theoretically, and its predictive capabilities as well.

4.2 Analysis of techniques for verification of plankton population models

The verification of the presented model's performance has been intentionally limited primarily to the laboratory verification of individual processes, such as encounter

rate (Figs. 2.8 and 2.9), and measures of the rates of processes, such as stable isotope fractionation (Chapter 3). By not using field data in the derivation of the model, any simulation run of a non-laboratory community (Figs. 2.12 and 2.13) is a forecast. This contrasts with models such as Hurtt and Armstrong (1999) and Fasham *et al.* (1990) who attempt to verify their models based on field data, some of which had been used to parameterise the model (in the case of the Hurtt and Armstrong (1999) model, this was seen as the ideal method of parameterisation). Using field data describing the state of the system alone, however, cannot resolve the performance of individual components of the model. Given the limited amount of field data on state variables such as nutrient concentrations, the verification based on state variables only may also be quite limited.

The work of Bissett *et al.* (1999a), which uses optical properties to test their model's ability to capture the dynamics of phytoplankton light capture, illustrates the advantages of using measures of the rate of processes to verify a model's field performance. As Bissett *et al.* (1999a) point out, this gives them a large number of highly measurable variables by which to test the model. Furthermore, they are able to diagnose weaknesses in specific parts of the model, to determine where more theoretical work is required. It is also worth pointing out that verification using state-variables is dependent on our ability to characterise the state of the whole system (i.e. all state variables simultaneously), while process-based verification does not require as complete a knowledge of the system (for example, knowledge of optical properties of phytoplankton is sufficient to test phytoplankton light capture equations). In plankton modelling, where knowledge of nutrient and non-pigmented cell concentration is very difficult to obtain over space and time, process-based verification has very significant advantages.

Chapter 3 extends our ability to use process-based verification techniques, by incorporating stable isotope fractionation in the phytoplankton growth model. The measurement of stable isotope fractionation in living plankton, as well as those in sediments, potentially allows verification of the equations describing phytoplankton growth in field simulations. Careful consideration of isotope fraction in herbivores (and in more com-

plex models, other levels of the food chain) may allow the process-based verification of animal grazing, ingestion and growth rates.

In summary, verification is the process of determining the usefulness of a model. It cannot be over-emphasised that data that is used to constructed the model should not be used to test it, as done systematically by Hurtt and Armstrong (1999), and partially by other authors (Fasham *et al.*, 1990; Steele and Henderson, 1981). Such models (especially Hurtt and Armstrong (1999)) provides nothing more than a format for summarising field data sets. Furthermore, the use of state-variables from field data sets alone to verify models is limited by the expense of ocean sampling programs, and their ability to describe a complete ecosystem over time and space. Process-based verification, both in the laboratory and the field does not have the same restrictions. I expect process-based verification to dominate the verification of process-based biogeochemical models, especially those of systems, such as plankton populations, where quantifying the state of the whole system is unfeasible.

4.3 Scaling in the model

Chapter 1 introduced the need for global, decadal predictions of primary productivity. Yet to satisfy the assumptions under which the model has been constructed, time is scaled to cellular processes (minutes), biomass is scaled to species, and length is scaled to volumes with equal mixing rates. This represents a several orders of magnitude increase in computation compared to the Steele and Henderson (1981) and Fasham *et al.* (1990) models. This section briefly outlines the resolution of biomass, time and length required by the presented model, and discusses its implications for running global simulations of plankton population dynamics.

4.3.1 Biomass scale

There are tens of thousands of species of plankton in the ocean. In one particular region, however, the biomass is generally dominated by one, or perhaps a few, phytoplankton groups. For example, Zubkov *et al.* (1998) found a changing picoplankton

community structure along a Atlantic transect from 50°N to 50°S. For much of the transect, however, the picoplankton was dominated by one of two groups of cyanobacterium: *Prochlorochoccus* or *Synechococcus*. Alternatively, rather than using an assemblage of identified species, it may turn out that species parameterisation is more representative of the plankton community if size-based relationships are used. Using either identified species, or size-based relationship, it is quite likely that global primary productivity simulations will require less than 10 species, perhaps as few as 4 (such as a cyanobacterium, a blue-green algae, a diatom, and a herbivore, or a 1, 5, and 10 μm phytoplankton cell, and a 10 μm herbivore).

4.3.2 Time scale

The time between integration steps in the Steele and Henderson (1981) and Fasham *et al.* (1990) models is around a day. For the process-based model of Bissett *et al.* (1999b), and the model presented in Chapter 2, integration steps are around a couple of minutes. Equations based on individuals must have time scales equivalent to the processes individuals undertake. For example, in Chapter 2, the phytoplankton cells can saturate in nitrogen in only minutes, and must be numerically solved using equivalent sized time-steps. However, since variations of this time-scale are not important for annual global productivity forecasts, can we solve for Q and q directly, reducing the number of state-variables by 2 per phytoplankton species, and perhaps increase the time between integration steps ?

Eqs. 2.58 and 2.59 solve for the growth rate of phytoplankton, k_3Qq, directly, as a function of N (k_1) and I (k_2) only. If the solution of Eqs. 2.58 and 2.59 were used in Table 2.6, there would be no need for the differential equations for Q and q. By reducing the number of state-variables, the number of calculations may be reduced. However, there are significant computational costs in solving for Q and q directly. To determine the value of k_3Qq required solving two non-linear simultaneous equations (Eqs. 2.58 and 2.59), a computationally expensive processes is its own right. It is worth noting that the equation for Q only has P in the mixing term, and does not have H in it, while q has P

in the mixing and light capture terms. As a result, there is only a weak coupling between Q and q and N, P and H, which will not significantly reduce the integration time step. The mixing term has a larger timescale (the POM circulation model, for example, is stable with 15 minute time steps) than the biological processes, and so does not reduce the time-step required for integration. It is therefore not clear whether using Eqs. 2.58 and 2.59 instead of the differential equations for Q and q would save computational time.

The loss of model integrity by solving for Q and q directly is significant. The nutrient and light history of a cell is lost, because the value of Q and q is dependent only on the present values of N and I, rather than the values of Q and q at the last time point. The loss of the history of Q and q would not allow the use of resources obtained in one location (such as nutrient obtain at the bottom of the mixed layer, or light from the euphotic zone) or time (such as energy obtained during the day) for growth when the resources aren't available.

In summary, the benefits of using Eqs. 2.58 and 2.59 instead of the differential equations for Q and q in Table 2.6 are questionable, and the costs significant.

4.3.3 Space scale

The space scale required for the model is limited by the scale at which mixing rates vary significantly. Ocean circulation models have the same limitation for space resolution. In the vertical direction, this is of the order of metres in the surface ocean, and hundreds of metres in the deep ocean. In the horizontal direction, the resolution will determine the features observed. Coarse resolution models (say 5° grid) will resolve basin scale circulation, while mesoscale eddies can be resolved with 1/3° meridional and 2/5° zonal resolution (Oschlies and Garçon, 1999). The effect of small-scale turbulence on plankton, which is many orders of magnitude smaller than the spatial resolution, is parameterised by the mean dissipation rate of turbulent kinetic energy, ϵ. This parameterisation is also used by turbulent closure mixing models (such as the POM and MOM) as a closure term.

4.3.4 Summary of scale discussion

Plankton models, like all models of biogeochemical processes, are being resolved at smaller and smaller scales as speed of computers increases. While the presented model certainly demands high resolution time, space and biomass scales, present plankton populations models are employing these scales anyway (Bissett *et al.*, 1999b).

The resolution of time, space and biomass chosen always represents a trade-off of between the three, as a result of finite computing power. The final choice of resolution will depend on the application of the model.

4.4 Complex behaviour in plankton models and populations.

Complex non-linear behaviour can affect our ability to simulate natural phenomena. In particular, chaotic behaviour, given uncertainty in initial conditions, limits the ability to predict time evolving characteristics of a system. Chaotic behaviour in deterministic models is characterised by sensitivity to initial conditions, while exhibiting coherent global properties such as period-doubling and attractors (for a basic text on chaos in dynamical systems see Ott (1993)). The dynamics of even extremely simple ecological models can exhibit chaotic behaviour (May, 1987). Plankton population models, as well as natural plankton populations, have the potential to exhibit chaotic behaviour, affecting our ability to predict population dynamics.

4.4.1 Complex behaviour in plankton models

It has been demonstrated (Edwards and Brindley, 1999; Yool, 1997; Edwards and Brindley, 1996; Truscott and Brindley, 1994) that simple plankton population models can exhibit complex behaviour. These studies have focused on the existence of limit cycles in unforced systems, particularly of predator-prey interactions during numerical simulations. A limit cycle is the periodic oscillation of state variables. The method of investigation used by the above authors has been to vary parameters values, while

keeping forcing functions constant, and look for steady oscillations in the output. The simple empirical models of plankton population dynamics used by the above authors have parameter values obtain from field data. The range of field-determined parameters values in the literature is usually quite large (for example, Edwards and Brindley (1999) found literature values of the grazing half-saturation coefficient of between 0.02 - 0.1 g C m^{-3}). This gives a wide range of parameters values to search for complex behaviour.

Edwards and Brindley have found oscillations in the Steele and Henderson (1981) model, with both a linear (Edwards and Brindley, 1999) and quadratic (Edwards and Brindley, 1996) zooplankton mortality term. Yool (1997) found equivalent oscillations in the more complex Fasham (1993) model. Neither Yool nor Edwards and Brindley, however, found chaotic behaviour. Edwards and Brindley searched the parameter space of the Steele and Henderson (1981) model for two common routes to chaos: period-doubling of limit cycles and saddle foci, without success. Given the failure of both Edwards and Brindley and Yool to find chaotic behaviour, it may be that simple NPZ plankton models do not exhibit chaotic behaviour. A complete search of parameter space would be necessary to confirm this.

4.4.2 Periodic behaviour in the presented plankton model

Fig. 4.1 shows the trajectories in phase-space of an unforced simulation with one phytoplankton species, *S. costatum*, and a $r = 10\mu$m herbivore species. The simulation reached steady state values at $N = 1.78 \times 10^{-3}$ mol m^{-3}, $P = 8.95 \times 10^{-15}$ mol m^{-3} and $H = 1.65 \times 10^{-16}$ mol m^{-3}. Short-term oscillations with a period around 20 days can be observed (Fig. 4.2).

A lengthy examination of the dynamics of the unforced model in phase-space has not been undertaken because the model's development is not complete, and any conclusions may be premature. However, the presented model is even less likely than the Steele and Henderson (1981) and Fasham *et al.* (1990) model's to exhibit chaotic behaviour because (1) the herbivore loss rate is approximately equal the phytoplankton loss rate,

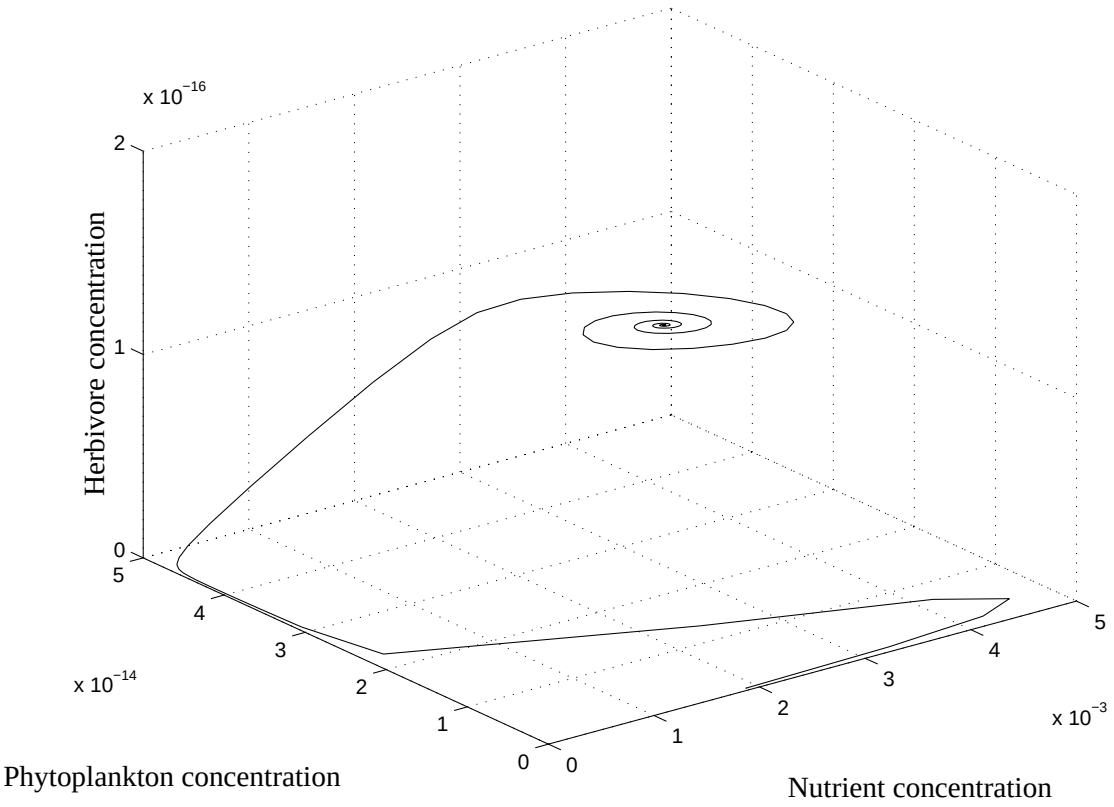

Figure 4.1: Phase space trajectories of an unforced simulation.

both being primarily due to mixing and (2) rather than a rectangular hyperbola, a linear particle encounter rate equation is used.

4.4.3 Complex behaviour in natural populations

Under some circumstances, short-term oscillations can exist in natural plankton populations (Plymouth Marine Laboratory, 1990a; Ryabchenko *et al.*, 1997). However, chaotic behaviour has not been observed in natural plankton populations. Nonetheless, plankton populations are coupled to ocean circulation and climate dynamics. What appears to be environmental noise at the scale of plankton populations, may be feedbacks from chaotic behaviour of environmental variables. The experimental data required to find chaotic behaviour in natural populations is presently unavailable, although data collected in the next decade from the SeaWiFS satellite, which measures global chlorophyll concentration, may reveal complex behaviour not observed from ship-board measurements.

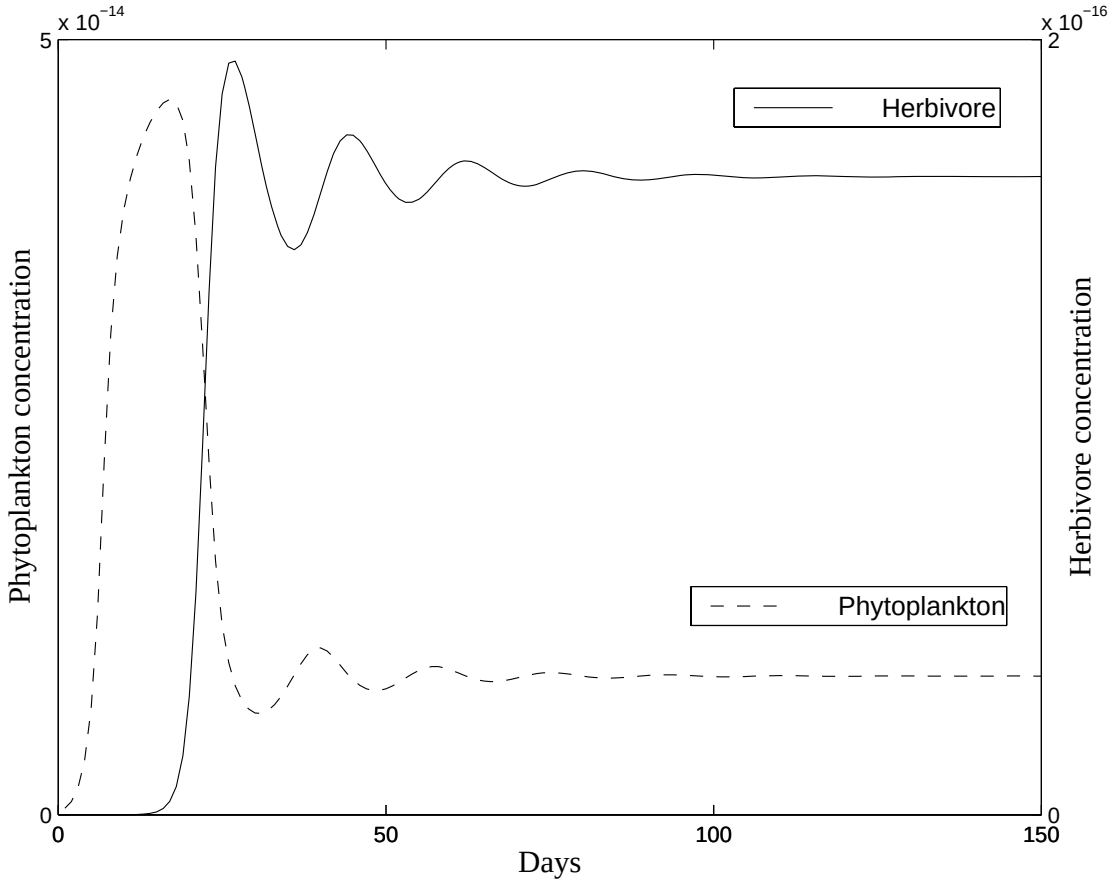

Figure 4.2: Short term oscillations in an unforced simulation of the model presented in Chapter 2, using *Skeletonema costatum* and a $r = 10\mu$m herbivore.

4.4.4 Forecasting in a non-linear system

Given that global plankton population dynamics is non-linear, and perhaps chaotic, it is worth looking at the limitations this places on forecasting in other biogeochemical systems. Non-linear systems can be sensitive to initial conditions. Simulations with negligibly different initial conditions can, over time, produce divergent outputs. This divergence sets a limit for the predictive capability of the model. The rate of divergence, and its eventual magnitude, is a characteristic of the phenomena. For example, the prediction of weather is possible for only 5-7 days ahead, primarily due to a sensitivity to initial conditions. Nonetheless, the same initial conditions and model can be used to gain meaningful long term forecasts of seasonal climate patterns (Kerr, 1998). While the rate of divergence of simulations is a limit to detailed short term weather forecasts, the

magnitude does not seem to provide a limit to long term climate forecasts (Kerr, 1998).

In conclusion, non-linear behaviour does present difficulties in the forecasting of plankton population dynamics. Nonetheless, deterministic model such as presented in Chapter 2, remain a useful prognostic tool.

4.5 Forecasting global biogeochemical cycles

The presented plankton population model, if coupled to a 3 dimensional ocean circulation model, will capture much of the coupling between ecosystem biogeochemical processes and the global climate. This level of coupling cannot be achieved by empirical models of plankton population dynamics. Examples of other biogeochemical components which have been coupled to the global climate include the many ocean-atmosphere models (Stockdale *et al.*, 1998), and the process-based models of atmospheric methane (Ridgwell *et al.*, 1999) and terrestrial productivity (Cao and Woodward, 1998b). Process-based models attempt to resolve feedbacks between components of global biogeochemical by understanding the underlying processes that govern these systems. These models are in many ways complementary. Each, by advancing their field, suggests that a process-based, mechanistic modelling methodology is the most likely approach to provide reliable forecasts, and coupled together, provide the best chance of predicting global climate change.

It may also be that these models eventually become competitors. Significant anthropogenically induced climate change is unlikely to be averted by mitigation of our present impact on the global climate. In fact, even the most optimistic assessment by the IPCC (IS92c) anticipates CO_2 emissions will increase until 2025, with a globally averaged warming of 1.5 K. To avert such change, many propose the sequestering of released carbon, rather than reduction in its emission (which is costly and may simply not be achieved). Amongst the ideas circulated is the perturbing of existing biogeochemical cycles to enhance sinks and remove sources of CO_2. Marine biota and terrestrial biota are the most obvious cycles to perturb. Before such a perturbation is applied, however,

predictive models will be required to ensure that the perturbation provides the required sequestration, with only acceptable side effects. Process-based models such as the Cao and Woodward (1998b) model of terrestrial productivity, and the plankton population model presented in this thesis, are the most likely candidates for such a task.

Appendix A

Biogeochemical values

In a sensible theory there are no [dimensionless] numbers whose values are obtainable only empirically. I can, of course, not prove that ... dimensionless constants in the laws of nature, which from a purely logical point of view can just as well have other values, should not exist. To me in my 'Gottvertrauen' [faith in God] this seems evident ...

Albert Einstein

Application of a model of this complexity to global scale processes is a daunting task. The following is a list of biogeochemical constants, and equations describing biogeochemical variables. Some have been used in the simple simulations of the mixed layers of Bermuda and OWS India found in Chapter 2. Others (such as the diffusivity of nutrients other then nitrogen) will be useful for more general simulation of plankton populations.

A.1 Properties of the earth

Gravitational field. Gravitational acceleration is used to calculate sinking rates of cells (Eq. 2.38). The earth's gravitational field is not uniform, but varies as a result of the earth's geometry. The earth is an oblate spheroid, with a equatorial radius of 6378 km, and a polar radius of 6357 km, and a mass of 5.977×10^{24} kg. A sphere of the same volume would have a radius of 6371 km. The surface of the earth roughly approximates a surface of equal acceleration towards the centre of mass. The increased gravitational acceleration of the equatorial bulge approximately balances the opposing

increase in centrifugal acceleration of a body further away from the axis of rotation. The balance is not perfect, and a small latitudinal and height above sea level correction gives the effective gravitational acceleration, g [m s^{-2}] (Gill, 1982):

$$g = \left(9.78302 + 0.005172 \sin^2 \varphi - 0.000006 \sin^2 2\varphi\right) \left(1 + z/6371000\right)^{-2} \tag{A.1}$$

where φ = latitude and z = height above sea level [m]. In the simulations in Chapter 2, g is assumed to be 9.81 m s^{-2}.

Solar Irradiance. The incident solar radiation on the sea surface is used in Chapter 2 to determine the light captured by phytoplankton cells (Eq. 2.18). The incident solar radiation on the earth's surface is a function of latitude, time of the day, and day of the year. Following Brock (1981), to calculate the solar irradiance at the earth's surface in the northern hemisphere, first calculated the declination of the earth, $D1$:

$$D1 = 0.409230 \sin\left(\frac{2\pi(284 + day)}{365}\right) \tag{A.2}$$

the radius vector of the earth, $R1$:

$$R1 = \frac{1}{\sqrt{1 + 0.033 \cos\left(\frac{2\pi day}{365}\right)}} \tag{A.3}$$

the hour angle, $W2$,

$$W2 = (hour - 12)\frac{\pi}{12} \tag{A.4}$$

and the zenith angle, Z:

$$Z = \cos^{-1}\left(\sin D1 \sin\varphi + \cos D1 \cos\varphi \cos W2\right) \tag{A.5}$$

The wavelength-resolved irradiance at the top of the earth's atmosphere, $I_{top,\lambda}$, is given by:

$$I_{top,\lambda} = I_{solar,\lambda}\frac{\cos Z}{R1^2} \tag{A.6}$$

where the $I_{solar,\lambda}$ is the spectrally resolved solar constant, and is given in Fig. 2.3. The total incident solar radiation varies between 1367 and 1369 W m^{-2} in an 11 year cycle.

The pathlength of the light through the atmosphere (assuming no scattering), M_{atm}, is given by (Gregg and Carder, 1990):

$$M_{atm} = \frac{1}{\cos Z + 0.15\,(93.885 - Z)^{-1.253}} \tag{A.7}$$

where M_{atm} is in units of airmass. (i.e. $M_{atm} = 1$ at the zenith sun). The wavelength-resolved irradiance at the earth's surface, $I_{0,\lambda}$, is given by:

$$I_{0,\lambda} = I_{top,\lambda}\tau_{\lambda}^{M_{atm}} \tag{A.8}$$

where τ_λ is the transmission coefficient of a cloudless atmosphere and zenith sun at wavelength λ [airmass^{-1}]. Light is further attenuated by clouds, also as a function of azimuth angle. In Chapter 2, a simple formulation (Smith and Dobson, 1984) was used for all wavelengths. There are a number of other formulations (Yool, 1997), and it is not clear which formulation is to be preferred.

A.2 Properties of seawater

Fluid viscosity. Fluid viscosity is required for the calculation of the Sherwood number, and hence nutrient uptake (Eq. 2.9) and the encounter rates of predators and prey (Table 2.5). Following Wolf-Gladrow and Riebesell (1997), the dynamic viscosity of freshwater, $\eta_{freshwater}$ [kg m^{-1} s^{-1}] as a function of temperature in degrees, T_C, is given by:

$$\log \frac{\eta(T_C)}{\eta(20)} = \frac{1.1709(20 - T_C) - 1.827 \times 10^{-3}(T_C - 20)^2}{T_C + 89.93} \tag{A.9}$$

The conversion of dynamic viscosity of freshwater to the dynamic viscosity of seawater is itself temperature dependent:

$$\frac{\eta_{fresh}}{\eta_{sea}} = 0.9508 - 0.0007379\,T_C \quad 0 < T_C < 25 \tag{A.10}$$

Fluid density. The density of water is required for the calculation of sinking rates of phytoplankton and herbivores (Eq. 2.38). The density of freshwater, ρ_{fresh} [kg m^{-3}], is given by Gill (1982):

$$\begin{aligned}\rho_{fresh} &= 999.842594 + 6.793952 \times 10^{-2} T_C - 9.095290 \times 10^{-3} T_C^2 \\ &\quad +1.001685 \times 10^{-4} T_C^3 - 1.120083 \times 10^{-6} T_C^4 + 6.536332 \times 10^{-9} T_C^5\end{aligned} \tag{A.11}$$

The density of seawater at atmospheric pressure:

$$\begin{aligned}\rho_{sea} &= \rho_{fresh} \\ &\quad +S \left(0.824493 - 4.0899 \times 10^{-3} T_C + 7.6438 \times 10^{-5} T_C^2 \right. \\ &\qquad \left. -8.2467 \times 10^{-7} T_C^3 + 5.3875 \times 10^{-9} T_C^4 \right) \\ &\quad +S^{2/3} \left(-5.72466 \times 10^{-3} + 1.0227 \times 10^{-4} T_C - 1.6546 \times 10^{-6} T_C^2 \right) \\ &\quad +S^2 4.8314 \times 10^{-4}\end{aligned} \tag{A.12}$$

where S is the salinity [ppt].

A.3 Diffusion coefficients

The diffusion coefficients of nutrient species are required in Chapter 2 and 3 to calculate nutrient uptake rates (Eq. 2.7 amongst others). Diffusion coefficients are usually measured in freshwater. The conversion to seawater is approximately inversely equal to the change in viscosity (Li and Gregory, 1974):

$$\frac{D_{sea}}{D_{fresh}} = \frac{\eta_{fresh}}{\eta_{sea}} \tag{A.13}$$

Chemical species	Oceanic Concentrations [mol m^{-3}]		Molecular Diffusivity	References
	Range	Bottom water	[10^{-10} m^2 s^{-1}]	
NO_3^-	$0.1 - 45 \times 10^{-3}$	2.0×10^{-3}	17.5	L92 M60 L74
$H_2PO_4^-$	$\sum P =$ $1 - 3.5 \times 10^{-3}$	$\sum P =$ 1×10^{-3}	7.78	M60, L92
HPO_4^{2-}			6.84	
HP_4^{3-}			5.63	
H_4SiO_4	$1 - 180 \times 10^{-3}$	10×10^{-3}	10	L92 M60 W71
$Fe(OH)_3$	$0.1 - 2.5 \times 10^{-6}$		5.58	L92
CO_2	$\sum CO_2 = 2.1$ - 2.5	2.5	17.8	
HCO_3^-	1.6 - 2.4	2.4	10.9	L92 WG97
CO_3^{2-}	$10 - 35 \times 10^{-3}$	10×10^{-3}	8.79	

Table A.1: Geochemical properties of oceanic water. Molecular diffusivity at 25^oC and $35^o/_{oo}$. For interpolation between 0 and 25^oC and 0 and $35^o/_{oo}$ see Li and Gregory (1974). Concentration conversions assume $\rho_{\text{seawater}} = 1000\,\text{kg}\,\text{m}^{-3}$. Bottom water values for Bermuda 32^o N, 65^oW, except carbon species which are based on Pacific Deep Water L92 - Libes (1992); M60 - Menzel and Ryther (1960); W71 - Wollast and Garrels (1971) and WG97 - Wolf-Gladrow and Riebesell (1997). See also Strass and Woods (1991)

A.4 Approximating absorptions bands as Gaussian curves

In Chapter 2, the light captured by a cell is a function of the absorbance of the pigments in the cell, and the pathlength of light through the cell. The absorbance of each pigment is a function of wavelength. To integrate the light captured over the photosynthetic range, Gaussian curves have been used to approximate the absorption bands (Fig. 2.1). The data used to create the Gaussian curves is tabulated in Table A.2.

Band number b	Pigment	Specific absorption coefficient γ_b [m^2 mg(pig)$^{-1}$]	Band half-width W_b [nm]	Peak wavelength λ_b [nm]
1	Chl *a*	0.037	53.8	384
2	Chl *a*	0.012	21.3	413
3	Chl *a*	0.039	32.1	435
4	Chl *c*	0.051	27.2	461
5	Chl *b*	0.061	45.0	464
6	Carot.	0.038	45.4	490
7	Carot.	0.017	45.9	532
8	Chl *c*	0.012	46.3	583
9	Chl *a*	0.005	35.0	623
10	Chl *a*	0.010	28.9	644
11	Chl *b*	0.022	24.4	655
12	Chl *a*	0.020	21.6	676
13	Chl *a*	0.002	33.5	700

Table A.2: Coefficients for fitting pigment specific absorption spectra to Gaussian curves (Hoepffner and Sathyendranath, 1991) Chl *a*, *b*, *c* = Chlorophyll *a b c*; Carot = Carotenoids. Specific absorption coefficient has units of [m^2mg(pig)$^{-1}$], where Chl. is measured in mg, and carot. in mSPU.

Appendix B

The geometry of plankton cells

God does not care about our mathematical difficulties. He integrates empirically.

Albert Einstein

In this thesis, plankton cells have generally been assumed to be ellipsoidal in shape. The geometric properties of ellipsoids have been used in the derivation of ψ (Table 2.1), $\overline{aA}$ (Table 2.3), and C_D (Table 2.4). Most plankton shapes are well approximated by ellipsoids. Nonetheless, plankton can take more elaborate shapes. This appendix provides both a source of information for the geometric shapes used, and as an example of the methodology required to solve for geometric properties of more elaborate shapes.

Fig. B.1 illustrates some geometric shapes used to approximate natural plankton morphology, and Table B.1 gives the formulae for calculating volume V, surface area, A_s, and diffusion shape factor, ψ, for each shape. The derivation of formulae for volume and surface area can be found in standard undergraduate mathematical texts (Edwards and Penny, 1986), and will not be re-derived here. The calculation of the diffusion shape factor, ψ, is less easily available. We will follow the methodology for solving the Laplace equation, $\nabla^2 C = 0$,

in orthogonal curvilinear coordinates presented in Wong (1991).

Shape	Volume, V [m^3]	Surface area, A_s [m^2]	Diffusion shape factor, ψ [m]
Sphere	$\frac{4}{3}\pi r^3$	$4\pi r^2$	$4\pi r$
Oblate spheroid	$\frac{4}{3}\pi r_1^2 r_2$	$2\pi r_1 r_2 \left[\frac{r_1}{r_2} + \frac{r_2}{\sqrt{r_1^2 - r_2^2}} \ln\left(\frac{r_1 + \sqrt{r_1^2 - r_2^2}}{r_2}\right)\right]$	$4\pi r_1 e \left(\frac{1}{\tan^{-1}\frac{e}{\sqrt{1-e^2}}}\right)$
Prolate spheroid	$\frac{4}{3}\pi r_1 r_2^2$	$2\pi r_1 r_2 \left[\frac{r_2}{r_1} + \frac{r_1}{\sqrt{r_1^2 - r_2^2}} \sin^{-1}\frac{\sqrt{r_1^2 - r_2^2}}{r_1}\right]$	$8\pi r_1 e \left(\frac{1}{\ln\frac{1+e}{1-e}}\right)$
Circular cylinder	$\pi r^2 h$	$2\pi r(r+h)$	$\left(8 + 6.95\left(\frac{h}{2r}\right)^{0.76}\right) r$

Table B.1: Geometric properties of shapes used for phytoplankton. Volume, V, and surface area, A_s, from (Edwards and Penny, 1986) and diffusion shape factor, ψ, from Table 2.1. The volume of an ellipsoid is given by $V = (4/3)\pi r_1 r_2 r_3$, but the surface area and diffusion shape factor must be solved numerically (Wolf-Gladrow and Riebesell, 1997). r, r_1, r_2, r_3 are orthogonal radii, where $r_1 > r_2 > r_3$, h = height of a cylinder, and $e = \sqrt{1 - (r_2/r_1)^2}$ is the eccentricity of the oblate and prolate spheroid.

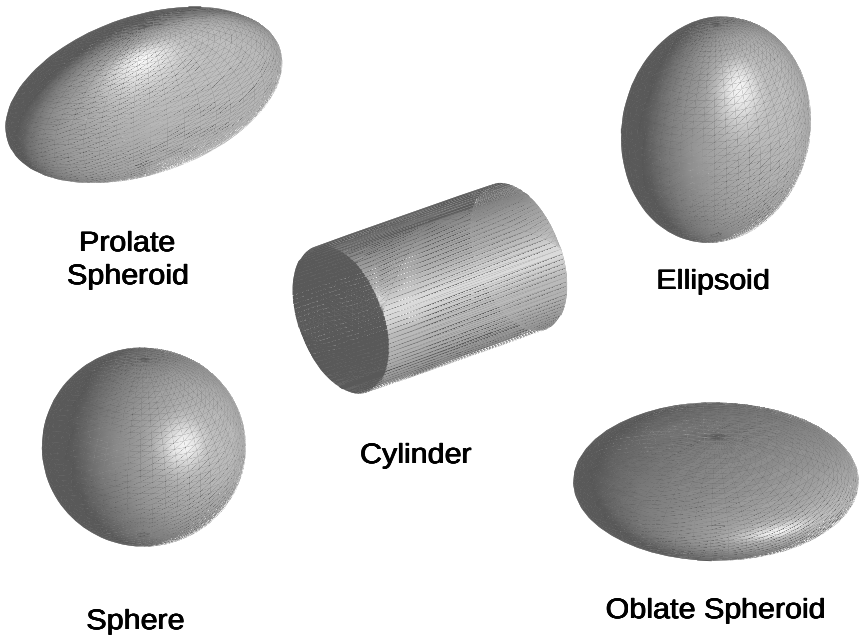

Figure B.1: Image of shapes used to approximate plankton morphology. In this diagram each shape has the same volume, but have different surface areas, A_s, diffusion shape factors, ψ, and average pathlengths of light, $\overline{aA}$.

B.1 Derivation of the diffusion shape factor, ψ, for any shape

For fluid with no motion, the concentration of a nutrient in a fluid is given by:

$$\frac{\partial C}{\partial t} = \kappa D \nabla^2 C \tag{B.1}$$

where κ is a constant, D is the molecular diffusivity, C is the concentration field, and $\nabla^2 = \nabla \cdot \nabla$ is the divergence of the gradient. Placing a sink for the nutrient, (i.e. a phytoplankton cell) into the fluid, changes the value for $\nabla^2 C$. We can solve Eq. B.1 for the case when the concentration gradient is not changing with time ($\nabla^2 C = 0$). If we do

so in a coordinate system that can also be used to simply define the surface of the cell, we are able to calculate the flux of nutrient at the cell surface. The diffusion shape factor, ψ, which is a coefficient that quantifies the surface flux in terms of the concentration of the fluid at the cell wall and the average concentration in the surrounding fluid, can then be calculated.

B.1.1 Solving $\nabla^2 C = 0$

The choice of the appropriate coordinate system greatly simplifies this problem. For each step, I will present the general solution for orthogonal curvilinear coordinates (OCC), and then apply it to spherical coordinates (SC) as an example.

Step 1. Define the coordinate system. We will represent OCC by $x = u_1, y = u_2, z = u_3$. SC are given by:

$$\begin{aligned} x &= r\sin\theta\cos\phi \\ y &= r\sin\theta\sin\phi \\ z &= r\cos\theta \end{aligned} \tag{B.2}$$

Step 2. Calculate the scale factors. In OCC for $i = 1, 2, 3$:

$$h_{u_i} = \left[\left(\frac{\partial x}{\partial u_i}\right)^2 + \left(\frac{\partial y}{\partial u_i}\right)^2 + \left(\frac{\partial z}{\partial u_i}\right)^2\right]^{1/2} \tag{B.3}$$

In SC h_r, h_θ and h_ϕ are given by:

$$\begin{aligned} h_r &= \sqrt{\left(\frac{\partial r\sin\theta\cos\phi}{\partial r}\right)^2 \left(\frac{\partial r\sin\theta\sin\phi}{\partial r}\right)^2 \left(\frac{\partial r\cos\theta}{\partial r}\right)^2} \\ &= \sqrt{\sin^2\theta\cos^2\phi + \sin^2\theta\sin^2\phi + \cos^2\theta} = 1 \end{aligned} \tag{B.4}$$

$$\tag{B.5}$$

and similarly, $h_\theta = r$ and $h_\phi = r\sin\theta$

Step 3. Solve for the gradient, ∇C. In OCC, the gradient, ∇C, is given by:

$$v_i = \frac{\partial}{h_i \partial u_i} C \tag{B.6}$$

So $(\nabla C)_r$, $(\nabla C)_\theta$ and $(\nabla C)_\phi$ are given by:

$$\begin{aligned} (\nabla C)_r &= \frac{\partial C}{\partial r} \\ (\nabla C)_\theta &= \frac{1}{r}\frac{\partial C}{\partial r} \\ (\nabla C)_\phi &= \frac{1}{r\sin\theta}\frac{\partial C}{\partial r} \end{aligned} \tag{B.7}$$

Step 4. Solve for divergence. The divergence, p_i, for an OCC system is given by:

$$p_i = \frac{h_1 h_2 h_3}{h_i} \tag{B.8}$$

so in SC, $p_r = h_\theta h_\phi = r^2 \sin\theta$, $p_\theta = h_r h_\phi = r\sin\theta$, and $p_\phi = h_r h_\theta = r$

Step 5. Solve for $\nabla^2 C = \nabla \cdot \nabla C$. The order of operations is $\nabla \cdot (\nabla C)$, so:

$$\nabla^2 C = \frac{1}{p_1}\frac{\partial}{h_1 \partial u_1}\left(p_1 \frac{\partial C}{h_1 \partial u_1}\right) + \frac{1}{p_2}\frac{\partial}{h_2 \partial u_2}\left(p_2 \frac{\partial C}{h_2 \partial u_2}\right) + \frac{1}{p_3}\frac{\partial}{h_3 \partial u_3}\left(p_3 \frac{\partial C}{h_3 \partial u_3}\right) \tag{B.9}$$

In SC Eq. B.9 becomes:

$$\nabla^2 C = \frac{1}{r^2\sin\theta}\frac{\partial}{\partial r}\left(r^2 \sin\theta \frac{\partial C}{\partial r}\right) + \frac{1}{r\sin\theta}\frac{\partial}{r\partial\theta}\left(r\sin\theta \frac{\partial C}{r\partial\theta}\right) + \frac{1}{r}\frac{\partial}{r\sin\theta\partial\phi}\left(r\frac{\partial C}{r\sin\theta\partial\phi}\right) \tag{B.10}$$

which reduces to:

$$\nabla^2 C = \frac{1}{r^2}\frac{\partial}{\partial r}\left(r^2 \frac{\partial C}{\partial r}\right) + \frac{1}{r^2\sin\theta}\frac{\partial}{\partial\theta}\left(\sin\theta \frac{\partial C}{\partial\theta}\right) + \frac{1}{r^2\sin^2\theta}\frac{\partial^2 C}{\partial\phi^2} \tag{B.11}$$

The appropriate coordinate system and solution of $\nabla^2 C = 0$ for a sphere, circular-cylinder, prolate spheroid, oblate spheroid and general ellipsoid are found in Tables B.2 and B.3.

Coordinate system		$\nabla^2 C$
Spherical coordinates (r, θ, ϕ), Sphere defined by $r =$ constant		
$0 \leq r < \infty$ $0 \leq \theta \leq \pi$ $0 \leq \phi < 2\pi$	$x = r\sin\theta\cos\phi$ $y = r\sin\theta\sin\phi$ $z = r\cos\theta$	$\frac{1}{r^2}\frac{\partial}{\partial r}\left(r^2\frac{\partial C}{\partial r}\right) + \frac{1}{r^2\sin\theta}\frac{\partial}{\partial\theta}\left(\sin\theta\frac{\partial C}{\partial\theta}\right) + \frac{1}{r^2\sin^2\theta}\frac{\partial^2 C}{\partial\phi^2}$
Circular-cylinder coordinates (r, ϕ, z), Cylinder defined by $r =$ constant		
$0 \leq r < \infty$ $0 \leq \phi < 2\pi$ $-\infty < z < \infty$	$x = r\cos\phi$ $y = r\sin\phi$ $z = z$	$\frac{1}{r}\frac{\partial}{\partial r}\left(r\frac{\partial C}{\partial r}\right) + \frac{1}{r^2}\frac{\partial^2 C}{\partial C^2} + \frac{\partial^2 C}{\partial z^2}$
Prolate spheroidal coordinates (η, θ, ϕ), Prolate spheroid defined by $\eta =$ constant		
$0 \leq \eta < \infty$ $0 \leq \theta \leq \pi$ $0 \leq \phi < 2\pi$	$x = a\sinh\eta\sin\theta\cos\phi$ $y = a\sinh\eta\sin\theta\sin\phi$ $z = a\cosh\eta\cos\theta$	$\frac{1}{a^2\left(\sinh^2\eta + \sin^2\theta\right)}\left(\frac{\partial^2 C}{\partial\eta^2} + \coth\eta\frac{\partial C}{\partial\eta} + \frac{\partial^2 C}{\partial\theta^2} + \cot\theta\frac{\partial C}{\partial\theta}\right) + \frac{1}{a^2\sinh^2\eta\sin^2\theta}\frac{\partial^2 C}{\partial\phi^2}$

Table B.2: The solution of $\nabla^2 C$ sphere, cylinder and prolate spheroid for a (Moon and Spencer, 1971; Wong, 1991). Moon and Spencer (1971) also give solutions for elliptic-cylinder, parabolic-cylinder, parabolic, conical and paraboloidal coordinates, although these solutions have not been used in this thesis. a is the foci of the ellipse that is rotated to form the prolate and oblate spheroids, and is given by $a = \sqrt{r_1^2 - r_2^2}$ where r_1 and r_2 are orthogonal radii and $r_1 > r_2$.

Coordinate system		$\nabla^2 C$
Oblate spheroidal coordinates (η, θ, ϕ), Oblate spheroid defined by $\eta =$ constant		
$0 \leq \eta < \infty$ $0 \leq \theta \leq \pi$ $0 \leq \phi < 2\pi$	$x = a\cosh\eta\sin\theta\cos\phi$ $y = a\cosh\eta\sin\theta\sin\phi$ $z = a\sinh\eta\cos\theta$	$\dfrac{1}{a^2\left(\cosh^2\eta - \sin^2\theta\right)}\left(\dfrac{\partial^2 C}{\partial\eta^2} + \tanh\eta\dfrac{\partial C}{\partial\eta} + \dfrac{\partial^2 C}{\partial\theta^2} + \cot\theta\dfrac{\partial C}{\partial\theta}\right) + \dfrac{1}{a^2\cosh^2\eta\sin^2\theta}\dfrac{\partial^2 C}{\partial\phi^2}$
General ellipsoidal coordinates (η, θ, ϕ), Ellipsoid defined by $\eta =$ constant		
$c^2 < \eta^2 < \infty^2$ $b^2 < \theta^2 < c^2$ $0 \leq \lambda^2 < b^2$	$(x)^2 = A_1$ $(y)^2 = A_2$ $(z)^2 = A_3$	$\dfrac{\sqrt{(\eta^2-b^2)(\eta^2-c^2)}}{(\eta^2-\theta^2)(\eta^2-\lambda^2)}\dfrac{\partial}{\partial\eta}\left[\sqrt{(\eta^2-b^2)(\eta^2-c^2)}\dfrac{\partial C}{\partial\eta}\right]$ $+\dfrac{\sqrt{(\theta^2-b^2)(c^2-\theta^2)}}{(\eta^2-\theta^2)(\theta^2-\lambda^2)}\dfrac{\partial}{\partial\theta}\left[\sqrt{(\theta^2-b^2)(c^2-\theta^2)}\dfrac{\partial C}{\partial\theta}\right]$ $+\dfrac{\sqrt{(b^2-\lambda^2)(c^2-\lambda^2)}}{(\eta^2-\lambda^2)(\theta^2-\lambda^2)}\dfrac{\partial}{\partial\lambda}\left[\sqrt{(b^2-\lambda^2)(c^2-\lambda^2)}\dfrac{\partial C}{\partial\lambda}\right]$
$A_1 = \left(\dfrac{\eta\theta\lambda}{bc}\right)^2$, $A_2 = \dfrac{(\eta^2-b^2)(\theta^2-b^2)(b^2-\lambda^2)}{b^2(c^2-b^2)}$ and $A_3 = \dfrac{(\eta^2-c^2)(c^2-\theta^2)(c^2-\lambda^2)}{c^2(c^2-b^2)}$		

Table B.3: The solution of $\nabla^2 C$ for an oblate spheroid, and general ellipsoid (Moon and Spencer, 1971; Wong, 1991). Moon and Spencer (1971) also give solutions for elliptic-cylinder, parabolic-cylinder, parabolic, conical and paraboloidal coordinates, although these solutions have not been used in this thesis. a is the foci of the ellipse that is rotated to form the prolate and oblate spheroids, and is given by $a = \sqrt{r_1^2 - r_2^2}$ where r_1 and r_2 are orthogonal radii and $r_1 > r_2$.

B.1.2 Solve for ψ using cell wall boundary conditions

The flux to a cell by diffusion along a concentration gradient is given by:

$$J = \psi D_i (C_b - C_w) \tag{B.12}$$

where J is the uptake rate to a cell [mol cell^{-1} s^{-1}]; D_i is the molecular diffusivity of chemical species i [m^2 s^{-1}], C_w is the nutrient concentration at the cell wall [mol m^{-3}] and C_b is the nutrient concentration in the bulk fluid [mol m^{-3}]. At this point we will restrict ourselves to the spherical case, because simplifications are shape dependent. In SC, concentration varies only radially, $\partial C/\partial\phi = \partial C/\partial\theta = 0$, and Eq. B.11 becomes:

$$\frac{1}{r}\frac{\partial}{\partial r} r^2 \frac{\partial C}{\partial r} = 0 \tag{B.13}$$

Multiply both sides of Eq. B.13 by r, and apply the chain rule of differentiation:

$$\frac{d^2 C}{dt^2} + \frac{2}{r}\frac{dC}{dt} = 0 \tag{B.14}$$

which is an ordinary differential equation. Substitute $K = dC/dt$, and by separation of variables, and integrating, we arrive at:

$$K = \frac{dC}{dt} = \frac{A_1}{r^2} \tag{B.15}$$

Integrating this becomes:

$$C = \frac{-2A_1}{r} + A_2 \tag{B.16}$$

where A_1 and A_2 are constants. At $r = \infty$, $C = C_b$, so $A_2 = C_b$, and at $r = a$, the radius of the cell, $C = C_w$ so $2A_1 = (C_b - C_w)a$. The flux per unit area is then given by (Fick's law):

$$J = D\frac{\partial C}{\partial r} = -\frac{(C_b - C_w)\, a}{r^2} \tag{B.17}$$

so for a surface area of $4\pi a^2$, the total flux becomes:

$$J = 4\pi a D \left(C_b - C_w\right) \tag{B.18}$$

and the value for $\psi = 4\pi a$. In the notation of rest of the thesis, where r represents the radius (not the radial coordinate), $\psi = 4\pi r$.

Bibliography

The researches of many commentators have already thrown much darkness on this subject, and it is probable that, if they continue, we shall soon know nothing at all about it.

Mark Twain

Arrigo, K. R., Robinson, D. H., Worthen, D. L., Dunbar, R. B., DiTullio, G. R., VanWoert, M. and Lizotte, M. P. (1999) Phytoplankton community structure and the drawdown of nutrients and CO_2 in the Southern Ocean. *Science*, **283**, 365–367.

Atkins, P. W. (1994) *Physical Chemistry*. Oxford University Press, Oxford, 5th edn.

Atkinson, M. J. (1992) Productivity of Eniwetak atoll reef predicted from mass-transfer relationships. *Cont. Shelf Res.*, **12**, 799–807.

Atkinson, M. J. and Bilger, B. W. (1992) Effects of water velocity on phosphate uptake in coral reef-flat communities. *Limnol. Oceanogr.*, **37**, 273–279.

de Baar, H. J. W. (1994) Von Liebig's law of the minimum and plankton ecology (1899-1991). *Prog. Oceanogr.*, **33**, 347–386.

Baird, M. E. and Atkinson, M. J. (1997) Measurement and prediction of mass transfer to experimental coral reef communities. *Limnol. Oceanogr.*, **42**, 1685–1693.

Baird, M. E. and Emsley, S. M. (1999) Towards a mechanistic model of plankton population dynamics. *J. Plankton Res.*, **21**, 85–126.

Bees, M. A., Mezić, I. and McGlade, J. M. (1998) Planktonic interactions and chaotic advection in langmuir circulation. *Mathematics and Computers in Simulation*, **44**, 527–544.

Berg, H. C. and Purcell, E. M. (1977) Physics of chemoreception. *Biophysical Journal*, **20**, 193–219.

Bidigare, R. R., Fluegge, A., Freeman, K. H., Hanson, K. L., Hayes, J. M., Hollander, D., Jasper, J. P., King, L. L., Laws, E. A., Milder, J., Millero, F. J., Pancost, R., Popp, B. N., Steinberg, P. A. and Wakeham, S. G. (1997) Consistent fractionation of ^{13}C in nature and in the laboratory: Growth-rate effects in some haptophyte algae. *Global Biogeochemical Cycles*, **11**, 279–292.

Bilger, R. W. and Atkinson, M. J. (1992) Anomalous mass transfer of phosphate on coral reef flats. *Limnol. Oceanogr.*, **37**, 261–272.

Bissett, W. P., Carder, K. L., Walsh, J. J. and Dieterle, D. A. (1999a) Carbon cycling in the upper waters of the Sargasso Sea: II. Numerical simulation of apparent and inherent optical properties. *Deep-Sea Res. I*, **46**, 271–317.

Bissett, W. P., Walsh, J. J., Dieterle, D. A. and Carder, K. L. (1999b) Carbon cycling in the upper waters of the Sargasso Sea: I. Numerical simulation of differential carbon and nitrogen fluxes. *Deep-Sea Res. I*, **46**, 205–269.

Blake, J. R. and Otto, S. R. (1996) Ciliary propulsion, chaotic filtration and a 'blinking' stokeslet. *J. Eng. Math.*, **30**, 151–168.

Blanchard, D. C. (1989) The ejection of drops from the sea and their enrichment with bacteria and other materials: a review. *Estuaries*, **12**, 127–137.

Bold, H. C. and Wynne, M. J. (1985) *Introduction to the Algae*. Prentice-Hall, Inc., New Jersey, 2nd edn.

Botsford, L. W., Castilla, J. C. and Peterson, C. H. (1997) The management of fisheries and marine ecosystems. *Science*, **277**, 509–515.

Brauner, N. and Shacham, M. (1996) Using power-law rate expression parameters for discrimination among mechanistic models in rate data regression. *Chem. Eng. Comm.*, **155**, 1–18.

Brenner, H. (1963) Forced convection heat and mass transfer at small Peclet numbers from a particle of arbitrary shape. *Chem. Eng. Sci.*, **18**, 109–122.

Bricaud, A., Morel, A. and Prieur, L. (1981) Absorption by dissolved organic matter of the sea (yellow substance) in the UV and visible domains. *Limnol. Oceanogr.*, **26**, 43–53.

Brock, T. D. (1981) Calculating solar radiation for ecological studies. *Ecol. Modelling*, **14**, 1–19.

Brunet, C., Davoult, D. and Casotti, R. (1996) Physiological reactions to a change in light regime in cultured *Skeletomena costatum* (Bacillariophyta): implications for estimation of phytoplankton biomass. *Hydrobiologia*, **333**, 87–94.

Brunk, B. K., Koch, D. L. and Lion, L. W. (1998) Turbulent coagulation of colloidal particles. *J. Fluid Mech.*, **364**, 81–113.

Buizza, R. and Palmer, T. N. (1998) Impact of ensemble size on ensemble prediction. *Mon. Wea. Rev.*, **126**, 2503–2518.

Cao, M. and Woodward, F. I. (1998a) Dynamic responses of terrestial ecosystem carbon cycling to global climate change. *Nature*, **393**, 249–252.

Cao, M. and Woodward, F. I. (1998b) Net primary and ecosystem production and carbon stocks of terrestial ecosystems and their responses to climate change. *Global Change Biol.*, **4**, 158–198.

Caperon, J. (1968) Population growth response of *Isochrysis galbana* to nitrate variation at limiting concentration. *Ecology*, **49**, 866–872.

Caperon, J. (1969) Time lag in population growth response of *Isochrysis galbana* to a variable nitrate environment. *Ecology*, **50**, 188–192.

Chen, D. X. and Coughenour, M. B. (1996) A mechanistic model for submerged aquatic macrophyte photosynthesis: *Hydrilla* in ambient and elevated CO_2. *Ecol. Modelling*, **89**, 133–146.

Clary, D. C. (1998) Quantum theory of chemical reaction dynamics. *Science*, **279**, 1879–1882.

Clift, R., Grace, J. R. and Weber, M. E. (1978) *Bubbles, drops and particles*. Academic Press, New York.

Dabros, T., Adamczyk, Z. and deVen, T. G. M. V. (1984) Transfer of colloidal particles to a cylinder in combined simple shear and uniform flow. *PhysioChemical Hydrodynamics*, **5**, 67–83.

Darwin, C. (1859) *The Origin of Species by Means of Natural Selection*. John Murray, London.

Denman, K., Hoffman, E. and Marchant, H. (1996) Marine biotic response to environmental change and feedbacks to climate. In Houghton *et al.* (1996), pp. 482–516.

Denman, K. L. and Gargett, A. E. (1995) Biological-physical interactions in the upper ocean: the role of vertical and small-scale transport processes. *Annu. Rev. Fluid Mech.*, **27**, 225–255.

Dixon, M. and Webb, E. C. (1979) *Enzymes*. Longman Group Limited.

Doney, S. C., Glover, D. M. and Najjar, R. G. (1996) A new coupled, one-dimensional biological-physical model for the upper ocean: Applications to the JGOFS Bermuda Alantic Time-series Study (BATS) site. *Deep-Sea Res. II*, **43**, 591–624.

Dower, J. F., Miller, T. J. and Leggett, W. C. (1997) The role of microscale turbulence in the feeding ecology of larval fish. *Adv. Mar. Biol.*, **31**, 169–220.

Driscoll, W. G. and Vaughan, W. (1978) *Handbook of Optics*. McGraw-Hill, New York.

Droop, M. R. (1968) Vitamin B-12 and marine ecology IV. The kinetics of uptake, growth and inhibition in *Monochrysis lutheri*. *J. Mar. Biol. Assoc. UK*, **48**, 689–733.

Droop, M. R. (1974) The nutrient status of algal cells in a continuous culture. *J. Mar. Bio. Ass. U.K.*, **54**, 825–855.

Dugdale, R. C. (1967) Nutrient limitation in the sea: dynamics, identification and significance. *Limnol. Oceanogr.*, **12**, 685–695.

Dyhrman, S. T. and Palenik, B. P. (1997) The identification and purification of a cell-surface alkaline phosphatase from the dinoflagellate *Prorocentrum minimum* (Dinophyceae). *J. Phycol.*, **33**, 602–612.

Eccleston-Parry, J. D. and Leadbeater, B. S. C. (1994) A comparison of the growth kinetics of six marine heterotrophic nanoflagellates fed with one bacterial species. *Mar. Ecol. Prog. Ser.*, **105**, 167–177.

Edwards, A. M. and Brindley, J. (1996) Oscillatory behaviour in a three-component plankton population model. *Dynamics and Stability of Systems*, **11**, 347–370.

Edwards, A. M. and Brindley, J. (1999) Zooplankton mortality and the dynamical behaviour of plankton population models. *Bull. Math. Bio.*, **61**, 303–339.

Edwards, C. H. and Penny, D. E. (1986) *Calculus and Analytic Geometry*. Prentice Hall International, Inc., 2nd edn.

Falkowski, P. G., Barber, R. T. and Smetacek, V. (1998) Biogeochemical controls and feedbacks on ocean primary production. *Science*, **281**, 200–206.

Falkowski, P. G., Dubinsky, Z. and Wyman, K. (1985) Growth-irradiance relationships in phytoplankton. *Limnol. Oceanogr.*, **30**, 311–321.

Farquhar, G. D., O'Leary, M. H. and Berry, J. A. (1982) On the relationship between carbon isotope discrimination and the intracellular carbon dioxide concentration in leaves. *Aust. J. Plant Physiol.*, **9**, 121–137.

Fasham, M. J. R. (1993) Modelling the marine biota. In Heimann, M. (editor), *The Global Carbon Cycle*, Springer-Verlag, New York. pp. 457–504.

Fasham, M. J. R., Ducklow, H. W. and McKelvie, S. M. (1990) A nitrogen-based model of plankton dynamics in the oceanic mixed layer. *J. Mar. Res.*, **48**, 591–639.

Flynn, K. J., Fasham, M. J. R. and Hipkin, C. R. (1997) Modelling the interactions between ammonium and nitrate uptake in marine phytoplankton. *Phil. Trans. R. Soc. Lond. B*, **352**, 1625–1645.

Geider, R. J., MacIntrye, H. L. and Kana, T. M. (1996) A dynamic model of photoadaptation in phytoplankton. *Limnol. Oceanogr.*, **41**, 1–15.

Geider, R. J., MacIntyre, H. L. and Kana, T. M. (1997) Dynamic model of phytoplankton growth and acclimation: responses of the balanced growth rate and the chlorophyll *a*:carbon ratio to light, nutrient-limitation and temperature. *Mar. Ecol. Prog. Ser.*, **148**, 187–200.

Geider, R. J. and Osbourne, B. A. (1992) *Algal Photosynthesis*. Chapman and Hall, New York.

Geider, R. J., Osbourne, B. A. and Raven, J. A. (1985) Light dependence of growth and photosynthesis in *Phaeodactylum tricornutum* (Bacillariophyceae). *J. Phycol.*, **21**, 609–619.

Gerritsen, J. and Strickler, J. R. (1977) Encounter probabilities and community structure in zooplankton: a mathematical model. *J. Fish. Res. Board Can.*, **34**, 73–82.

Gill, A. E. (1982) *Atmosphere-Ocean Dynamics*. Academic Press, Inc., London.

Goldman, J. C., Hansell, D. A. and Dennett, M. R. (1992) Chemical characterization of three large oceanic diatoms: potential impact on water column chemistry. *Mar. Ecol. Prog. Ser.*, **88**, 257–270.

Gregg, W. W. and Carder, K. L. (1990) A simple spectral solar irradiance model for cloudless maritime atmospheres. *Limnol. Oceanogr.*, **35**, 1657–1675.

Hansen, P. J., Bjornsen, P. K. and Hansen, B. W. (1997) Zooplankton grazing and growth: Scaling within the 2-2,000 μm body size range. *Limnol. Oceanogr.*, **42**, 687–704.

Hill, P. S. (1992) Reconciling aggregation theory with observed vertical fluxes following phytoplankton blooms. *J. Geophys. Res.*, **97**, 2295–2308.

Hill, R. and Whittingham, C. P. (1955) *Photosynthesis*. Methuen, London.

Hoepffner, N. and Sathyendranath, S. (1991) Effect of pigment composition on absorption properties of phytoplankton. *Mar. Ecol. Prog. Ser.*, **73**, 11–23.

Hoffman, J. D. (1992) *Numerical Methods for Engineers and Scientists*. McGraw-Hill, New York.

Houghton, J. T., Filho, L. G. M., Callander, B. A., Harris, N., Kattenberg, A. and Maskell, K. (editors) (1996) *Climate Change 1995 - The Science of Climate Change. Contributions of Working Group I to the Second Assessment Report of the Intergovernmental Panel on Climate Change*. Cambridge University Press.

Huppert, H. E. (1986) The intrusion of fluid mechanics into geology. *J. Fluid Mech.*, **173**, 557–594.

Hurtt, G. C. and Armstrong, R. A. (1999) A pelagic ecosystem model calibrated with BATS and OWSI data. *Deep-Sea Res. I*, **46**, 27–61.

Jackson, G. A. (1995) Coagulation of marine algae. In Huang, C. P., O'Melia, C. R. and Morgan, J. J. (editors), *Aquatic Chemistry: Interfacial and Interspecies Processes*, American Chemical Society, Washington, DC. pp. 203–217.

Jackson, G. A. and Lochmann, S. E. (1992) Effect of coagulation on nutrient and light limitation of an algal bloom. *Limnol. Oceanogr.*, **37**, 77–89.

Jeffery, S. W. and Wright, S. W. (1994) Photosynthetic pigments in the haptophyta. In Green, J. C. and Leadbeater, B. S. C. (editors), *The Haptophyte Algae*, Clarendon Press, Oxford. pp. 111–132.

Joos, F., Plattner, G., Stocker, T. F., Marchal, O. and Schmittner, A. (1999) Global warming and marine carbon cycle feedbacks on future atmospheric CO_2. *Science*, **284**, 464–467.

Karp-Boss, L., Boss, E. and Jumars, P. A. (1996) Nutrient fluxes to planktonic osmotrophs in the presence of fluid motion. *Oceanography and Marine Biology: an Annual Review*, **34**, 71–107.

Kennett, J. P. (1982) *Marine Geology*. Prentice-Hall, Inc., New Jersey.

Kerr, R. A. (1998) Models win big in forecasting El Niño. *Science*, **280**, 522–523.

Kiørboe, T. (1993) Turbulence, phytoplankton cell size, and the structure of pelagic food webs. *Adv. Mar. Biol.*, **29**, 1–72.

Kiørboe, T., Hansen, J. L. S., Alldredge, A. L., Jackson, G. A., Passow, U., Dam, H. G., Drapeau, D. T., Waite, A. and Garcia, C. M. (1996) Sedimentation of phytoplankton during a diatom bloom: rates and mechanisms. *J. Mar. Res.*, **54**, 1123–1148.

Kirk, J. T. O. (1975a) A theoretical analysis of the contribution of algal cells to the attenuation of light within natural waters. I. General treatment of suspensions of pigmented cells. *New Phytol.*, **75**, 11–20.

Kirk, J. T. O. (1975b) A theoretical analysis of the contribution of algal cells to the attenuation of light within natural waters. II. Spherical cells. *New Phytol.*, **75**, 21–36.

Kirk, J. T. O. (1976) A theoretical analysis of the contribution of algal cells to the attenuation of light within natural waters. III. Cylindrical and spheroidal cells. *New Phytol.*, **77**, 341–358.

Kirk, J. T. O. (1981) A Monte Carlo study of the nature of the underwater light field in, and the relationship between optical properties of, turbid yellow waters. *Aust. J. Mar. Freshwater Res.*, **32**, 517–532.

Kirk, J. T. O. (1984) Dependence of relationship between inherent and apparent optical properties of water on solar altitude. *Limnol. Oceanogr.*, **29**, 350–356.

Kirk, J. T. O. (1991) Volume scattering function, average cosines, and the underwater light field. *Limnol. Oceanogr.*, **36**, 455–467.

Kirk, J. T. O. (1994) *Light and Photosynthesis in Aquatic Ecosystems*. Cambridge University Press, Cambridge, 2nd edn.

Koller, L. R. (1965) *Ultraviolet Radiation*. John Wiley and Sons, Inc., New York, 2nd edn.

Korb, R. E., Raven, J. A. and Johnston, A. M. (1998) Relationship between CO_2 concentrations and stable carbon isotope discrimination in the diatoms *Chaetoceros calcitrans* and *Ditylum brightwellii*. *Mar. Ecol. Prog. Ser.*, **171**, 303–305.

Kuchel, P. W. and Ralston, G. B. (1988) *Schuam's outline of theory and problems of biochemistry*. McGraw-Hill, Inc., Sydney.

Laws, E. A., Bidigare, R. R. and Popp, B. N. (1997) Effects of growth rate and CO_2 concentration on carbon isotopic fractionation by the marine diatom *Phaeodactylum tricornutum*. *Limnol. Oceanogr.*, **42**, 1552–1560.

Laws, E. A., Popp, B. N., Bidigare, R. R., Kennicutt, M. C. and Macko, S. A. (1995) Dependence of phytoplankton carbon isotope composition on growth rate and $[CO_2]_{aq}$: theoretical considerations and experimental results. *Geochim. Cosmochim. Acta*, **59**, 1131–1138.

Laws, E. A., Thompson, P. A., Popp, B. N. and Bidigare, R. R. (1998) Sources of inorganic carbon for marine microalgal photosynthesis: A reassessment of $\delta^{13}C$ data from batch culture studies of *Thalassiosira pseudonana* and *Emiliania huxleyi*. *Limnol. Oceanogr.*, **43**, 136–142.

Lazier, J. R. N. and Mann, K. H. (1989) Turbulence and the diffusive layers around small organisms. *Deep-Sea Res.*, **36**, 1721–1733.

Legovic, T. and Cruzado, A. (1997) A model of phytoplankton growth on multiple nutrients based on Michaelis-Menton-Monod uptake, Droop's growth and Liebig's law. *Ecol. Model.*, **99**, 19–31.

Lewis, M. R., Ulloa, O. and Platt, T. (1988) Photosynthetic action, absorption, and quantum yield spectra for a natural population of *Oscillatoria* in the North Atlantic. *Limnol. Oceanogr.*, **33**, 92–98.

Li, Y. and Gregory, S. (1974) Diffusion of ions in sea water and in deep-sea sediments. *Geochim. Cosmochim. Acta*, **38**, 703–714.

Libes, S. M. (1992) *An Introduction to Marine Biogeochemistry*. John Wiley and Sons, Inc., New York.

von Liebig, J. (1840) *Chemistry in its Application to Agriculture and Physiology*. Taylor and Walton, London.

Lohmann, H. (1902) Die coccolithophoridae, eine monographie der coccolith en bildenden flagellaten, zuglish ein beitrag zur kenntrnis des mittelmeerauftriets. *Archi. Protistenkunde*, **1**, 89–165.

Loyalka, S. K. and Griffin, J. L. (1994) Rotation of non-spherical axi-symmetric particles in the slip regime. *J. Aerosol Sci.*, **25**, 509–525.

Mann, K. H. and Lazier, J. R. N. (1991) *Dynamics of Marine Ecosystems*. Blackwell Scientific Publications Inc., Oxford.

Marchal, O., Stocker, T. F. and Joos, F. (1998) A latitude-depth, circulation-biogeochemical ocean model for paleoclimate studies. Development and sensitivities. *Tellus*, **50B**, 290–316.

May, R. M. (1987) Chaos and the dynamics of biological populations. *Proc. R. Soc. Lond. A*, **413**, 27–44.

McGillicuddy Jr., D. J. (1995) One-dimensional numerical simulation of primary production: Lagrangian and eulerian formulations. *J. Plankton Res.*, **17**, 405–412.

Mellor, G. L. and Yamada, T. (1974) A hierarchy of turbulent closure models for planetary boundary layers. *Journal of Atmospheric Sciences*, **31**, 1791–1806.

Mellor, G. L. and Yamada, T. (1982) Development of a turbulent closure model for geophysical fluid problems. *Rev. Geophys. Space Phys.*, **20**, 851–875.

Menzel, D. W. and Ryther, J. H. (1960) The annual cycle of primary production in the Sargasso Sea off Bermuda. *Deep-Sea Res.*, **6**, 351–367.

Mierle, G. (1985a) Kinetics of phosphate transport by *Synechococcus leopoliensis* (cyanophyta): evidence for diffusion limitation of phosphate uptake. *J. Phycol.*, **21**, 177–181.

Mierle, G. (1985b) A method for estimating the diffusion resistance of the unstirred layer of microorganisms. *Biochim. Biophys. Acta*, **812**, 827–834.

Moon, P. and Spencer, D. E. (1971) *Field Theory Handbook*. Springer-Verlag, 2nd edn.

Morel, A., Ahn, Y., Partensky, F., Vaulot, D. and Claustre, H. (1993) *Prochlorococcus* and *Synechococcus*: A comparative study of their optical properties in relation to their size and pigmentation. *J. Mar. Res.*, **51**, 617–649.

Morel, A. and Bicaud, A. (1986) Inherent properties of algal cells including picoplankton: theoretical and experimental results. In Platt, T. and Li, W. K. W. (editors),

Photosynthetic picoplankton, Can. Bull. Fish. Aquat. Sci. **214**: 583 p., Ottawa. pp. 521–559.

Morel, F. M. M. (1987) Kinetics of nutrient-uptake and growth in phytoplankton. *J. Phycology*, **23**, 137–150.

Murray, A. G. and Jackson, G. A. (1992) Viral dynamics: a model of the effects of size, shape, motion and abundance of single-celled planktonic organisms and other particles. *Mar. Ecol. Prog. Ser.*, **89**, 103–116.

Newell, G. E. and Newell, R. C. (1973) *Marine Plankton*. Hutchinson Educational Ltd., London, 3rd edn.

Nielsen, M. V. and Sakshaug, E. (1993) Photobiological studies of *Skeletonema costatum* adapted to spectrally different light regimes. *Limnol. Oceanogr.*, **38**, 1576–1581.

Oschlies, A. and Garçon, V. (1999) An eddy-permitting coupled physical-biological model of the North Atlantic 1. sensitivity to advection numerics and mixed layer physics. *Global Biogeochem. Cycles*, **13**, 135–160.

Ott, E. (1993) *Chaos in Dynamical Systems*. Cambridge University Press.

Pahlow, M., Riebesell, U. and Wolf-Gladrow, D. A. (1997) Impact of cell shape and chain formation on nutrient acquisition by marine diatoms. *Limnol. Oceanogr.*, **42**, 1660–1672.

Pais, A. (1982) *Subtle is the Lord - the science and life of Albert Einstein*. Oxford University Press.

Pasciak, W. J. and Gavis, J. (1975) Transport limited nutrient uptake rates in *Dictylum brightwellii*. *Limnol. Oceanogr.*, **20**, 604–617.

Piontkovski, S. A., Williams, R., Peterson, W. T., Yunev, O. A., Minkina, N. I., Vladimirov, V. L. and Blinkov, A. (1997) Spatial heterogeneity of the plankton fields in the upper mixed layer of the open ocean. *Mar. Ecol. Prog. Ser.*, **148**, 145–154.

Plymouth Marine Laboratory (1990a) *Ocean Weather Station India 1971-1975 Part I*. Natural Environment Research Council.

Plymouth Marine Laboratory (1990b) *Plymouth Culture Collection: List of Strains*. Natural Environment Research Council.

Pond, S. and Pickard, G. L. (1983) *Introductory Dynamical Oceanography*. Pergamon, Oxford, 2nd edn.

Popp, B. N., Kenig, F., Wakeham, S. G., Laws, E. A. and Bidigare, R. R. (1998a) Does growth rate affect ketone unsaturation and intracellular carbon isotopic variability in *Emiliania huxleyi*. *Paleooceanography*, **13**, 35–41.

Popp, B. N., Laws, E. A., Bidigare, R. R., Dore, J. E., Hanson, K. L. and Wakeham, S. G. (1998b) Effect of phytoplankton cell geometry on carbon isotope fractionation. *Geochim. Cosmochim. Acta*, **62**, 69–77.

Rau, G. H., Riebesell, U. and Wolf-Gladrow, D. (1996) A model of photosynthetic ^{13}C fractionation by marine phytoplankton based on diffusive molecular CO_2 uptake. *Mar. Ecol. Prog. Ser.*, **133**, 275–285.

Raven, J. A. (1997) Phagotrophy in phototrophs. *Limnol. Oceanogr.*, **42**, 198–205.

Raven, J. A. and Geider, R. J. (1988) Temperature and algal growth. *New Phytol.*, **110**, 441–461.

Ridgwell, A. J., Marshall, S. J. and Gregson, K. (1999) Consumption of atmospheric methane by soils: a process-based model. *Global Biogeochem. Cycles*, **13**, 59–70.

Riley, G. A. (1947) A theoretical analysis of the zooplankton population of Georges Bank. *J. Mar. Res.*, **6**, 104–113.

Rothschild, B. J. and Osborn, T. R. (1988) Small-scale turbulence and plankton contact rates. *J. Plankton Res.*, **10**, 465–474.

Ryabchenko, V. A., Fasham, M. J. R., Kagan, B. A. and Popova, E. E. (1997) What causes short-term oscillations in ecosystem models of the ocean mixed layer. *J. Mar. Syst.*, **13**, 33–50.

Saffman, P. G. and Turner, J. S. (1956) On the collision of drops in turbulent clouds. *J Fluid. Mech.*, **1**, 16–30.

Sakshaug, E., Andresen, K. and Kiefer, D. A. (1989) A steady state description of growth and light absorption in the marine planktonic diatom *Skeletonema costatum*. *Limnol. Oceanogr.*, **34**, 198–205.

Sarmiento, J. L., Hughes, T. M. C., Stouffer, R. J. and Manab, S. (1998) Simulated response of the ocean carbon cycle to anthropogenic climate warming. *Nature*, **393**, 245–249.

Sarmiento, J. L., Slater, R. D., Fasham, M. J. R., Ducklow, H. W., Toggweiler, J. R. and Evans, G. T. (1993) A seasonal three-dimensional ecosystem model of nitrogen cycling in the North Atlantic euphotic zone. *Global Biogeochem. Cycles*, **7**, 417–450.

Sharples, J. and Tett, P. (1994) Modelling the effect of physical variability on the mid-water chlorophyll maximum. *J. Mar. Res.*, **52**, 219–238.

Shimeta, J., Jumars, P. A. and Lessard, E. J. (1995) Influences of turbulence on suspension feeding by planktonic protozoa: experiments in laminar shear fields. *Limnol. Oceanogr.*, **40**, 845–859.

Smith, F. A. and Walker, N. A. (1980) Photosynthesis by aquatic plants: effects of unstirred layers in relation to assimilation of CO_2 and HCO_3^- and to carbon isotopic discrimination. *New Phytol.*, **86**, 245–259.

Smith, S. D. and Dobson, F. W. (1984) The heat budget at Ocean Weather Station *Bravo*. *Atmosphere-Ocean*, **22**, 1–22.

Sommer, U. (1988) Some size relationships in phytoflagellate motility. *Hydrobiologia*, **161**, 125–131.

Steele, J. H. and Clark, C. W. (1998) Relationship between individual- and population-based plankton models. *J. Plankton Res.*, **20**, 1403–1415.

Steele, J. H. and Henderson, E. W. (1981) A simple plankton model. *The Am. Nat.*, **117**, 676–691.

Stockdale, T. N., Anderson, D. L. T., Alves, J. O. S. and Balmaseda, M. A. (1998) Global seasonal rainfall forecasts using a coupled ocean-atmosphere model. *Nature*, **392**, 370–373.

Straile, D. (1997) Gross growth efficiencies of protozoan and metazoan zooplankton and their dependence on food concentration, predator-prey weight ratio, and taxonomic group. *Limnol. Oceanogr.*, **42**, 1375–1385.

Strass, V. H. and Woods, J. D. (1991) New production in the summer revealed by the meridional slope of the deep chlorophyll maximum. *Deep-Sea Res.*, **38**, 35–56.

Sunda, W. G. and Huntsman, S. A. (1996) Antagonism between cadmium and zinc toxicity and manganese limitation in a coastal diatom. *Limnol. Oceanogr.*, **41**, 373–387.

Suttle, C., Chan, A. and Cottrell, M. (1990) Infection of phytoplankton by viruses and reduction of primary productivity. *Nature*, **347**, 467–469.

Tang, E. P. Y. (1995) The allometry of algal growth rates. *J. Plankton Res.*, **17**, 1325–1335.

Taylor, A. H., Geider, R. J. and Gilbert, F. J. H. (1997) Seasonal and latitudinal dependencies of phytoplankton carbon-to-chlorophyll *a* ratios: results of a modelling study. *Mar. Ecol. Prog. Ser.*, **152**, 51–66.

Taylor, A. H. and Stephens, J. A. (1993) Diurnal variations of convective mixing and the spring bloom of phytoplankton. *Deep-Sea Res. II*, **40**, 389–408.

Thompson, P. A. and Calvert, S. E. (1994) Carbon isotope fractionation by a marine diatom: The influence of irradiance, daylength, pH, and nitrogen source. *Limnol. Oceanogr.*, **39**, 1835–1844.

Thompson, P. A. and Calvert, S. E. (1995) Carbon isotope fractionation by *Emiliania huxleyi*. *Limnol. Oceanogr.*, **40**, 673–679.

Todling, R., Cohn, S. E. and Sivakumaran, N. S. (1998) Suboptimal schemes for retrospective data assimilation based on the fixed-lag Kalman smoother. *Mon. Wea. Rev.*, **126**, 2274–2286.

Truscott, J. E. and Brindley, J. (1994) Equilibria, stability and excitability in a general class of plankton population models. *Phil. Trans. R. Soc. Lond., Ser. A*, **347**, 703–718.

Valiela, I. (1992) *Marine Ecological Processes*. Springer-Verlag, New York, 2nd edn.

Wolf-Gladrow, D. and Riebesell, U. (1997) Diffusion and reactions in the vicinity of plankton: a refined model for inorganic carbon transport. *Mar. Chem.*, **59**, 17–34.

Wollast, R. and Garrels, R. M. (1971) Diffusion coefficient of silica in seawater. *Nature*, **229**, 94.

Wong, C. W. (1991) *Introduction to Mathematical Physics*. Oxford University Press.

Wroblewski, J. (1977) A model of phytoplankton plume formation during variable Oregon upwelling. *J. Mar. Res.*, **35**, 357–394.

Yool, A. (1997) *The Dynamics of Open-Ocean Plankton Ecosystem Models*. Ph.D. thesis, Dept. of Biological Sciences, University of Warwick.

Zubkov, M. V., Sleigh, M. A., Tarran, G. A., Burkill, P. H. and Leakey, R. J. G. (1998) Picoplanktonic community structure on an Atlantic transect from 50 N to 50 S. *Deep-Sea Res. I*, **45**, 1339–1355.

Publications

Baird, M. E. and Emsley, S. M. (1999) Towards a mechanistic model of plankton population dynamics. *J. Plankton Res.*, **21**, 85-126.

Baird, M. E., Emsley, S. M. and McGlade, J. M. (submitted) Verifying a phytoplankton growth model using population dynamics and carbon isotope fractionation. *Mar. Ecol. Prog. Ser.*